DEVELOPMENT OF ADVANCED METHODS TO CHARACTERISE THE FRACTURE BEHAVIOUR OF FLEXIBLE BONDED JOINTS

Julen Manterola Najera

Universitat de Girona

Doctoral Thesis

DEVELOPMENT OF ADVANCED METHODS TO CHARACTERISE THE FRACTURE BEHAVIOUR OF FLEXIBLE BONDED JOINTS

by
Julen Manterola Najera

2020

Doctoral Thesis

DEVELOPMENT OF ADVANCED METHODS TO CHARACTERISE THE FRACTURE BEHAVIOUR OF FLEXIBLE BONDED JOINTS

by
Julen Manterola Najera

2020

Doctoral Programme in Technology

supervised by
Dr. Albert Turon Travesa
Dr. Jordi Renart Canalias
Dr. Javier Zurbitu González

Thesis submitted to the University of Girona for the degree of Doctor of Philosophy

Acknowledgements

I would like to present my deepest gratitude to my advisors Javier Zurbitu, Jordi Renart and Albert Turon for their support and advice given during the thesis, specially in tough moments when time pressed and inspiring ideas were needed. I also thank work mates in Ikerlan for their contributions in different tasks, being always predisposed to help. The work environment in Ikerlan was friendly and productive, perfect for developing such a project.

I would also like to thank PhD candidates in AMADE research group for hosting me and for the support received at any time I needed. The different stays in Girona have been refreshing and motivating to continue working on the thesis.

I would like to mention the support received from coauthors Mario Cabello, Marcos Aguirre and Iker Urresti in Ikerlan, and Julien Jumel at I2M in University of Bordeaux to address the technical challenges found during the development of the thesis.

Eskerrik asko familiari, batez ere ama eta aiteri zuon eguneroko baldintza bako laguntzagaitik, arrebei dekozuen bizitasune kutsatzeagaitik, eta Idow eta Gasteizko kuadrilari bakoitza bere erara nire psikologo pertsonalak iziteagaitik.

Danori, eskerrik asko benetan!

Preface

The work developed in this thesis was conducted at Ikerlan Technology Research Centre in Arrasate-Mondragón, being part of the Structural Reliability team in the Applied Mechanics Area. The thesis was funded by Ikerlan and part of the research presented was developed at AMADE research group (Department of Mechanical Engineering and Industrial Construction, University of Girona) in Girona, Spain.

Publications

The present Ph.D. thesis has been written as a compendium of peer-reviewed journal papers in accordance with the regulations of the University of Girona. The thesis is comprised of the following papers:

Peer-reviewed journal articles

- **J. Manterola**, M. Cabello, J. Zurbitu, J. Renart, A. Turon, J. Jumel and I. Urresti. Effect of the width-to-thickness ratio on the mode I fracture toughness of flexible bonded joints. *Engineering Fracture Mechanics*, 2019; 218: 106584.
  doi:10.1016/j.engfracmech.2019.106584

  ISSN: 0013-7944, Impact Factor: 2.908, ranked 27/134 in the category of *Mechanics* (1st quartile)[a].

- **J. Manterola**, M. Aguirre, J. Zurbitu, J. Renart, A. Turon and I. Urresti. Using acoustic emissions (AE) to monitor mode I crack growth in bonded joints. *Engineering Fracture Mechanics*, 2020; 224: 106778.
  doi: 10.1016/j.engfracmech.2019.106778

  ISSN: 0013-7944, Impact Factor: 2.908, ranked 27/134 in the category of *Mechanics* (1st quartile)[a].

- **J. Manterola**, J. Zurbitu, J. Renart, A. Turon and I. Urresti. Durability study of flexible bonded joints: the effect of sustained loads in mode I fracture tests. *Polymer Testing*, 2020; 88: 106570.
  doi: 10.1016/j.polymertesting.2020.106570

[a] According to the 2018 Journal Citation Reports

ISSN: 0142-9418, Impact Factor: 2.943, ranked 5/33 in the category of *Materials science, characterization & testing* (1st quartile)[a].

- **J. Manterola**, J. Renart, J. Zurbitu, A. Turon and I. Urresti. Mode I fracture characterisation of rigid and flexible bonded joints using an advanced Wedge-Driven Test. *Mechanics of Materials*, 2020; 148: 103534. doi: 10.1016/j.mechmat.2020.103534

  ISSN: 0167-6636, Impact Factor: 2.958, ranked 24/134 in the category of *Mechanics* (1st quartile)[a].

Patent request

- **J. Manterola**, J. Zurbitu, M. Cabello, I. Urresti, J. Renart and A. Turon. Process and apparatus for determining the energy release rate of a test piece. 2020; WO2021152187A1.

Conference proceedings

- **J. Manterola**, M. Cabello, F. Martínez, J. Renart, A. Turon and J. Zurbitu. Design methodology to maximize the strength of a bonded joint using flexible adhesives. XVIII Congreso Internacional de Adhesión y Adhesivos. Barcelona (Spain), September 2017.

- **J. Manterola**, J. Zurbitu, J. Renart, A. Turon and I. Urresti. Towards an experimental method for the fracture characterization of bonded joints subjected to environmental ageing. XX Congreso Internacional de Adhesión y Adhesivos. San Sebastián (Spain), September 2019.

- **J. Manterola**, J. Zurbitu, M. Aguirre, J. Renart, A. Turon and I. Urresti. Crack growth propagation measurement in bonded joints using acoustic emission (AE) technique. XX Congreso Internacional de Adhesión y Adhesivos. San Sebastián (Spain), September 2019.

Universitat de Girona

Dr. Albert Turon Travesa and Dr. Jordi Renart Canalias Associate Professors at University of Girona, and Dr. Javier Zurbitu González, Researcher at Ikerlan Technology Research Centre in Mondragón

hereby CERTIFY that:

The thesis entitled *Development of advanced methods to characterise the fracture behaviour of flexible bonded joints*, submitted for the degree of Doctor of Philosophy by Julen Manterola Najera, has been conducted under my supervision.

Dr. Albert Turon
University of Girona

Dr. Jordi Renart
University of Girona

Dr. Javier Zurbitu
Ikerlan, S.COOP

Girona, February 2020

List of Figures

List of Tables

Acronyms

AE	Acoustic Emissions
ASTM	American Society of Testing Materials
AVG	Average
CBBM	Compliance Based Beam Method
CBT	Corrected Beam Theory
CFRP	Carbon Fibre Reinforced Polymer
CHAN	Channel
COF	Coefficient of Friction
DCB	Double Cantilever Beam
DIC	Digital Image Correlation
ERR	Energy Release Rate
EU	European Union
FBG	Fibre Bragg Grating
FE	Finite Element
FPZ	Fracture Process Zone
ISO	International Organization for Standardization
LEFM	Linear Elastic Fracture Mechanics
LUCY	Location Uncertainty
MSE	Mean Squared Error
NDT	Non-destructive Techniques
NLFM	Non-linear Fracture Mechanics
OBR	Optical Backscatter Reflectometer
PLB	Pencil Lead Break
QSR	Quasi-static Strain Rate
SBT	Simple Beam Theory
SD	Standard Deviation
SHM	Structural Health Monitoring
SW	Smart Wedge
TRL	Technology Readiness Level
WDD	Wedge Driven Delamination
WDT	Wedge Driven Test
WDT+	Wedge Driven Test Plus
WT	Wedge Test

List of symbols

A_{th}	signal peak amplitude
a	crack length
a_c	corrected crack length
a_e	equivalent crack length
a_0	initial crack length
B	total width of the specimen
B^*	effective width of the adhesive layer before fracture occurs
C	compliance
D	distance between sensors
D_w	diameter of the curvature in the rounded tip of a wedge
d	distance from first hit sensor, or wedge position
d_{ini}	wedge position when crack starts to propagate
d_{lim}	wedge position before being inserted into the adhesive layer
E_a	adhesive's Young's modulus
E_f	flexural modulus of the joint
E_i	Young's modulus for the adherend in direction i
E_x	Young's modulus of the adherend
F_{push}	load needed to push the wedge forward
F^c_{push}	critical pushing load to propagate a crack
G_I	mode I energy release rate
G_{IC}	critical ERR, fracture toughness
G_{IC_e}	fracture toughness considering the exact contact
G_{IC_s}	fracture toughness considering the simplified contact
G_{13}	out-of-plane shear modulus of the adherend
h	adherend thickness
I	moment of inertia
J_I	mode I J-integral
J^{ext}	fracture energy measured in the external face
$J^{(eq)}$	equivalent fracture energy of bonded joint
$J^{(eq)}_{PE}$	equivalent fracture energy under plane-strain state
$J^{(eq)}_{(B/t_a)}$	equivalent fracture energy for a given B/t_a configuration
$J_{(B/t_a)}$	fracture energy for a given B/t_a configuration

P	openinig load
r_w	radius of the tip in a rounded wedge
t	exposure time
t_a	bondline thickness
$\mathbb{U}$	elastic potential energy
V	volume, or velocity of dispersion waves
x	longitudinal location of the crack tip
Δ	crack length correction factor
Δ_a	crack growth
Δc	maximum longitudinal deformation of the crack tip
ΔP	increment of the opening load
ΔT	arrival time delay
$\Delta\delta_y$	increment of the opening displacement
δ_x	longitudinal displacement
δ_y	opening displacement
ϵ_{xy}	shear strain in the x-y local plane
θ	relative rotation angle between adherends
θ^c	critical rotation angle to propagate a crack
μ	friction coefficient between the wedge and adherends
ν_a	adhesive's Poisson ratio
$\zeta^{(eq)}_{(B/t_a)}$	equivalent correction factor for a given B/t_a
σ_y^{max}	maximum peel stress

Contents

Abstract

Joining technologies play an important role in one of the most important technical challenges of today: climate change. The main objectives are to reduce the carbon footprint and to increase the environmental sustainability and for this purpose, industry has to develop more efficient and durable systems that may favour the reduction of CO2 emissions and renewable energy generation. Transport or energy sectors support innovation in lightweight materials (e.g. composites) and structures to reduce energy consumption, and multi-material structures are used to provide their integrity. While conventional joining technologies show limitations when mechanical requests are high, advanced joining technologies such as adhesive joints take advantage. The lack of knowledge about the mechanical behaviour of bonded joints, however, produce oversized structures and duplicated joints by adding extra mechanical joints for precaution.

Most studies are based on rigid bonded joints using epoxy adhesives although the catalogue of structural adhesives is extensive. Thus, experimental studies are lacking to analyse the structural behaviour of flexible adhesives, which may provide improved properties against dynamic loads or harsh environments. The most widely used test standards are the DCB test (ISO-25217) and the Wedge Test (ASTM D3762) to evaluate the quality and the durability of bonded joints, respectively. Their principal limitation, however, is that crack length measuring is needed and that results show a strong dependence on joint dimensions. Moreover, there is not yet consensus regarding the use of the appropriate method specially when using flexible adhesives or in durability studies.

The present Thesis gives a step forward and proposes different solutions for the characterisation of the fracture behaviour of flexible bonded joints, contributing to the use of bonded joints in industry. In this way, the influence of the width-to-thickness ratio (i.e. stress state) on the mode I fracture toughness of flexible bonded joints has been evaluated through an experimental study. An analytical model has been developed to predict the fracture toughness of flexible bonded joints and it is proved that the fracture behaviour of flexible bonded joints is dominated by the elastic behaviour of the adhesive. Acoustic emissions technique is proposed to reduce subjectivity in crack length measurement and mode I crack growth is monitored in bonded

joints, providing an estimation of the size of the fracture process zone (FPZ). The method is valid for rigid and flexible bonded joints and evidences in numerical and experimental results show the nature of acoustic events.

Bonded joints applied in industrial environments, however, must also withstand environmental conditions (e.g. temperature and humidity), but the selection of the appropriate method to characterise their durability is not evident. A durability study of flexible bonded joints has been conducted to evaluate the suitability of different experimental methods available in the literature. For this purpose, bonded joints have been subjected to load and environmental conditions and the fracture toughness has been evaluated at different exposure times. It is concluded that neither the Wedge Test (ASTM D3762) nor the experimental methods that require crack length measurement are appropriate to evaluate the durability of flexible bonded joints exposed to the combined effect of loads, temperature and humidity. To compensate the lack of experimental methods to address durability studies, a new data reduction method named Wedge Driven Test Plus (WDT+) has been developed. It is valid for rigid and flexible bonded joints and avoids crack length measurement to evaluate the fracture toughness. The influence of test speed and the wedge diameter on the test procedure have been analysed by comparing the WDT+ and the DCB test. It is proved that the proposed method is robust, less sensitive to test speed than the DCB test (ISO-25217) and applicable in bonded joints with any bondline thickness. Finally, a new experimental method has been developed to evaluate the durability of bonded joints exposed to load and environmental conditions. The test method applies the WDT+ to provide the evolution of the energy release rate (ERR) during the test. For this purpose, a new test rig has been developed and, despite its low TRL level, the proposed method shows a great potential to be used in future projects with an industrial application.

Resumen

Las tecnologías de unión juegan un papel relevante en uno de los retos técnicos más importantes de la actualidad: el cambio climático. Los objetivos principales son reducir la huella de carbono y aumentar la sostenibilidad ambiental y para ello, la industria tiene que desarrollar sistemas más eficientes y duraderos que favorezcan la reducción de las emisiones de CO2 y la generación de energía por fuentes renovables. Sectores como el transporte o el energético apoyan la innovación en búsqueda de materiales y estructuras ligeras (p. ej. composites) para el ahorro en el consumo de energía y utilizan a estructuras multi-material para no reducir su integridad. Cuando las solicitaciones mecánicas son elevadas, los métodos de unión convencionales muestran limitaciones y otras tecnologías de unión más avanzadas como las adhesivas toman ventaja. No obstante, la falta de conocimiento sobre el comportamiento mecánico de las uniones adhesivas provoca que las estructuras se sobredimensionen y que, en última instancia, se añada una unión mecánica por precaución.

A pesar del amplio catálogo de adhesivos estructurales, los estudios generalmente se basan en uniones rígidas con adhesivos en base epoxy. De este modo, existe una falta de estudios experimentales que analicen el comportamiento mecánico de uniones adhesivas flexibles, las cuales muestran mejores propiedades frente a cargas dinámicas o ambientes hostiles. En este aspecto, los métodos normalizados que generalmente se utilizan son el ensayo sobre probetas de doble viga en voladizo (también denominado como ensayo DCB, ISO-25217) y el ensayo *Wedge Test* (ASTM D3762), utilizados para evaluar la calidad y la durabilidad de las uniones adhesivas respectivamente. La limitación principal de estos métodos es que requieren medir la longitud de grieta visualmente y que los resultados muestran una gran dependencia de las dimensiones de la unión. Además, no existe un consenso en la utilización de los métodos, especialmente cuando se usan adhesivos flexibles o se realizan estudios de durabilidad.

La presente tesis da un paso adelante y propone diferentes soluciones para la caracterización del comportamiento a la fractura de las uniones adhesivas flexibles, contribuyendo en la utilización de este tipo de uniones en la industria. En esta dirección, en primer lugar, se ha evaluado experimentalmente la influencia del ratio ancho-espesor (estado tensional) sobre la tenaci-

dad a la fractura en modo I de uniones adhesivas flexibles. Se ha desarrollado un modelo analítico para predecir la tenacidad a la fractura de uniones adhesivas flexibles y se ha demostrando que el comportamiento elástico del adhesivo domina el comportamiento a la fractura de las uniones adhesivas flexibles. Se propone utilizar sensores de emisiones acústicas para reducir la subjetividad en la medición de la grieta y se monitoriza el crecimiento de grieta en modo I, estimando el tamaño de la zona de proceso de fallo (FPZ). El método es aplicable tanto en uniones rígidas como en flexibles y se determina la naturaleza de los eventos acústicos tras una correlación entre los modelos numéricos y los resultados experimentales.

Las uniones adhesivas aplicadas en entornos industriales deben soportar también las condiciones ambientales (p. ej. temperatura y humedad), pero no es evidente qué método seguir para evaluar su durabilidad. Con el objetivo de evaluar la aplicabilidad de los diferentes métodos disponibles en la literatura, se ha realizado un estudio de durabilidad sobre uniones adhesivas flexibles. Para ello, las uniones se han expuesto a unas condiciones concretas de carga y de ambiente y se ha evaluado su tenacidad a la fractura en diferentes tiempos de exposición. Se ha concluido que el ensayo *Wedge Test* (ASTM D3762) y los métodos que requieren medir la longitud de grieta no son válidos para evaluar la durabilidad de uniones adhesivas flexibles expuestas al efecto combinado de la carga, la temperatura y la humedad. En respuesta a la falta de métodos experimentales para evaluar la durabilidad de las uniones adhesivas, se ha desarrollado un método de reducción de datos llamado Wedge Driven Test Plus (WDT+), válido para uniones rígidas y flexibles.

El método consiste en insertar una cuña dentro de la capa de adhesivo de una unión adhesiva de geometría prismática y no depende de la longitud de grieta para evaluar la tenacidad a la fractura. Se han analizado la influencia de la velocidad del ensayo y del espesor de la cuña sobre el proceso de ensayo comparando el WDT+ con el ensayo DCB. Se demuestra que el método propuesto es robusto y menos sensible a la velocidad del ensayo que el ensayo DCB, con la posibilidad de hacer ensayos sobre uniones adhesivas con diferentes espesores. Por último, se ha desarrollado un nuevo método experimental para evaluar la durabilidad de uniones adhesivas expuestas a condiciones de carga y de ambiente. El nuevo método de ensayo aplica el WDT+ para mostrar la evolución de la tasa de liberación de energía (ERR) durante el ensayo. Para ello, se ha desarrollado un nuevo utillaje y, aunque todavía se encuentre en un nivel de TRL bajo, el método propuesto tiene potencial para ser aplicado en futuros proyectos con aplicación industrial.

Resum

Les tecnologies d'unió juguen un paper rellevant en un dels reptes tecnològics més importants de l'actualitat: el canvi climàtic. Els objectius principals són reduir la petjada de carboni i augmentar la sostenibilitat ambiental i per a això, la indústria ha de desenvolupar sistemes més eficients i duradors, afavorint la reducció de les emissions de CO2 i la generació d'energia mitjançant fonts renovables. Sectors com el transport o l'energètic donen suport a la innovació en recerca de materials i estructures lleugeres (per exemple els compòsits) per a l'estalvi en el consum d'energia i utilitzen estructures multimaterial per mantenir-ne la seva integritat estructural. Quan les sol·licitacions mecàniques són elevades, els mètodes d'unió convencionals tenen certes limitacions, i altres tecnologies d'unió més avançades com les adhesives prenen la iniciativa. No obstant, la manca de coneixement sobre el comportament mecànic de les unions adhesives provoca que les estructures es sobredimensionin i que, en darrera instància, aquestes es reforcis mitjançant una unió mecànica convencional.

Malgrat l'existència d'un ampli catàleg d'adhesius estructurals, els estudis generalment es centren en unions rígides amb adhesius en base epoxi, i hi ha una manca d'estudis experimentals que analitzin el comportament mecànic d'unions adhesives flexibles, encara que s'hagi observat que tenen millors propietats quan estan sotmesos a càrregues dinàmiques o ambients hostils. En aquest aspecte, els mètodes d'assaig normalitzats que s'utilitzen per avaluar la qualitat de les unions adhesives i la seva durabilitat són l'assaig de doble biga en voladís (altrament anomenat assaig DCB, ISO-25217) i l'assaig de cunya o "wedge" (ASTM D3762), respectivament. La limitació principal d'aquests mètodes d'assaig és que requereixen realitzar mesures de la longitud d'esquerda visualment i que els resultats mostren una gran dependència de les dimensions de la unió. Per altra banda, no hi ha un consens en la utilització dels mètodes, especialment quan es fan servir adhesius flexibles o es realitzen estudis de durabilitat.

La present Tesi fa un pas endavant i proposa diferents solucions per a la caracterització del comportament a fractura de les unions adhesives flexibles, contribuint a la utilització d'aquest tipus d'unions en la indústria. En aquesta direcció, en primer lloc, s'ha realitzat un estudi experimental sobre el comportament a fractura en mode I d'unions adhesives flexibles i s'ha avaluat

la influència de l'estat tensional sobre la tenacitat a la fractura de la unió. S'ha desenvolupat un model analític capaç de predir la tenacitat a la fractura d'unions adhesives flexibles, demostrant que el comportament elàstic de l'adhesiu domina el comportament a la fractura de les unions adhesives flexibles. En segon lloc, amb l'objectiu de reduir la subjectivitat en el mesurament de l'esquerda, es proposa utilitzar sensors d'emissions acústiques en unions adhesives per localitzar la posició del creixement d'esquerda en mode I, i també per estimar la mida de la zona de procés de fallada (FPZ). S'ha comprovat, a través d'una campanya experimental, que el mètode és aplicable tant en unions rígides com en flexibles i després d'una correlació amb models numèrics, s'ha determinat la naturalesa dels esdeveniments acústics.

Una unió adhesiva aplicada en un entorn industrial ha de suportar també les condicions ambientals de l'entorn (com per exemple la temperatura i la humitat), però actualment no està clarament identificada la metodologia que cal utilitzar per avaluar la durabilitat d'aquestes unions adhesives. Amb l'objectiu d'avaluar l'aplicabilitat dels diferents mètodes d'assaig disponibles a la literatura, s'ha realitzat un estudi de durabilitat sobre unions adhesives flexibles, sotmetent-les a una càrrega sostinguda, i a diferents condicions ambientals. S'ha analitzat com mesuren els difuntes mètodes de caracterització de la tenacitat a la fractura la degradació de capa d'adhesiu, concloent que l'assaig Wedge Test (ASTM D3762) i els mètodes que requereixen mesurar la longitud d'esquerda no són vàlids per avaluar la durabilitat d'unions adhesives flexibles exposades a efectes combinats de la càrrega, la temperatura i la humitat. Per tal de donar resposta a la manca de mètodes experimentals per avaluar la durabilitat de les unions adhesives, s'ha desenvolupat un nou mètode d'assaig i de reducció de dades anomenat "Wedge Driven Test Plus (WDT+)", vàlid tant per a unions rígides com flexibles.

El mètode consisteix en inserir una cunya dins la capa d'adhesiu d'una unió adhesiva de geometria prismàtica per tal de propagar una esquerda. El mètode no depèn de la longitud d'esquerda per avaluar la tenacitat a la fractura. S'ha analitzat la influència de la velocitat de l'assaig i del diàmetre de la cunya en els resultats del mètode d'assaig WDT+. Finalment els resultats s'han comparat amb els de l'assaig DCB. Es demostra que el mètode proposat és robust i menys sensible a la velocitat de propagació de l'esquerda (velocitat d'assaig) que l'assaig DCB, amb la possibilitat de fer assajos sobre unions adhesives amb diferents gruixos. Finalment, s'ha utilitzat el WDT+ per definir un nou mètode experimental per avaluar la durabilitat d'unions adhesives exposades a condicions de càrrega i ambientals conegudes. S'aplica el WDT+ per obtenir la evolució de la taxa d'alliberament d'energia (ERR) durant l'assaig. Per a això, s'ha desenvolupat un nou utillatge i, tot i que encara es trobi en un nivell de TRL baix, el mètode proposat té potencial per ser aplicat en futurs projectes amb aplicació industrial.

Laburpena

Lotura teknologiek rol garrantzitsua jokatzen dute egungo erronka teknologiko handienetariko batean: klima-aldaketa. Helburu nagusiak karbono aztarna murriztea eta ingurumenaren iraunkortasuna bermatzea dira eta horretarako, industriak sistema eraginkorragoak eta iraunkorragoak garatu behar ditu energia berriztagarriak sustatzearekin batera CO2 gasen isurketak murrizteko. Garraio edo energia sektoreek material (adibidez, konpositeak) eta estruktura arinen berrikuntza babesten dute energia kontsumoa aurrezteko eta horrela CO2 isurketak murrizteko. Material arin hauek material anitzeko egituretan erabiltzen dira eta egituren osotasuna bermatzea ezinbestekoa da. Tentsio mekanikoak altuak direnean material ezberdinen arteko lotura konbentzionalak mugatuak dauden bitartean, lotura teknologia aurretuagoek abantailak azaltzen dituzte, lotura adhesiboen kasua den moduan. Hala ere, lotura adhesiboen portaera mekanikoari buruzko ezagutza faltak gehiegizko dimentsionatzeak eta segurtasunezko lotura mekanikoen eransketak eragiten du.

Adhesibo estrukturalen katalogoa zabala izan arren, orokorrean, azterketak epoxi motako adhesibo zurrunetan oinarritzen dira eta ondorioz, adhesibo malguak aztertzen dituzten lan esperimentalak falta dira. Egindako esperimentuetan karga dinamikoen edo ingurugiro gogorren aurrean propietate onak erakusten dituzte, non lotura adhesiboen kalitatea eta iraunkortasuna ebaluatzeko erabiltzen diren metodo estandarrak DCB entseguak (*DCB test*, ISO-25217) eta *Wedge Test* entsegua (ASTM D3762) diren hurrenez hurren. Arrakalaren luzera bisualki neurtu beharrak eta loturaren dimentsionen menpekotasunak ordea metodo hauen aplikazioa asko murrizten du. Gainera, ez dago adostasunik metodoen erabileraren inguruan, batez ere adhesibo malguak erabiltzean edo iraunkortasun azterketak egiterakoan.

Tesi honek aurrerapauso bat emanen du eta irtenbide desberdinak proposatzen ditu adhesibo malguen hausturaren portaera karakterizatzeko erabiltzen diren metodoen mugei aurre egiteko. Era berean, industrian azaltzen diren erronka teknikoei lotura adhesiboen erabileraren bitartez erantzuna ematen zaiela uste da. Norabide honetan, I-motako haustura baten aurrean lotura adhesibo malguen portaera aztertu da esperimentalki eta tentsio egoeraren eragina neurtu da loturaren irmotasunean. Honetarako, lotura adhesibo malguen irmotasuna iragartzeko gai den eredu analitiko bat garatu da, hauen haustura adhesiboaren portaera malguak deskribatzen duela fro-

gatuz. Arrakalaren neurketan subjektibotasuna murrizteko helburuz emisio akustikoak neurtzen dituzten sentsoreak erabiltzea proposatzen da, Imotako haustura baten aurrean arrakalaren hazkuntza monitorizatu eta adhesiboan sortutako kaltearen (FPZren) tamaina estimatzeko. Honez gain, metodoa lotura adhesibo zurrun eta malguetan aplikagarria dela berretsi da esperimentalki eta zenbakizko ereduekin korrelazioa egin ondoren, emisio akustikoen izaera zehaztu da.

Ingurune industrial batean aplikaturiko lotura adhesibo batek ordea ingurumen baldintzak ere jasan behar ditu (adibidez, tenperatura eta hezetasuna), baina ez dago argi zein metodo jarraitu behar den lotura adhesiboen iraunkortasuna ebaluatzeko. Literaturan eskuragarri dauden metodo desberdinen aplikagarritasuna ebaluatzeko asmoz, iraunkortasun azterketa bat burutu da. Horretarako, lotura adhesibo malguak karga, tenperatura eta hezetasun baldintza jakin batzuen eraginpean jarri dira eta adhesiboan sortutako kalteak irmotasuna neurtzeko erabiltzen diren metodo esperimentaletan izan duen eragina ebaluatu da. Kanpo baldintza jakin hauen eraginpean dauden lotura adhesibo malguen iraunkortasuna ebaluatzean, ez *Wedge Test* (ASTM D3762) metodoa ezta arrakala neurtu beharra duten metodoak ere, ez direla aproposak ondorioztatu da. Lotura adhesiboen iraunkortasuna ebaluatzeko metodo esperimentalen faltari erantzunez, Wedge Driven Test Plus (WDT+) izeneko datu murrizketa metodoa garatu da, adhesibo zurrun zein malguetan aplikatzeko balio duelarik.

Metodoak geometria prismatikozko lotura adhesibo batean ziri bat sartzean datza baina honek ez du arrakalaren luzera neurtzeko beharrik irmotasuna ebaluatzeko. Gainera, entseguaren abiaduraren eta ziriaren lodieraren eragina WDT+ metodoarengan aztertu da eta emaitzak DCB entseguekin alderatu dira. Proposatutako metodoa sendoa dela eta DCB entseguekin konparaturik entseguaren abiadurarekiko sentikortasun maila baxuagoa duela frogatu da, adhesiboaren lodiera edozein dela balio duelarik. Bukatzeko, WDT+ metodoa erabiltzen duen metodo esperimental berri bat proposatu da lotura adhesiboen iraunkortasuna ebaluatzeko. Honek karga, tenperatura eta hezetasun kondizioak hartzen ditu kontuan eta WDT+ metodoaren bitartez, adhesiboaren irmotasuna (ERR) ebaluatzen da etengabeki. Horretarako, tresneria berri bat garatu da eta, nahiz eta TRL maila baxu batean aurkitu oraindik, proposaturiko metodoak etorkizunean eman daitezkeen aplikazio industrialdun proiektuetan erabili ahal izateko potentziala dauka.

Chapter 1

Introduction

1.1 The role of bonded joints in industry

Technical challenges in industry sectors such as transport, energy or space are aligned with the measures that the European Union (EU) and Member States are currently running to reduce carbon emissions in order to prevent climate change [1]. The strategy aims to reduce the carbon footprint and to increment environmental sustainability. For this purpose, different actions are being taken in each industry sector to develop new efficient and safety systems. For instance, recent regulations setting CO2 emission performance standards for vehicles ensure that from 2030 onwards new passenger cars will emit on average 37.5% less CO2 and new vans will emit on average 31% less CO2 compared to 2021 levels [2]. With regards to safety, the EU has recently introduced new regulations imposing enhanced safety standards for car manufacturers in an attempt to significantly reduce the number of road casualties and to contribute the goal of zero road fatalities and serious injuries by 2050 [3], reinforcing previous commitments [4]. Similarly, aerospace industry's agenda defines the path to reach in 2050 a 75% reduction in CO2 and 90% in NOx emissions per passenger kilometre relative to the year 2000 [5]. Among other, the actions defined in [6] support innovation in lightweight materials and structures for weight-saving. The 2030 climate and energy framework [7] also includes key targets such as an improvement in energy efficiency of 32.5% and a share for renewable energy of 32%, namely wind, solar, geothermal or wave and other ocean energies [8]. Regarding space sector, it is considered to provide cutting-edge solutions to many kinds of societal challenges such as climate change by ensuring comprehensive monitoring of our planet using space-based Earth observation systems, becoming a strategic sector for innovation [9].

Since weight is synonym of energy consumption, more efficient and durable

systems are required and efforts should be focused on using new lightweight materials and multi-material structures increasing safety. Using materials with high specific strength (i.e. high strength-to-mass ratio), e.g. composites, enables to address technical challenges such as the existing in wind power stations. To be competitive, they need to increase capacity using higher wind towers and bigger turbines with larger rotor blades [10]. Then, multi-material structures must be joined and high mechanical loads sustained. While conventional joining technologies show limitations, new design and manufacturing approaches such as advanced joining technologies play an important role.

Adhesive bonding provides many advantages such as a lower structural weight, high strength-to-weight ratio, reduction of stress concentrations, design flexibility, high energy absorption capabilities, damping and isolation of components, sealing, increased fatigue life and corrosion resistance [11].

Overall, bonded joints contribute to structural integrity. They have found applications in high technology industries such as automotive, aeronautics, aerospace or energy. However, safety considerations for adhesively bonded structures often require mechanical fasteners as an additional safety precaution, specially in primary structures. This evinces the immaturity of the methodologies for analysing the structural integrity of bonded joints.

Regarding automotive industry, modern cars contain about 15 kg of adhesive and they are used mainly to avoid corrosion, to stiffen the car body, to obtain a better crash performance, to joint different materials that are not weldable and for sealing purposes [12]. In terms of durability, adhesive bonds must withstand constant and cyclic loads in combination with environmental influences like climate, radiation and oxidation. Moreover, adhesive is already present in the body in white of cars and they have to resist the anticorrosion coatings and the painting process, such as washing and bathing in tanks for the cataphoretic coating. In aircraft and spacecraft structures, bonded joints are exposed to extreme thermomechanical loads either cyclically or over long periods of time. Spacecraft structures work more than 15 years in orbital phase [13] while aircraft structures last about 30 years in service [14] and performing real-life representative tests through short term tests becomes a challenge. The combination of extreme high and low temperatures and humidity develop residual stresses in dissimilar materials such as titanium-composite structures typical in aerospace. In the limit case, residual stresses can cause bonded joints to self-destruct, specially when components are thick. Structures exposed to marine environment, e.g. offshore wind turbines, undergo extremely varied load and environmental conditions as a result of the immersion at a constant depth (hydrostatic pressure), waves and currents (cyclic loads), and wind gusts, wave slams or water hammer in pipework (dynamic loads) [15]. In marine environment, the effect of salinity, water acidity, exposure to sunlight and biological fouling must be considered

in addition to temperature and humidity.

The most appropriate adhesive must be selected depending load and exposure conditions in structures. If adhesives are classified into two large families, rigid and flexible adhesives can be defined. In general, rigid adhesives have Young modulus greater than 1 GPa and show small deformations until the break. However, flexible adhesives are characterised by low Young modulus and large deformations before the break, sometimes presenting even an incompressible behaviour. While many alternatives can be found in the market, rigid epoxies are the most used due to the good mechanical properties. Acrylics also provide high rigidity but most of these adhesives are too brittle and are not appropriate against dynamic loads (i.e. fatigue, impact and vibrations). Flexible adhesives such as polyurethanes or silicones have less strength but provide better properties against dynamic loads due to their higher resistance to fracture. Further, silicones are used for their stability at high temperature and good behaviour to harsh environment. Thus, many of the durability problems exposed in transport, energy or space sectors may be solved using new adhesive types instead of the classical epoxies [16].

In any case, the mechanical performance of bonded joints is evaluated through experimental procedures and multiple studies have analysed the fracture behaviour of rigid bonded joints [17–21] considering either mechanical loads [22–27], environmental factors [28–30] or their combination [31–38]. In contrast, only few studies have analysed the mechanical performance of flexible bonded joints and the suitability of experimental procedures to evaluate their fracture behaviour [39–41], where environmental conditions are hardly considered. In addition, standardised experimental methods [42, 43] show limitations to characterise the fracture properties of bonded joints considering load and environmental conditions. Thus, new approaches are needed to understand the fracture behaviour of flexible bonded joints and to get representative test methods to characterise the behaviour of flexible bonded joints in service conditions.

1.2 Assessment of the quality of bonded joints

The quality of a bonded joint is defined by its mechanical capacity to withstand external loads and service environment. The evaluation of the mechanical performance of a bonded joint is a complex process. However, it is often based on a simplified description of its geometry and on the simple mechanical properties of the bonding interface such as its fracture strength and toughness. The opening mode, i.e. mode I, is the most severe fracture mode to quantify the quality of a bonded joint and it is determined by the critical energy release rate (critical ERR, G_{IC}). It defines the capacity of a material to sustain mechanical loadings in the presence of flaws and it is evaluated using

different experimental procedures, evidencing a strong dependence on specimen dimensions, type of adhesive, environmental conditions, external loads and the time of exposure. These effects have a primary relevance in bonded joints with flexible adhesives specially when large structural components are designed, and they will be analysed in the following subsections.

1.2.1 Adhesive interface and the fracture of bonded joints

The stress and strain distribution along the interface is known to be highly dependent on geometrical parameters such as the thickness (t_a) and width (B) of the adhesive layer. In consequence, the fracture toughness exhibits a strong dependence on the bondline geometry.

The bondline–thickness dependence could be attributed to the confinement of the plastically deformed area near the crack tip [17]. In fact, the extension of the plastic zone along the bondline is constrained by the adherends and its size influences the fracture toughness of the bonded joint. Moreover, the parametric study carried out in [18] shows that the total bond toughness not only depends on the bondline thickness but is also significantly affected by the adherend's stiffness. Thus, the plastic zone size may also derive from the adhesive–adherend thickness configuration.

For a given bondline thickness, the measured critical ERR varies with the width of the bonded joint. Indeed, the stress state near the crack tip varies from plane stress in a very thin specimen to plane strain near the centre of a wide plate. Consequently, the degree of plasticity that develops at the crack tip also varies [19]. For wide specimens, the plane stress to plane strain zone transition remains small enough in comparison with the total width of the adhesive layer so that it has little influence on the overall performance of the specimen.

However, the vast majority of previous works are based on studies with rigid bonded joints and experimental research is lacking for flexible bonded joints. In relation to flexible adhesives, the influence of the stress distribution along the specimen width on the fracture behaviour of a bonded joint has been analysed in double cantilever beam (DCB) specimens [39, 40]. As a result, a relation is obtained between the equivalent fracture energy of the bonded joint ($J^{(eq)}$) and the fracture energy measured for a specific zone in the adhesive layer that is purely under the plane stress state, i.e. the external face of the bonded joint (J^{ext}):

$$J^{(eq)} = \xi^{(eq)}_{(B/t_a)} J^{ext} \tag{1.1}$$

The correction factor $\xi^{(eq)}_{(B/t_a)}$ depends on B, t_a and the adhesive's Poisson's ratio (ν_a), and reads:

$$\xi^{(eq)}_{(B/t_a)} = 1 - \frac{\nu_a^2}{(1-\nu_a)} + \frac{6\nu_a^3}{(1-\nu_a)} \frac{\left[1 - e^{-(1/6\nu_a)(B/t_a)}\right]}{B/t_a} \tag{1.2}$$

In addition, in [39] the relation B/t_a is used to identify the stress state of an adhesive layer. Although the stress distribution in an adhesive layer is fully influenced by the Poisson's ratio, the B/t_a ratio may define the equivalent stress state of the adhesive layer in a bonded joint. Low values for the B/t_a ratio may indicate a plane-stress-prevailing stress state and large values of B/t_a may indicate a plane-strain-dominated stress state.

The simple approach in Equation 1.1 is experimentally and numerically validated in [40] as a way to describe the stress state and its effect on the fracture toughness in a specific bonded joint. However, experimental work is lacking not only on a more general validation but also to understand the mechanisms explaining the dependence of the fracture energy on specimen dimensions. Such a study may promote an efficient application of adhesives in large bonded structures.

1.2.2 Standard methods for mode I fracture characterisation

ISO-25217 test standard [42] is the most widespread standardized method to measure the mode I fracture toughness in structural adhesives. DCB specimens are used as test samples due to their simplicity and crack length measurement (a) is required to determine the fracture toughness (Figure 1.1).

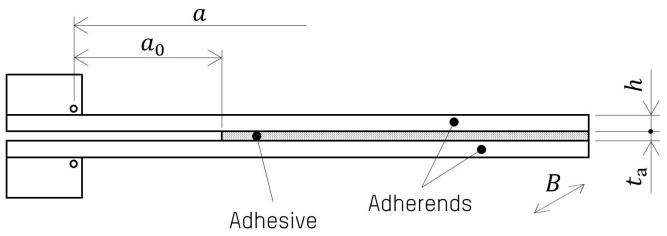

Fig. 1.1: DCB specimen with load blocks.

Data reduction methods such as the corrected beam theory (CBT) correct the crack length a to compensate the rotation of specimen arms near the crack front produced by the flexibility of the specimen [44]. The corrected crack length (a_c) reads:

$$a_c = a + \mid \Delta \mid \tag{1.3}$$

For the correction, the crack length correction factor (Δ) is needed, and it is obtained by plotting the cube root of the compliance $y = C^{(1/3)}$, as a

function of crack length a. Then, a linear fit is extrapolated through the data in the plot $y - a$ to yield Δ as the $x-$intercept of the function $y = 0$.

Based on linear elastic fracture mechanics (LEFM) considerations, the equation to evaluate the fracture toughness reads:

$$G_{IC} = \frac{3P\delta_y}{2Ba_c} \tag{1.4}$$

where P is the applied opening load and δ_y is the opening displacement.

For durability analyses, the most widely used test standard is the Wedge Test (WT) following ASTM D3762 [43] standard. The test method is used to make a qualitative evaluation of the environmental durability of bonded joints with metal adherends and it consists of stressing a bonded joint by inserting a wedge into the bonded path (Figure 1.2). Then, the specimen is exposed to an aggressive environment and, when propagation finishes, the crack length is measured since it is related to the toughness of the joint [27,33, 34]. Crack lengths of different bonded joints may be compared to evaluate the performance of each joint, but additional data reduction methods are needed to get the value of the fracture toughness of the bonded joint.

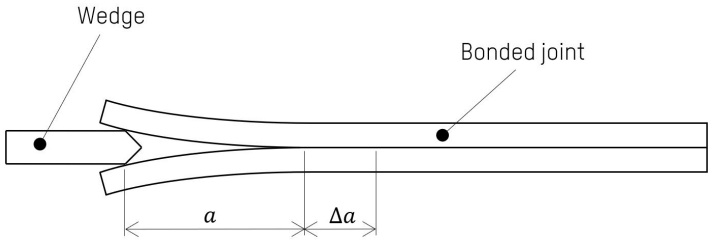

Fig. 1.2: Wedge Test (WT) method and crack growth after environmental exposure (Δa).

In [45], a simplified formulation is proposed to calculate the fracture toughness of bonded joints with a negligible bondline thickness. Later, the elasticity of the adhesive is included to this formulation [46], which reads:

$$G_{IC} = \frac{\delta_y^2 E_1 \left(h + \frac{t_a}{2}\right)^3 \left(1 - \frac{t_a}{2h+t_a}\right)^3 \left(a + \beta\right)^2}{48\left(\frac{a^3}{3} + a^2\beta + a\beta^2\right)^2} \tag{1.5}$$

where E_i is the elastic modulus of the adherend in direction i and h is the adherend thickness. In this case, δ_y is equal to the wedge thickness. β is expressed as follows:

$$\beta = 0.667\left(h + \frac{t_a}{2}\right)\left\{\left(1 - \frac{t_a}{2h + t_a}\right)^3\left[1 + \frac{t_a}{2h + t_a}\left(\frac{2E_1}{E_a} - 1\right)\right]\right\}^{-4} \quad (1.6)$$

where E_a is the elastic modulus of the adhesive.

However, it is difficult to obtain an accurate visual determination of the crack length in bonded joints due to large fracture process zones (FPZs) or barely visible crack propagations. For instance, in [39], large FPZs are developed ahead of the crack tip as a consequence of the elasto-plastic behaviour of the adhesive. In flexible bonded joints, the FPZ may extend several decades of millimetres [41] in the interior of the adhesive layer while small errors in the measurement of the crack length result in large errors of the fracture toughness [47]. Further, bonded joints in real structures are often hidden and it is not possible to measure the crack length visually. To compensate, alternative methods such as structural health monitoring (SHM) can be used for crack growth monitoring and numerous techniques with different degrees of precision and success exist.

1.2.3 SHM for crack length measurement

For SHM purposes, non-destructive techniques (NDTs) are of great interest for industry due to their capacity to examine materials and structural components without changing or destroying their usefulness. NDTs comprise different crack length monitoring techniques [48], such as strain measurement, ultrasonics and acoustic emissions (AE). They can be classified in three different groups: non-contacting techniques, embedded sensors and backface techniques.

Non-contacting techniques such as high-speed photography help during image processing to reduce subjectivity in the visual measurement of the crack length, even when monitoring high crack growth rates [49]. Alternatively, [50] demonstrates how digital image correlation (DIC) software can be used to analyse displacements in successive images recorded during fracture tests. This allows to identify continuously the location of the zero-vertical displacement in adherends, assuming that the crack tip is located at this point because the DIC signal is lost on the edges of the adherends. Despite the increased accuracy afforded by this technique, crack length measurement is still subjective because the location of the crack tip is determined observing the outer edge of the bonded joint, rather than along the entire width. Further, differentiation between elastic deformation and breakage is not evident. Advanced thermographic methods are also used to monitor the crack growth by analysing external surfaces [51, 52]. Scanning is not required and the access to measure is just from one side of the specimen. However, despite its

accuracy even in cases when cracking is not visible [51], thermography only works when the rise of temperature around the crack tip is high enough and, thus, when damage is in an advanced stage [52].

Sensors can be also embedded in bonded joints, inserted in the adherends when composite laminates are used [53,54], in the adhesive layer [55] or in the interface between the adherend and the adhesive [56]. The most commonly used sensor is the Fiber Bragg Grating (FBG), which provides strain distribution measurements along the bonded joint. The crack tip and FPZ are located by interpreting the variations in the longitudinal strain distribution. As a further step, in [57] a sensor-free SHM is observed to form a built-in sensing network with graphene nanoparticles diffused in fibre-reinforced polymers. Using this network, guided ultrasonic waves are transmitted at any site of the composite component, and there is no need to attach any conventional ultrasonic transducer. However, embedding sensors increases the complexity of composite and adhesive manufacturing, and monitoring strategy must be foreseen before the manufacturing process.

An alternative is the use of the backface techniques which consist of attaching sensors to the outer surface of adherends so as to monitor the behaviour of the bonded joint during testing. Different techniques with different levels of sophistication are available to characterise the crack length of a bonded joint. For example, in [34], a simple micrometre is used to find the zero-vertical displacement of the adherends and it is assumed that the crack tip is located at this point. Alternatively, in [58] strain gauges are bonded along the central line of a thin adherend to perform an asymmetric test. Longitudinal strains on the thin adherend are measured and strain gauge measurements are interpreted using simple beam theory to estimate the crack length. More sophisticatedly, optical fibres can be bonded to the outer face of the adherend to yield a higher spatial resolution using such technologies as an optical backscatter reflectometer (OBR) [59,60]. The ability to characterise crack length in bonded joints tested in static [59] and fatigue [60] conditions makes the optic fibre a versatile technology. However, these technologies use fungible components and provide only external information of the bonded joint.

In ultrasonic analysis, which is an advanced backface technique, ultrasonic waves are transmitted into materials to detect internal flaws or for characterisation purposes. Ultrasonic devices are widely used for the local inspection of aerospace structures composed of multi-layer, adhesively bonded metallic and composite components that are difficult to access. In multi-layer metallic components, wave propagation [61] and the localization of hidden defects such as fatigue cracks and localized disbonds [62] are analysed using high-frequency guided ultrasounds. In [63], defect sizes created in multi-layer composite bonded structures are evaluated. Nevertheless, continuous information about the evolution of components condition is lacking

when using ultrasonic technology.

Acoustic emissions (AE) testing provides continuous real-time information about the integrity of structures. Some literature exists about detecting, locating and identifying damage events to predict failure in early stages—such as [64]'s reference to timber structures. These damage events may be produced by deformations, crack formation, corrosion or defects, and AE can be deployed within a wide range of applications such as fabrication processes, pressure equipment, aerial structures, aerospace structures, bonded joints and composite structures. Regarding composite structures, different types of damage mechanisms such as fibre breakage, core failure, matrix cracking or debonding are studied using AE techniques in delamination of sandwich structures [65] and woven composites [66]. Moreover, in [67], the delamination damage evolution is monitored using AE in unidirectional carbon fibre reinforced polymer (CFRP) specimens and acoustic activity is analysed to identify the delamination onset and crack propagation. The fracture process of concrete and masonry structures is also analysed with AE testing [68–70]. In [68], the spatial distribution of damage is characterised using AE signals emerging from the growing of cracks in a concrete specimen. Further, the crack propagation is localized using AE in a repaired multiple leaf stone masonry [69] and in an FRP-concrete beam [70], proving the effectiveness of the AE technique in bi-material structural components. Regarding bonded structures, [20] shows how AE events are produced following the pencil lead break (PLB) test procedure. For this purpose, wave propagation on a present adhesive layer is analysed in bonded large aluminium sheets at different distances and source orientations. The study provides guidance for locating and identifying AE events occurring within adhesive joints, but neither fracture tests nor adhesive cracking are examined. In [21], a modal AE analysis of mode I and mode II fractures is carried out. AE source events are analysed, and location and identification guidance is provided. A correlation between AE source location and the visually observed crack front is suggested. However, experimental evidence is lacking for any rigorous conclusions, specially since the presence of an FPZ ahead of the crack tip also denotes damage [41].

These studies exemplify the lack of experimental data on techniques such as AE that do not use fungible sensors to detect, locate and identify cracks when obtaining the fracture properties of bonded joints with metallic adherends.

1.2.4 Alternative methods to evaluate the fracture toughness

Alternatively, crack length independent data reduction methods that are primarily for laboratory purposes are also available in the literature. For instance, the compliance-based beam method (CBBM) avoids measuring the crack length during the test and an equivalent crack length (a_e) is evaluated

instead [22]:

$$G_{IC} = \frac{6P^2}{B^2 h}\left(\frac{2a_e^2}{h^2 E_f} + \frac{1}{5G_{13}}\right) \tag{1.7}$$

where E_f is the corrected flexural modulus and G_{13} is the out-of-plane shear modulus of the adherend. Although crack length tracking is avoided, additional experimental tests are required to determine adherend elastic properties. Moreover, the flexural modulus is obtained through an iterative procedure in which the initial compliance of the bonded joint should be used to obtain a converged value. Thus, following CBBM becomes laborious when specimens with different materials and geometries are tested.

The J-integral method is another alternative to characterise the fracture toughness of bonded joints, which is based on non-linear fracture mechanic (NLFM) considerations [23]. In this case, crack length measurement is avoided since the relative rotation between the adherends is measured, e.g. with inclinometers (Figure 1.3) [24,41]:

$$G_I = J_I = \frac{P}{B}\theta \tag{1.8}$$

where θ is the relative rotation between adherends at the position where the load is applied with respect to the bondline of the DCB specimen.

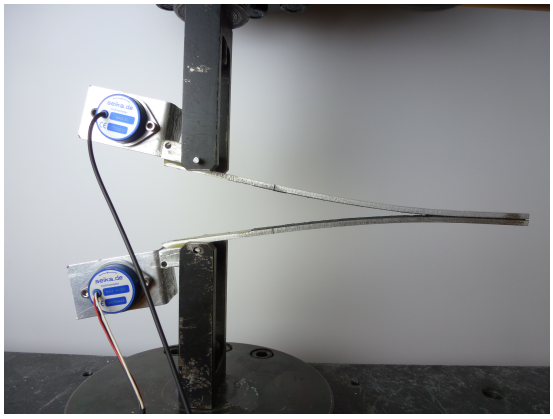

Fig. 1.3: DCB test in progress, with inclinometers.

In [71], a different test procedure based on the WT is proposed. The Wedge Driven Delamination (WDD) method is designed to characterise the interlaminar mode I fracture toughness of unidirectional carbon fibre composites. In the WDD testing design, the sample is forced upon a stationary low-friction wedge and, unlike in DCB tests, the crack front position relative to the contact point between the wedge and adherends remains constant on

average during the crack propagation (Figure 1.4). A steady crack growth is obtained and the data reduction method is simplified to $G_{IC} = F_{push}/B$, being F_{push} the longitudinal load needed to move the wedge forward. Then, crack length measurement is avoided but the data reduction method ignores the bondline thickness.

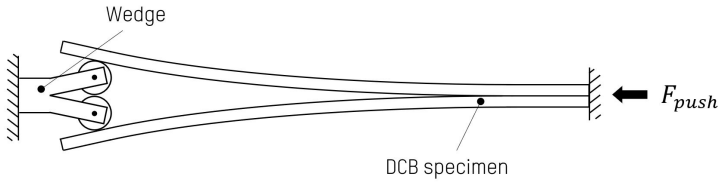

Fig. 1.4: WDD method with frictionless rollers in substitution of a wedge.

In [25], an analytical expression is developed to consider the equivalent coefficient of friction (COF) between wedge and adherends in wedge-driven tests. A forced driven wedge is simulated for the separation of a thin adherend bonded to an infinitively rigid adherend. Simulations are not validated by own experimental work and some experimental data are taken from the literature for comparison. In [26], the Wedge Driven Test (WDT) is proposed as an alternative method to evaluate the fracture strength of composite structures bonded with thin adhesive layers. Unlike WDD, this method takes into account the friction between wedge and adherends and the wedge design is much simpler. However, in order to avoid crack length measurement to determine the fracture toughness, the equivalent COF must be deduced by fitting experimental data to analytical expressions based on the simple beam theory. The ERR is calculated as follows:

$$G_I = \frac{F_{push}}{B}\frac{3r_w}{2a_c}\frac{\left(1+\mu\frac{3r_w}{2a_c}\right)}{\left(\mu+\frac{3r_w}{2a_c}\right)} \tag{1.9}$$

where μ is the COF between the wedge and adherends and r_w is the radius of the curvature in the wedge tip. For this application, a_c can be obtained by solving the roots of the following polynomial function:

$$(4F_{push})\cdot a_c^4 - (6r_w\mu F_{push})\cdot a_c^3 - (2E_1Bh^3r_w\mu)\cdot a_c - 3E_1Bh^3r_w^2 = 0 \tag{1.10}$$

Finally, an advanced WDT method named Smart Wedge (SW) test is presented in [31]. It proposes a new test rig to get experimental results out of a universal testing machine (Figure 1.5). During the insertion of the wedge, the vertical opening load is monitored using load transductors and, appar-

ently, the crack length measurement is avoided. The expression to evaluate the fracture toughness reads:

$$G_{IC} = \left[\frac{9P^4\delta_y^2}{4B^3(E_f I)}\right]^{1/3} \tag{1.11}$$

where E_f is the flexural modulus of adherends and I is the moment of inertia.

However, the flexural stiffness ($E_f I$) must be obtained using a post-tested wedge specimen under DCB type loading and, at this point, the crack length has to be measured, following:

$$E_f I = \frac{2a^3}{3}\left(\frac{\Delta P}{\Delta \delta_y}\right) \tag{1.12}$$

Thus, although the Equation 1.11 only depends on the opening load, the crack length measurement is inherent to the data reduction method.

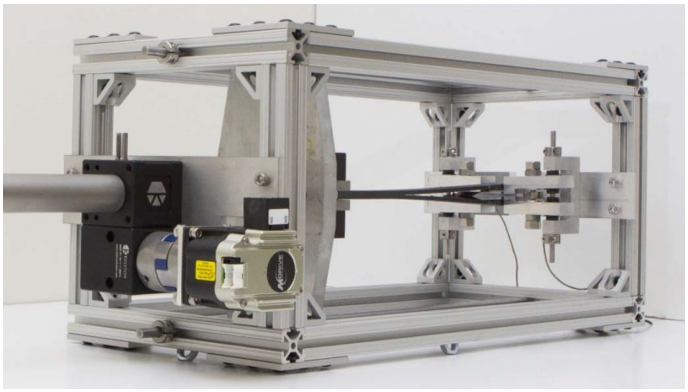

Fig. 1.5: Smart Wedge (SW) test rig [31].

All in all, the aforementioned experimental methods provide different useful solutions. The primary limitation of DCB tests is that neither the load nor the crack growth rate are constant during crack propagation. In contrast, wedge-type tests are steady and once fracture initiates the load required to move the wedge forward and the crack length remain constant. Although the aim of wedge-type tests is to provide simple, objective and fast test procedures, they are still subject of study. As there is a contact between the wedge and the specimen, making data reduction methods that avoid crack length measurement or friction coefficient estimation is yet to be assessed.

1.2.5 Assessment of the durability of bonded joints

Bonded joints in real applications are exposed to service environment and adhesive strength may be affected by many common environments such as

temperature, moisture or outdoor weathering. The combination of external loads with service environment may cause an adhesive bond to degrade at a faster rate and thus, to fail in early stages [29,72]. This is of particular concern in primary structures, e.g. in aircraft structures [14,16], in which the coupled effect of environmental ageing and mechanical loads on bonded joints must be considered [73].

In applications where bonded joints are not subjected to high loads for prolonged periods, as in non-stressed bonded joints, only the effect of environmental degradation is typically evaluated on elements. Then, adhesive bonds are exposed either to simulated service conditions or to accelerated ageing [28], following ASTM D1151-00(2013) [74] for constant conditions and ASTM D1183-03(2019) [75] for cyclic conditions. After completion of exposure, adhesive bonds are tested to evaluate their fracture resistance e.g. following DCB tests. However, an accurate visual determination of crack length may be difficult since large FPZs are expected in degraded bonded joints. Thus, advanced SHM techniques or crack length independent data reduction procedures may be used to ensure the correct characterisation of bonded joints.

Specific test setups that control the environment and monitor changes in bonded joint performance are required to assess the service lifetime of bonded joints exposed to external loads, i.e. stressed bonded joints. Qualitative results are obtained when using the WT method [43], which may not be objective enough when rigorous studies are required. Expressions in [45,46] allow to get a quantitative value of the fracture toughness, but both depend on the crack length measurement. In accordance with [27], even with sophisticated equations, the subjectivity of the crack length makes this a questionable method of determining the fracture toughness. Moreover, the WT method is a stress-relaxation test and creep tests are more representative of the load state of bonded joints. In [35,36], a state-of-the-art study on the use of the ASTM D3762 standard test method to assess the durability of metal bonded joints for aeronautical applications is carried out. The effect of several parameters such as surface preparation and bondline thickness on the crack propagation are studied in rigid bonded joints during the exposure period. Further, in [37], the previous study is continued with composite bonded joints and the effect of adherend thickness, i.e. flexural stiffness, on the crack propagation and the fracture toughness calculation is evaluated. Despite the extensive study, low modulus adhesives or bonded joints having thick bondline thicknesses are out of the scope of the analysis. Thus, the applicability of the WT in flexible bonded joints for durability studies is yet to be assessed.

In general, few works other than [27] have discussed the suitability of different test methods for assessing the durability of bonded joints. While the authors of this study concluded that both the DCB test and the WT are valid for assesing the durability of rigid bonded joints, the results obtained

through these methods are not comparable. In [38], the effect of different environmental exposures on the crack growth is investigated, following DCB tests and WT tests. Although the crack path or failure modes are analysed, the evaluation of the fracture toughness is out of the discussion. To compensate the lack of consensus on methodologies and the recent withdrawal with no replacement of ASTM D3762, new experimental procedures are needed to evaluate the durability of bonded joints. The WDT [26], the SW [31] or the dual-actuator test rig in [32] (Figure 1.6) are examples of this.

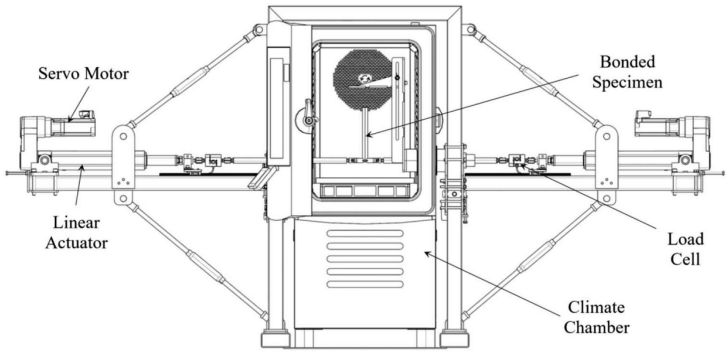

Fig. 1.6: Scheme of the dual actuator test rig with a DCB specimen [32].

The WDT [26] avoids crack length measurement and the load needed to insert the wedge must be tracked to evaluate the fracture toughness of degraded bonded joints. However, the influence of the environmental exposure may difficult the deduction of the friction factor, having different COFs depending on the time of exposure and the specimen. Thus, the application of this test procedure for durability studies is dubious. The SW [31] proposes a new test rig to expose specimens to environmental conditions while the inserted wedge is halted inside of the bonded path, essentially as the Wedge Test. The test rig does not depend on the tensile testing machine and it can be inserted in a climate chamber. While the test procedure is similar to the WT, the main advantage of the SW test is that the fracture toughness is continuously evaluated by tracking the opening load and avoiding crack length measurement. Although material resources are reduced, the flexural stiffness of the bonded joint may continuously change with exposure, specially when non-metallic adherends are used [76,77]. Thus, the determination of the fracture toughness would not be precise, reinforcing the crack length dependency of the data reduction method.

Alternatively, the dual-actuator test rig proposed in [32] enables mechanical testing in an ageing environment (Figure 1.6). Static and dynamic tests in mode I, mode II and mixed-mode failure modes can be performed in DCB

specimens. Further, while the test rig allows the application of standard test procedures such as the ISO-25217 to evaluate the fracture toughness of bonded joints, wedge test-based methods cannot be applied. However, the test rig is coupled to a climate chamber and the set-up is large having an overall length of 4 m, a width of 1.8 m and a height of 2 m (Figure 1.6). Moreover, standard procedures depend on the crack length to evaluate the fracture toughness. Although the test procedure suggests using DIC technology to monitor the crack growth, it must be made from the outside through the window of the environmental chamber. Thus, the location of the crack tip is even more subjective.

1.3 Criticism of the state-of-the-art

Concerning flexible bonded joints, studies in [39, 40] analyse the influence of the stress distribution along the width of the specimen on the fracture behaviour of DCB bonded joints and the approach in Equation 1.1 is proposed to describe the stress state and its effect on the fracture toughness in a specific bonded joint. However, there is a lack of experimental work to understand the mechanisms explaining the dependency of the fracture toughness on specimen dimensions. A general validation of the Equation 1.1 may relate the fracture toughness of flexible bonded joints with different configurations, promoting their application in large bonded structures usual in industrial applications.

While standard methods such as ISO-25217 and ASTM D3762 depend on the visual measurement of the crack length, they are specific for rigid and thin bonded joints. Thick bondline thicknesses or flexible adhesives [39, 41] develop larger FPZs ahead of the crack tip and large errors in the evaluation of the fracture toughness are produced due to the small errors in the crack length measurement [47]. Then, an accurate visual determination of the crack length is often difficult to obtain and alternative methods such as SHM or crack length independent procedures are applied to reduce subjectivity. AE technique is of great interest for industry and avoids using fungible sensors to detect, locate and identify cracks in bonded joints. However, studies show the lack of experimental work in bonded structures for AE source location [21, 41], specially when dealing with flexible bonded joints. While wedge-type tests [26, 31] are promising, they are still subject of study because they implicitly depend on the measurement of the crack length. Moreover, they are specific for rigid or thin bonded joints, and flexible adhesives as well as thick adhesive layers are excluded from the experimental validation.

Durability analyses also are focused on rigid bonded joints with thin adhesive layers [35–37]. Few works such as [27, 38] discuss about the suitability of test methods to evaluate the durability of bonded joints. Then, the applica-

bility of the DCB test or the WT to test specimens with flexible adhesives or thick adhesive layers is yet to be assessed. DCB tests do not allow the control of load conditions during crack propagation while wedge-type tests require crack length measurement. Moreover, the new test rigs and experimental procedures such as the WDT [26], the SW [31] or the dual-actuator test rig in [32] are specific for rigid bonded joints with thin adhesive layers and do not solve the limitations in load control or crack length measurement. Thus, experimental work is lacking to understand the fracture behaviour of flexible bonded joints in service conditions, increasing the scope of experimental procedures to bonded joints with flexible adhesives or thick adhesive layers.

1.4 Objectives

The scope of the present Thesis is to develop new experimental methods for the evaluation of the strength and toughness of joints bonded with flexible adhesives and large bondline thicknesses. Following the general scope, some specific objectives are contemplated:

- To prove the influence of the stress state on the mode I fracture toughness of thick and flexible bonded joints, considering the elastic deformation of the adhesive layer.
- To assess the application of acoustic emissions (AE) for crack location to avoid subjectivity in crack length measurements.
- To demonstrate the limitations of current experimental methods to evaluate the fracture toughness of degraded bonded joints for durability studies.
- To develop a new experimental method to evaluate the durability of flexible bonded joints, considering environmental conditions and sustained loads.

1.5 Structure of the document

The document describes the work developed in the thesis and it is structured as follows.

Chapter 2 describes the methodology followed during the thesis to overcome the technical challenges detected in the revision of the state of the art. Analytical, experimental and numerical methods are described making continuous references to the elaborated papers in the Appendix, as recommended for theses by compendium of peer-reviewed journal papers. These documents contain the specific methodologies and procedures followed for

each contribution and describe extensively the experimental campaigns and analytical developments.

Chapter 3 discusses the results obtained in the experimental campaigns and the analytical models. Then, the suitability of the proposed methods is evaluated by fracture mechanics concepts, experimental observation or numerical modelling. Papers in the Appendix are continuously referenced and contributions are identified, emphasising on the improvements introduced in comparison with the existing methods. Finally, Chapter 4 determines the scope of each contribution and possible future works are outlined to address the new challenges that arise from the current thesis.

Regarding the papers in the Appendix, the methodology presented in the paper "Effect of the width-to-thickness ratio on the mode I fracture toughness of flexible bonded joints" given in Appendix A is summarised in Section 2.1, while results and discussion are provided in Section 3.1. The methodology developed in the paper "Using acoustic emissions (AE) to monitor mode I crack growth in bonded joints" given in Appendix B is summarised in Section 2.2 and results and discussion are provided in Section 3.2. Subsection 2.3.1 summarises the methodology of the paper "Durability study of flexible bonded joints: the effect of sustained loads in mode I fracture tests" given in Appendix C. Results and discussion are provided in Section 3.3. The methodology presented in the paper "Mode I fracture characterisation of rigid and flexible bonded joints using an advanced Wedge-Driven Test" given in Appendix D is summarised in Subsection 2.3.2, while results and discussion are presented in Section 3.4.

Chapter 2

Methodology

New methods are proposed as alternatives to the limitations detected in the revision of the state of the art. Developed experimental methods are focused on mode I fracture characterisation of structural joints bonded with flexible adhesives and large bondline thicknesses. The different contributions in the form of analytical and experimental procedures are described in the following subsections.

2.1 Influence of the stress state on the fracture

2.1.1 The width-to-thickness ratio

Strength and toughness of bonded joints are determined using standard procedures and they evidence a strong dependence on specimen dimensions. While the width (B) and thickness (t_a) of the adhesive layer govern the stress distribution in the adhesive interface, the width-to-thickness ratio (B/t_a) determines the equivalent stress state of a bonded joint. Then, it can be used to relate the fracture toughness of bonded joints with different B/t_a configurations.

Equations 1.1 and 1.2 were used to find such a relationship. As these equations describe the stress distribution in the adhesive layer of a bonded joint and its effect on the equivalent fracture toughness [40], they were useful to relate the fracture toughness of bonded joints with different stress states. In addition, large deformations of the adhesive layer were observed in flexible bonded joints (Figure 2.1) and the fracture behaviour of the adhesive layer was analysed.

In this work, the fracture behaviour of a nearly incompressible flexible adhesive was studied. The silicone-based adhesive Sikasil SG-500 was used

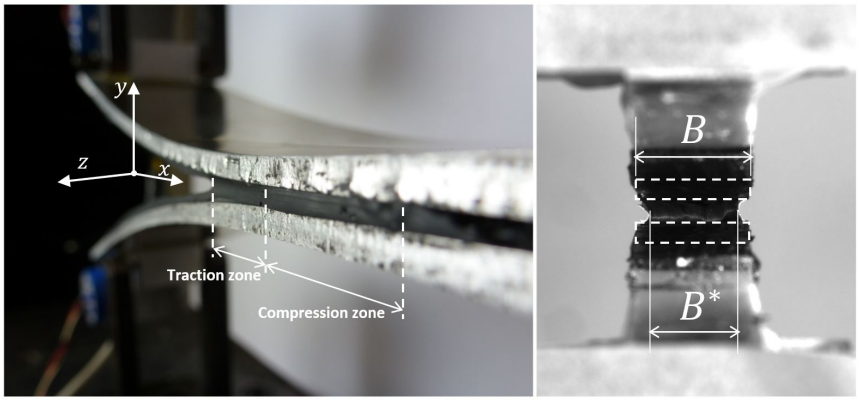

a) b)

Fig. 2.1: Out-of-plane deformation of the adhesive layer in a) the traction and compression zones, and b) along the width of the specimen, where B is the total width of the adhesive layer and B^* is the effective width before fracture occurs.

for this study. First, the elastic properties of the adhesive such as Young's modulus and Poisson's ratio were characterised. Then, DCB specimens with the same materials but with different widths and bondline thicknesses were manufactured. Specimens were divided in two batches depending on the bondline thickness (0.5 mm and 2.0 mm) and tested following the procedures described in the Appendix A. The J-integral data reduction method was used to evaluate the fracture toughness of bonded joints and the effect of the width-to-thickness ratio on the equivalent fracture toughness of flexible bonded joints was analysed. In agreement with previous experimental studies about the fracture behaviour of tough bonded joints, it was observed a pronounced lateral contraction of the adhesive layer. It was produced by shear deformations on the adhesive layer and the effective width of the adhesive layer was shortened near the crack tip, affecting on the fracture behaviour of the bonded joint (Figure 2.1).

An analytical relation between the lateral contraction, i.e. stretch ratio (B^*/B), and the stress state was developed to improve the analytical expression in Equation 1.1 to predict the fracture toughness of flexible bonded joints.

2.1.2 Analytical model to consider the bondline geometry

An analytical model based on the relation in [40] has been developed in order to gain a deeper understanding of the mechanisms explaining the dependence of the fracture toughness on specimen dimensions. Focusing on flexible bonded joints, the elastic deformation of the adhesive layer has been

studied using the constitutive equations for an isotropic linear elastic material. The stretch ratio B^*/B has been defined to describe the lateral contraction of the adhesive layer, showing that the effective width of the adhesive layer is reduced during loading. This reduction affects the fracture behaviour of bonded joints, especially when dealing with flexible bonded joints. Thus, the effect of the lateral contraction of the adhesive layer on the fracture toughness has been evaluated in flexible bonded joints.

Broadening the relation in Equation 1.1 to relate the equivalent fracture toughness of bonded joints to different width-to-thickness configurations, the expression results in:

$$J^{(eq)}_{B/t_a} = \frac{\xi^{(eq)}_{(B/t_a)}}{\xi^{(eq)}_{(B/t_a\to\infty)}} J^{(eq)}_{PE} \tag{2.1}$$

where $J^{(eq)}_{PE}$ is defined as the fracture toughness of a bonded joint under plane-strain-prevailing stress state ($B/t_a \to \infty$) and $\xi^{(eq)}_{(B/t_a\to\infty)}$ refers to the Equation 1.2 in the limit case. The ratio $\xi^{(eq)}_{(B/t_a)}/\xi^{(eq)}_{(B/t_a\to\infty)}$ defines a relationship between the equivalent stresses of a bonded joint with any B/t_a ratio and a bonded joint under plane-strain conditions ($B/t_a \to \infty$). Then, $J^{(eq)}_{B/t_a}$ might be the equivalent fracture energy for any B/t_a-configured bonded joint. The equivalent fracture toughness of a bonded joint under plane-strain conditions, $J^{(eq)}_{PE}$, is measurable by testing a large B/t_a-configured bonded joint.

Due to the almost incompressible nature of elastomeric flexible adhesives ($\nu_a \approx 0.5$), very pronounced lateral contractions were observed along the specimen sides near the crack tip (Figure 2.1). As a consequence, the effective width of the bonded joint was shortened. To consider this effect, the geometrical relation $B^*(x)/t_a$ defined in [39] is written as a function of the $B^*(x)/B$ ratio. This allows the evaluation of an effective width $B^*(x)$ as a function of the adhesive bondline thickness (t_a) and adhesive Poisson's ratio (ν_a). The longitudinal location of the crack tip (x) is shown in Figure 2.2, which may also vary depending on the deformation of the adhesive layer. The effective width $B^*(x)$ is the real width in the midsection of the adhesive layer just before fracture occurs, which differs with the total width of the specimen B due to the lateral contractions in the adhesive layer (Figure 2.1). The $B^*(x)/B$ ratio may be expressed as:

$$\frac{B^*(x)}{B} = 1 - \frac{t_a}{B} \ln\left[\left(\frac{1-\nu_a-\nu_a^2+\psi_x}{(1+\nu_a)(1-2\nu_a)+\psi_x+\psi_{(B/2)}}\right)^{6\nu_a}\right] \tag{2.2}$$

where ψ_x is a correction function that reads:

$$\psi_x = \nu_a^2 e^{\left(\frac{x}{3\nu_a t_a}\right)} \tag{2.3}$$

The correction function $\psi_{(B/2)}$ in Equation 2.2 is obtained by setting $x = B/2$ in Equation 2.3.

The analytical expression in Equation 2.2 depends on the measurable geometrical parameters B and t_a, the material property ν_a, and x. Regarding the latter, shear deformations appear in the adhesive layer when a DCB specimen with a flexible adhesive is subjected to an opening load. Thus, a concave-shaped crack front is produced. The maximum longitudinal deformation due to the shear effect, i.e. Poisson effect, is located in the midplane of the adhesive layer (Δ_c). Although the analytical model considers the bondline thickness, the problem is treated as if the adhesive layer would be a thin laminate in the midsection of the bonded area. Then, it is accepted that the longitudinal location of the crack tip is shifted following the relation $x = \Delta_c$ (Figure 2.2).

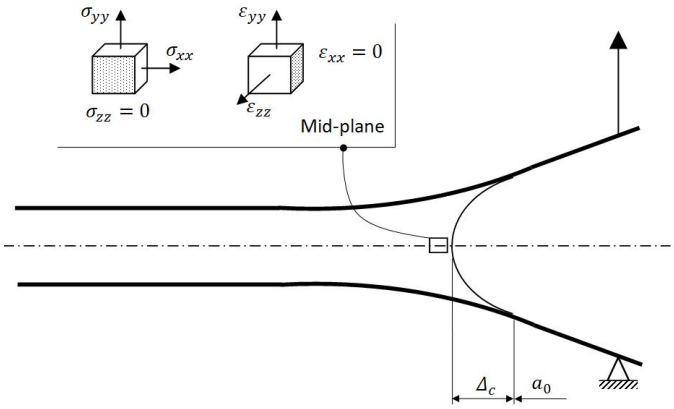

Fig. 2.2: Scheme of the strain and stress fields in the adhesive layer.

With regards to the longitudinal deformation of the crack tip, an energy-based analysis has been performed to evaluate $x = \Delta_c$. When the specimen is loaded, the adhesive layer accumulates elastic potential energy ($\mathbb{U}$) due to strains induced in it. When fracture occurs, the elastic potential energy reaches a maximum in the crack tip. Following the principle of minimum potential energy, the equilibrium condition $d\mathbb{U}/dV = 0$ results in the following equation for Δ_c, which is expressed as a function of the opening displacement (since $\varepsilon_{xy} = \Delta_c/t_a$):

$$\Delta_c = \sqrt{\frac{1}{2(1-\nu_a)}}\delta_y \tag{2.4}$$

Note that the correction function in Equation 2.4 still depends on δ_y and t_a. From experimental evidence (more detailed in Section 3.1), it is observed that for a given flexible adhesive, the $B^*(\Delta_c)/B$ ratio only depends on the B/t_a ratio. Thus, the effect of the lateral contraction is independent of the thickness of the adhesive layer, so $\delta_y = t_a$ is proposed.

As the fracture energy J_{B/t_a} experimentally evaluable for any B/t_a configured bonded joint depends on B^* and not on B (Figure 2.1b), it can be related to $J_{PE}^{(eq)}$ by considering the $B^*(\Delta_c)/B$ ratio,

$$J_{(B/t_a)} = \frac{B^*(\Delta_c)}{B} J_{(B/t_a)}^{(eq)} = \frac{B^*(\Delta_c)}{B} \frac{\tilde{\varsigma}_{(B/t_a)}^{(eq)}}{1 - \frac{\nu_a^2}{(1-\nu_a)}} J_{PE}^{(eq)} \tag{2.5}$$

Further details of the analytical development can be found in Section 2 of the Appendix A.

2.2 Acoustic emissions to monitor crack growth

2.2.1 Acoustic emissions technique

SHM techniques are commonly used when crack length measurement is required. An accurate visual determination of the location of the crack tip is often a challenge in bonded structures due to large FPZs and difficulties in reaching the bonded path. Similarly, crack fronts in the interior of large structures are not necessarily straight [78] and NDTs are of great interest due to their capacity to examine materials and components without changing or destroying their usefulness. Among non-fungible sensors, AE testing provides continuous real-time information about complete structures and it can be used to detect, locate and identify damage events in bonded structures.

On this way, AE was proposed to monitor the mode I crack growth in bonded joints as a feasible technique to provide information of the crack front position. DCB specimens were manufactured by bonding metallic adherends with rigid and flexible adhesives. While mode I fracture paths were generated following DCB test protocol in ISO-25217, acoustic sensors were coupled to the bonded specimens to process the acoustic events generated during crack growth. An appropriate filtering strategy was selected and location results of acoustic events were compared with the visually tracked crack propagation (a) and the corrected crack length (a_c) following Equation 1.3. Finite element (FE) simulations were carried out to correlate the experimental evidence to the FPZ.

AE monitoring involves measuring the mechanical vibration energy emitted by bonded joints after a sudden change or movement during testing pro-

duced, for example, by cracking or plastic deformation. These acoustic waves propagate from the source throughout the structure in an omni-directional manner with a velocity of dispersion (V in Figure 2.3a). An AE sensor in contact with the material being monitored detects the mechanical shock wave and converts the low-displacement, high-frequency mechanical wave into an electric signal, amplified by a pre-amplifier and processed by the AE instrument [79]. Recorded data can then be used to determine the location of the AE event (d in Figure 2.3a) between two sensors at a known distance (D in Figure 2.3a) by processing the arrival time delay in each sensor (ΔT in Figure 2.3a).

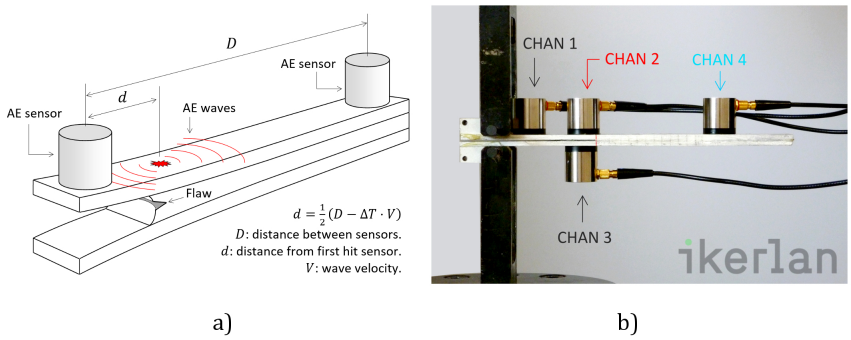

Fig. 2.3: a) Scheme of acoustic emissions (AE) principle, and b) test set-up with fastened AE sensors.

For location purposes, four AE piezoelectric sensors (VS45-H, Vallen Systeme GmbH) were coupled to the adherends with an external 34 dB pre-amplifier (Figure 2.3b). An elastic sticky band was used to produce hold-down pressure on the contact surface between the AE sensors and the aluminium adherends while measurements were being taken. A viscous gel was used to ensure continuity of the AE between the sensors and adherend surface. The AE device used to process the acoustic signal was a 4-channel AE system model (AMSY-6, Vallen Systeme GmbH).

AE sensors were attached to the adherends in a longitudinal direction by measuring the distance from the absolute 'zero', located in the left extreme of the specimen's adherend, to the centre of the sensor with a calliper. Later, the PLB test [80] was applied to check the correct coupling of AE sensors and to evaluate the acoustic attenuation of the structure. In accordance with the reference system, the locations of these events were calculated using the group velocity of dispersion curves given by Vallen Dispersion software. The group velocity was calculated by setting an aluminium sheet with a thickness of 3 mm for both types of adhesive. AE sensors were able to record AE waves in a frequency range from 40 kHz to 450 kHz. Within these frequency

values, the fastest type of Lamb wave was the symmetric wave with a group velocity of 5200 m/s, which was quite stable. One output channel (CHAN) was assigned to each AE sensor (Figure 2.3b): channels 2 and 4 (CHAN2 and CHAN4, respectively) were used for the longitudinal location of the acoustic events; CHAN1 was used to measure location uncertainty (LUCY) by evaluating the time delay between each pair of sensors by triangulation; CHAN3 was assigned as a guard sensor to avoid external noise in measurements, e.g. from test tools. As the minimum sensor quantity for 1D location is two, each pair of sensors estimates a location and the location difference in each acoustic event indicates the LUCY. Furthermore, acoustic events that hit a guard sensor before hitting any normal sensor are rejected. The location module from Vallen VisualAE software was used for the location analysis and, in order to filter out noise, the AE signal peak amplitude threshold (A_{th}) and an admissible LUCY limit were defined following a parametric analysis.

Although A_{th} depends on many parameters such as the sensitivity of sensors or the level of preamplification used, the correct selection of the A_{th} is a relevant point. Thus, the procedure in [81] was followed to set it and DCB specimens were loaded until crack initiation while the peak amplitude of AE events was monitored. In the initial elastic regime, the peak amplitude remained mostly below 60 dB while, when crack propagation started, the peak amplpitude raised above 60 dB. Thus, crack growth was associated to AE events with a peak amplitude $\geq$ 60 dB while AE events $<$ 60 dB were associated to other effects such as adherend or adhesive elastic deformations.

Similarly, the LUCY limit was set through PLB test results. Having 5 to 6 measurements depending on the specimen and 33 in total, 90% of PLB tests denoted a LUCY below 3.0 mm. It was considered an admissible limit to get accurate location results.

2.2.2 Numerical simulations

A 3D numerical model was implemented using FE method and ANSYS software was used to reproduce experimental DCB tests for the two types of adhesive. Adherends and the adhesive were modelled using SOLID185 8-node quadrilateral elements and a row of cohesive interface elements type INTER205 was added at the midplane of the adhesive layer. The cohesive law was assumed to be bilinear and the stiffness was set following the general analytical model described in [41]. It was considered that the adhesive layer started to damage when traction stresses overpassed the ultimate strength determined for each adhesive. Thus, the FPZ was defined as the region where traction forces exceeded the local maximum strength but still the debonding was not completed. The values for the fracture toughness used in numerical models as well as material properties were taken either from the experimental campaign or [41].

Mesh was constructed using the hexahedron meshing algorithms of the software ANSYS and manual resizing. This resulted in an element size of 0.25 mm in the longitudinal and transversal directions, and 0.143 mm in the out-of-plane direction. Simulations were used to analyse the size of the FPZ and to correlate the experimental evidence with the observed fracture process.

For further details the reader may refer to the Appendix B of the document.

2.3 Effect of service conditions on G_{IC}

There is a lack of consensus on methodologies to evaluate the durability of bonded joints simulating service conditions of an specific application. Although ASTM D3762 standard exists, other test standards such as ISO-25217 may be used to evaluate the evolution of the fracture toughness as a function of the degradation when a quantitative analysis is required. To do so, conditioning is applied prior testing and different specimens with different exposure durations are needed to evaluate the evolution of properties. Moreover, the damage induced in the adhesive layer may affect on the evaluation of the fracture toughness when large FPZs are produced because data reduction methods depend on the crack length. The suitability of existing test methods was analysed and a new wedge-type test method was proposed to perform durability tests.

2.3.1 Suitability of existing test methods for durability tests

A test campaign was carried out to assess the suitability of the existing experimental methods for the evaluation of the fracture toughness of bonded joints exposed to service conditions.

DCB-type flexible bonded joints were manufactured. Some specimens were stressed by inserting a wedge into the bonded joint as suggests the WT procedure in ASTM D3762. Then, all specimens were introduced in a climate chamber as described in the Appendix C. Stressed and non-stressed specimens were exposed to specific temperature and humidity conditions simulating service conditions. A 1000-hour exposure at 85% relative humidity and 82°C temperature was used as an accelerated fixed time condition, and the exposure times (t) studied were 0h, 10h, 100h, 300h and 1000h. When any of these exposure times was reached, four specimens in total were removed from the climate chamber, having two stressed and two non-stressed aged specimens. Immediately after, the crack tip was located in stressed bonded joints and the inserted wedge removed. Finally, DCB tests were carried out in stressed and non-stressed specimens and the fracture energy was evaluated

to analyse the influence of ageing on the evaluation of the fracture toughness.

WT and DCB test results were compared and their feasibility for durability studies was evaluated. Difficulties in visual crack length measurement were expected due to the degraded condition of the adhesive. Therefore, different data reduction methods were applied and their applicability to evaluate the fracture toughness of the bonded joints was analysed. While the applied crack length dependent methods were the one in [46] for the WT and the CBT [42] for the DCB tests, methods independent on the crack length were the CBBM [22] and the J-integral method [23]. CBT and WT methods are explained in the Subsection 1.2.2 and the Equations 1.4 and 1.5 were used respectively to evaluate the fracture toughness. CBBM and J-integral methods are described in Subsection 1.2.4 and the fracture energy was evaluated following Equations 1.7 and 1.8, respectively.

Fractured surfaces on the bonded area were photographed after the completion of DCB tests and damaged surfaces of stressed and non-stressed bonded joints were compared. For further details about the test set-up and execution the reader may refer to the Appendix C of the document.

2.3.2 Towards a durability test for bonded joints: development of an advanced wedge driven test

From the durability study it was deduced that the existing wedge-type tests do not allow [43] or are unfeasible [26, 31, 32] to evaluate the evolution of the fracture toughness while bonded joints are exposed to service conditions, specially when flexible adhesives are used. Therefore, an advanced data reduction method that allows to perform durability tests was developed for wedge-type tests. The data reduction method is presented in the current Subsection 2.3.2 while the new test set-up to perform durability tests is explained in Subsection 2.3.3.

Advanced test protocols based on the insertion of a wedge simplify the test procedure in favour of efficiency. However, even the most advanced test methods still evidence a strong dependence on the crack length when the fracture toughness is evaluated. To avoid so, an estimation of the coefficient of friction (COF) [26] or specific material properties [31] are needed.

In the present thesis, the WDT test procedure developed in [26] is improved and simplified to get fast and reliable results in accordance with the original aim of the test method. A new data reduction method named Wedge Driven Test Plus (WDT+) is proposed. The WDT+ avoids crack length measurement, load tracking or equivalent COF estimation by measuring the rotation of adherends to evaluate the fracture toughness of bonded joints. Inclinometers were fixed to adherends and the scope of the test procedure in [26] was incresed towards flexible bonded joints and thick adhesive layers by considering the adhesive thickness in the formulation.

The WDT+ consists on the insertion of a wedge between the adherends at a constant speed to generate a fracture in the adhesive layer, while the specimen is clamped to the frame of the testing machine (Figure 2.4a). During the insertion, the wedge moves towards the crack front and both the load needed to move the wedge forward (F_{push}) and the rotation angle of adhrends (θ) increase until the crack starts to propagate. At this moment, the longitudinal position of the wedge (d) is $d = d_{ini}$, and F_{push} and θ reach their maximum values around which will fluctuate during crack propagation: $F_{push} = F^c_{push}$ and $\theta = \theta^c$. During crack propagation ($d > d_{ini}$), it is assumed that the wedge moves at the same displacement rate as the crack front, keeping a constant distance a. Moreover, the wedge is in contact with metallic adherends in the adhesive-free surface. After several millimetres of crack propagation, the wedge is inserted into the adhesive layer ($d = d_{lim}$) and the wedge tears and sweeps the adhesive as shown for the flexible adhesive in Figure 2.4b. This produces an increase of F_{push} and θ above their critical values. Thus, only the data between d_{ini} and d_{lim} is considered of interest to calculate the fracture toughness. The wedge stops when $d = 125$ mm and it is pulled towards to the origin to finish the test.

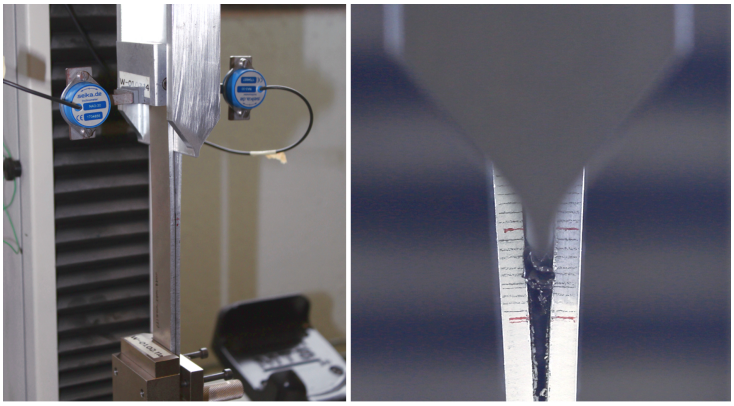

a) b)

Fig. 2.4: a) WDT+ test in progress with attached inclinometers and b) tearing and sweeping of the adhesive.

As stated, adherend rotation at the contact point between the wedge and the specimen was measured to evaluate the fracture toughness of bonded joints. To do so, two NA3-30 capacitive inclinometers from SEIKA Mikrosystemtechnik GmbH were fixed to each adherend (Figure 2.4a), providing that the rotation of the adherends at the fractured end is the same than at the contact point. Moreover, measuring the opening angle allowed to consider the root rotation of the specimen arms near the crack front and a_c was used

for the following instead of a. During the wedge insertion, the load needed to move the wedge and the individual opening angle of each adherend were recorded and averaged to determine θ. Considering the adherends in the fractured path as cantilever beams, the following geometrical equation was obtained for the corrected crack length [25]:

$$a_c = \frac{3}{2}\frac{\delta_y}{\tan\theta} \tag{2.6}$$

It is considered that the crack propagation phase of the WDT+ and the DCB test are equivalent. Then, the opening load following simple beam theory (SBT) with the corrected crack length reads:

$$P = \frac{E_x h^3 \delta_y}{4a_c^3} \tag{2.7}$$

where E_x is the Young's modulus of the adherend. The expression for the ERR considers LEFM. Thus, using Equations 1.4 and 2.7, it is given as follows:

$$G_I = \frac{3}{4}\frac{E_x h^3 \delta_y^2}{a_c^4} \tag{2.8}$$

Since small deviations in geometrical measurements may result in large errors in the evaluated fracture toughness, the contact point between a wedge with a rounded tip and the adherends was also analysed. A simplified and an exact contact point were considered for the analysis (Figures 2 and 3 in the Appendix D). Later, in Subsection 3.4.3, the relative error between the fracture toughness evaluated through the exact (G_{IC_e}) and the simplified (G_{IC_s}) contact points is determined. Besides, the influence of the bondline thickness is considered in the formulation.

A simplified contact point is assumed in the following as the a/r_w ratio is large enough in the tests carried out [26]. Considering the bondline thickness, the formulation for the opening displacement at the simplified contact point reads:

$$\delta_y = \frac{D_w - t_a}{2} \tag{2.9}$$

where D_w is the thickness of the wedge. Note that for thin adhesives or delamination tests it can be asssumed that $t_a \approx 0$. Using Equations 2.6, 2.8 and 2.9, an expression for the ERR is obtained:

$$G_I = \frac{16}{27}\frac{E_x h^3 \tan^4\theta}{(D_w - t_a)^2} \tag{2.10}$$

For further details about the analytical development, the reader may refer to the Appendix D of the document.

Regarding the experimental campaign, DCB specimens bonded with a rigid and a flexible adhesive were tested according to the procedures in [26] and [42] for the WDT+ and DCB tests, respectively. However, the fracture toughness was evaluated using Equation 2.10 and following J-integral method for the WDT+ and DCB tests. Fracture toughness results in WDT+ tests and DCB tests were compared for validation and tests were carried out at different displacement rates to evalute the effect of test speed on the test performance for the quasi-static characterisation. In addition, WDT+ tests were conducted using wedges with different thicknesses to analyse the influence of the wedge diameter on the results. Thus, specimens were classified in different batches depending on the test speed and the wedge thickness with which the test was conducted.

For the DCB tests, the displacement rate applied varied from 2 mm/min, as recommended in ISO-25217 for quasi-static tests, to 50 mm/min. For the WDT+, test conditions analogous to those in DCB tests were applied. For this purpose, the crack position data obtained in DCB tests was analysed and the average crack growth rate (da/dt) was calculated to specify equivalent displacement rates since, in WDT+, the crack growth rate is assumed to be the same as the wedge displacement rate. Thus, the analogous displacement rates for rigid bonded joints were within $10-250$ mm/min, while for flexible bonded joints varied within $6-150$ mm/min. Besides, three wedges with different thicknesses within $3.00-6.60$ mm were used.

For further details of the experimental campaign the reader may refer to the Appendix D of the document.

2.3.3 Towards a durability test for bonded joints: a new test set-up

Following wedge-type tests, a new test rig was developed that enables the simultaneous application of a constant load and environmental conditions to bonded joints. The proposed test rig (Figure 2.5) weights around 10 kg and its dimensions are 510 mm high and 200 mm wide in both directions. Thus, it is easy to manipulate by a technician, for example, to insert it in a conventional climate chamber. Moreover, the classical wedge is substituted by two frictionless rollers separated to a certain distance, which will minimise the effect of friction in experimental results. The distance between rollers is adjustable to adapt the test procedure to bonded joints with any bondline thickness (Figure 2.6).

The new test method applies a constant F_{push} load to a bonded joint that is exposed to environmental conditions. A wedge is inserted in a DCB specimen that is clamped to the frame of the test rig and its crack tip is stressed until the desired time of exposure is completed. Using the WDT+ for durability tests, both the applied load and the energy available to crack the adhesive remain

constant throughout the duration of the test and thus, either the crack growth rate or the opening angle are stable.

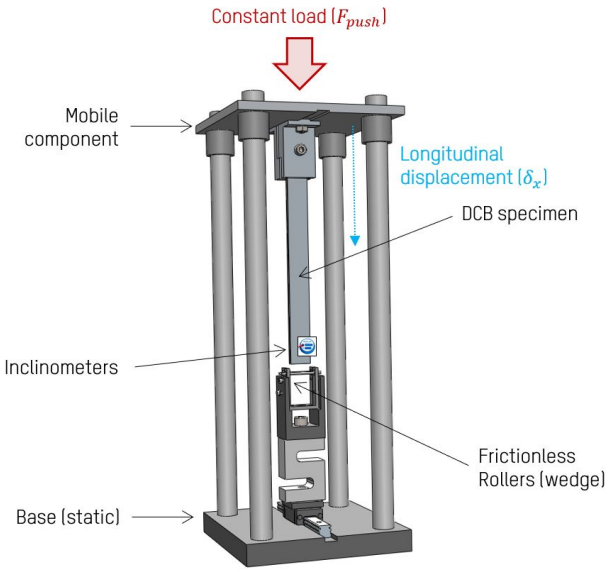

Fig. 2.5: Proposed test rig and the set-up to perform durability tests.

First, the wedge is inserted between the adherends and, second, a constant F_{push} load below the critical value at which the crack propagates is applied. Then, the wedge moves towards the crack front following the longitudinal direction in Figure 2.5, and it stops when the elastic potential energy of the bonded joint counteracts the external forces applied on it. At this moment, the bonded joint is in equilibrium and the distance between the wedge and the crack tip defines the initial crack length, being $a = a_0$ (Figure 2.6). Then, the bonded joint is ready to be exposed to environmental conditions. The coupled effect of the external load and environmental conditions damages the adhesive until it becomes too weak and the crack starts to propagate ($a > a_0$). From this moment, the damage induced in the adhesive layer is expected to grow ($a \gg a_0$).

The ERR is evaluated following the WDT+ data reduction method exposed in Subsection 2.3.2, which avoids crack length measurement or the estimation of a friction coefficient. The rotation of adherends at the contact point between the wedge and the specimen is measured by fixing two inclinometers to the adherends of the bonded joint and the Equation 2.10 is used monitor the ERR during the test. Then, the evolution of the damage in the adhesive layer is captured through the opening angle of adherends even when crack propagation is not visually noticeable due to adhesive relaxation.

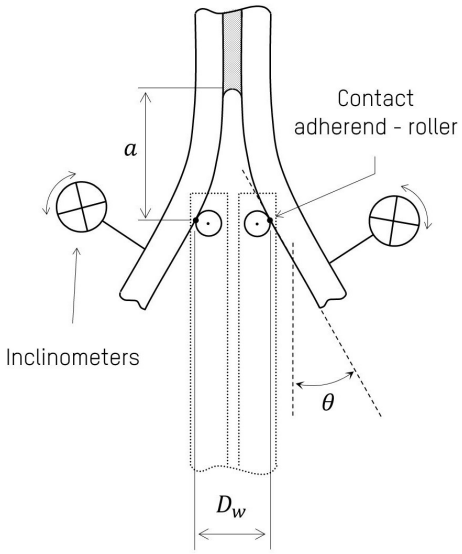

Fig. 2.6: Detail of the contact between rollers (wedge) and adherends.

Chapter 3

Results and discussion

Experimental and numerical results obtained through the methods developed in Chapter 2 are divided in four subsections. Each subsection corresponds to a research article in the Appendix.

3.1 Effect of the width-to-thickness ratio on G_{IC}

In summary of the results in Appendix A, Figure 3.1 shows the analytical curves given by Equation 2.2 and experimental results to describe the lateral contraction of the adhesive layer in flexible bonded joints with different widths and bondline thicknesses (0.5 mm and 2.0 mm).

Experimental results show that the lateral contraction of the adhesive layer at the crack tip is independent of the bondline thickness (Figure 3.1a). Following Section 2.1, the assumption $\delta_y = t_a$ in Equation 2.4 enables the correction $B^*(\Delta_c)/B$ in Equation 2.2 to be independent of t_a. Thus, it confirms that the fracture behaviour of a bonded joint is dominated by the stress state, i.e. B/t_a ratio. To evaluate the accuracy of the analytical model, the mean squared error (MSE) between the experimental data and the analytical approach was evaluated. It determined that the analytical curve given by $B^*(\Delta_c)/B$ accurately predicts the lateral contraction produced by the stretch-shortening phenomenon (Figure 14 in the Appendix A).

Therefore, the flexibility of the adhesive layer plays an important role in the fracture process of a bonded joint, specially when nearly incompressible adhesives are used. In such cases, the shortening of the effective width generated due to the elastic behaviour of the adhesive must be considered (Figure 3.2) through Equation 2.5, which completes the analytical model in Equation 1.1 with the correction in Equation 2.2.

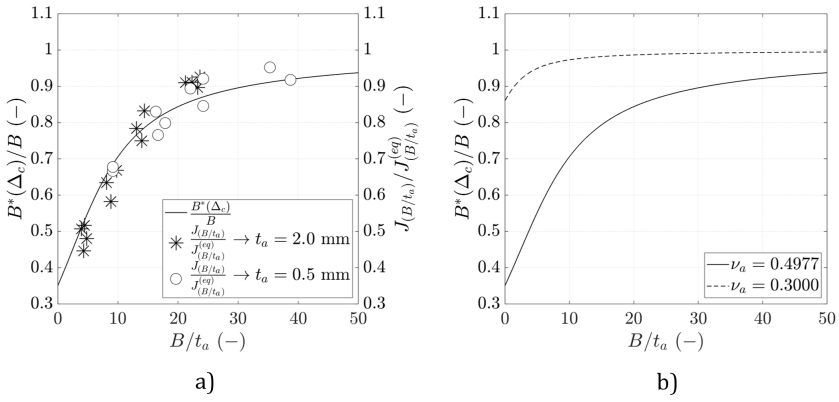

Fig. 3.1: a) Experimental validation of the lateral contraction in the flexible adhesive ($\nu_a = 0.4977$) and b) the lateral contraction for a rigid ($\nu_a = 0.3$) and an almost incompressible adhesive ($\nu_a = 0.4977$).

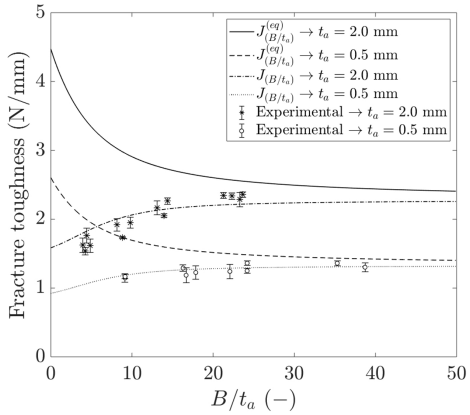

Fig. 3.2: Validation of the analytical prediction curves with experimental data in terms of fracture toughness.

Experimental findings about the existing relation between the fracture toughness and the stress state of bonded joints draw two curves superposed by two analytical curves. Each analytical curve corresponds to a specific bondline thickness since $J_{PE}^{(eq)}$ also changes. Thus, the corrected analytical model accurately predicts the experimental data whatever the stress state is. Under plane stress conditions, the curves drop in a non-parallel manner, and in plane strain conditions the fracture toughness is asymptotic and does not increase even though the total width increases.

The analytical model is valid either for rigid or flexible bonde joints but it has not been experimentally validated for rigid adhesives. In flexible bonded joints, the effective width shortens by up to 65% when $B/t_a \to 0$ (Figure 3.1b) and it is evidenced when the fracture toughness is predicted. In the case of rigid bonded joints, the effective width is almost constant and drops by 13% when $B/t_a \to 0$, which means that the elastic behaviour of the adhesive has less effect on the fracture toughness than stress state or plasticity, as anticipated in [19].

Different curves are then obtained if the individual effect of the bondline thickness on the fracture toughness is analysed. This arises due to the effect of the stress state and the elastic behaviour of the adhesive. If Equation 2.5 is analysed according to the effect of the bondline thickness, we get:

$$\frac{J_{(B/t_a)}}{J_{PE}^{(eq)}} = \frac{B^*(\Delta_c)}{B} \frac{\xi_{(B/t_a)}^{(eq)}}{\xi_{(B/t_a \to \infty)}^{(eq)}} \tag{3.1}$$

Thus, the effect of the bondline thickness on the fracture toughness can be evaluated merely by fixing the rest of the variables in Equation 2.10 (Figure 3.3).

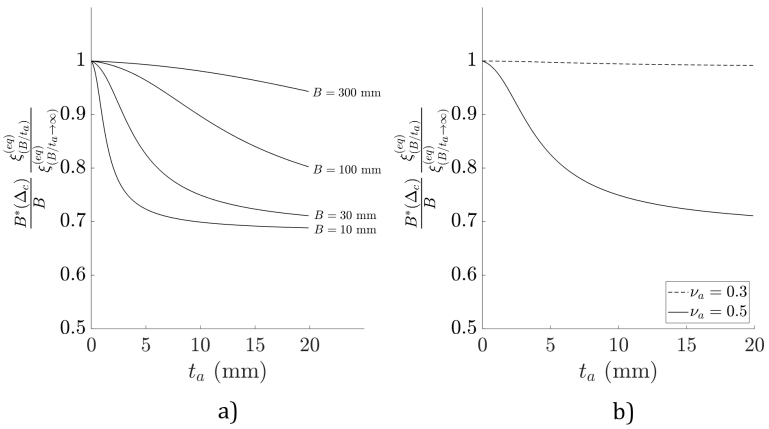

Fig. 3.3: Effect of the bondline thickness on the fracture toughness: a) for different widths of a flexible adhesive, and b) for 30-mm-wide rigid and flexible adhesives.

The different curves for small or large total-width values in Figure 3.3a corroborate the two typical curves defined in [19] through experimental finding. A similar trend is also captured varying Poisson's ratio (Figure 3.3b). However, note that the curves for very small bondline thicknesses ($t_a \to 0$) do not decrease as anticipated in [17] for rigid adhesives.

The advantage of this method is that only the experimental result of a bonded joint with a specific thickness but any width is needed to obtain the

whole analytical curve J_{B/t_a} versus B/t_a using Equation 2.5. By contrast, the curves obtained through Equation 2.5 correspond to bonded joints with a specific bondline thickness (Figure 3.2) since $J_{PE}^{(eq)}$ may change. Thus, if the bondline thickness is changed the procedure must be repeated and new test must be performed to obtain its corresponding analytical curve.

3.2 AE event location

3.2.1 Experimental correlation

Experimental results in the Appendix B are summarized in the following, emerging from the monitoring of the mode I crack growth using acoustic emissions.

Figure 3.4a and Figure 3.4b show the curves for the visual (a) and the corrected (a_c) crack lengths, as well as a point cloud of AE events, obtained for the longitudinal location of the crack tip in rigid and flexible bonded joints, respectively. Regarding the DCB test results, a_c followed the growth of a at a distance of 5.92 mm and 21.78 mm in the interior of the bonded area. The average crack growth rate was 9.62 mm/min and 6.37 mm/min in rigid and flexible bonded joints respectively, which accounts for the presence of a FPZ developed ahead of the crack tip.

Regarding AE data, AE event detection began when the visible crack propagation started. The point clouds followed the visually measured crack length, but with some dispersion. Linear regression fits of the point clouds revealed that the AE point clouds followed the crack length measured visually with an average offset of 4.98 mm and 25.32 mm in rigid and flexible bonded joints, respectively. The average linear slope was of 8.47 mm/min and 6.61 mm/min in rigid and flexible bonded joints respectively, which were approximate to the offsets and crack growth rates evaluated with the visual and corrected crack lengths. The coefficients of determination (R-square) were 0.8547 and 0.9394 for rigid and flexible bonded joints.

With regards to rigid bonded joints, most of AE events originated very close to the external crack tip just within the adhesive layer, while the visual method determined the external location of the crack tip. However, in flexible bonded joints a clear gap between the visual crack length and the AE data was observed. Thus, in accordance with [39, 41] where large FPZs were detected in flexible bonded joints, the results demonstrate that AE events originate in the interior of the adhesive far from the visually detected external crack tip. In fact, the location of these AE events was in close agreement with the corrected crack length calculations.

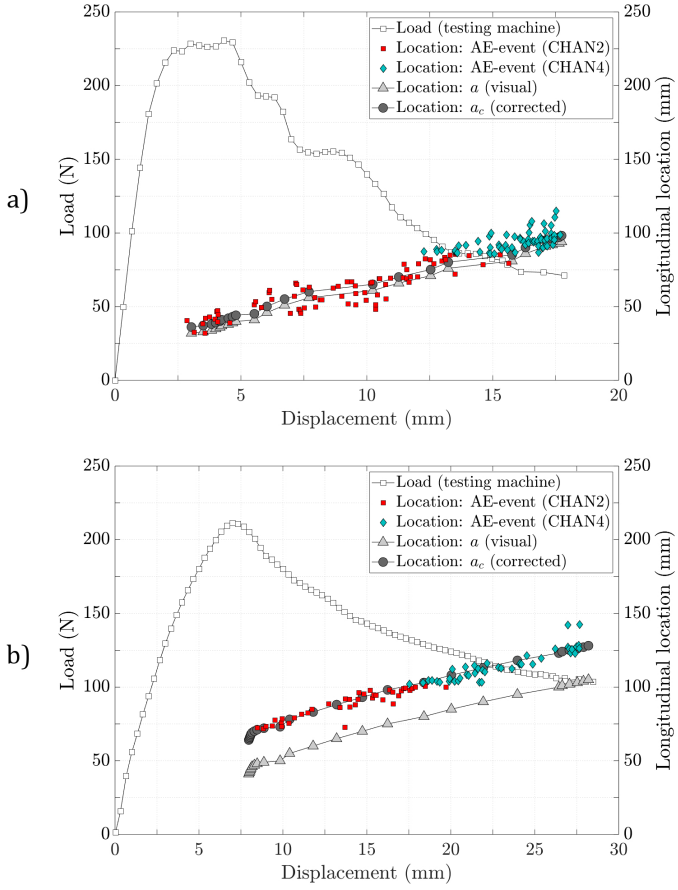

Fig. 3.4: Load-displacement curves and longitudinal locations of the crack tip, i.e. crack length, a) in the rigid adhesive, and b) in the flexible adhesive.

3.2.2 Size of the FPZ

FE models were developed to simulate experimental tests and a refined description is provided in the Appendix B. Simulations corroborated the presence of a large FPZ within the adhesive layer when a crack propagates (Figure 6 in the Appendix B). The FPZ measured at the time that crack started to propagate was 4.90 mm and 23.25 mm from the crack tip to the interior of the adhesive layer in rigid and flexible bonded joints, respectively. Figure 3.5 summarises the FPZ and maximum peel stress locations measured in the numerical simulations, AE event location and the crack length correction factor for both the rigid and flexible bonded joints.

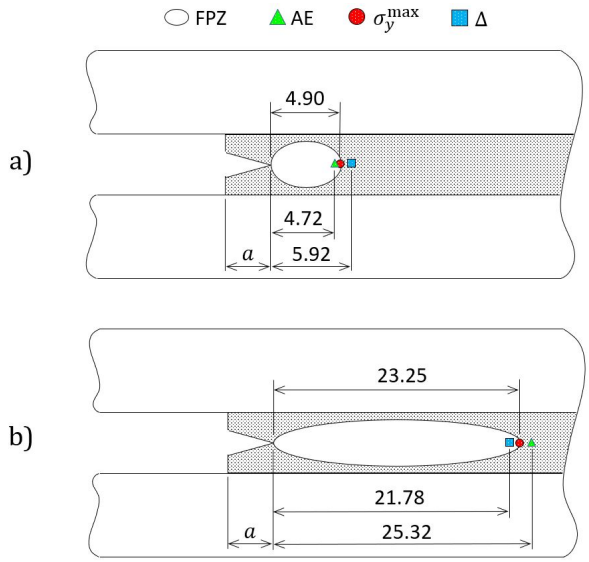

Fig. 3.5: Extension of the FPZ, AE event location, the point of maximum peel stress (σ_y^{max}) and the crack length correction factor (Δ) in a) rigid and b) flexible bonded joints, in mm.

These results confirm that a large damage zone, i.e. FPZ, is developed inside the adhesive layer when fracture conditions are met, specially in flexible bonded joints. However, this damage was not detected during visual inspection of the crack tip. To compensate, the CBT data reduction method corrects the visual crack length and proposes the use of the corrected crack length to evaluate fracture energy in bonded joints, which is associated with the flexibility of specimen arms and the FPZ. AE events were produced by real-time physical events, such as cracking or plastic deformation, and a good representation of the real behaviour of a bonded joint was obtained. Unlike in [21], where AE source location links to a visually measured crack length, the AE event location observed in this study strongly corresponded to the location of maximum peel stress induced in the adhesive layer under fracture conditions.

This demonstrates that AE testing is valid for mode I crack growth monitoring in rigid and flexible bonded joints. AE technique removes subjectivity in crack length measurement and the size of the FPZ can be quantified, regardless of the type of crack front either in samples or structural subcomponents.

3.3 Evaluation of G_{IC} in bonded joints exposed to service conditions

3.3.1 Stressed versus non-stressed exposure

Significant differences are observed in the fracture toughness evaluated in bonded joints stressed by sustaining an external load during environmental exposure and non-stressed bonded joints. Fracture toughness values were evaluated through DCB tests following CBT [42], CBBM [22] and J-integral [23] data reduction methods, and they are given in Table 3.1 and Table 3.2 for stressed and non-stressed bonded joints, respectively.

Table 3.1: Fracture toughness evaluated in stressed specimens, in N/mm.

	CBT		**CBBM**		**J-integral**	
Exposure time, t (h)	AVG	SD	AVG	SD	AVG	SD
0	1.526	0.046	1.481	0.123	1.510	0.099
10	1.111	0.147	1.154	0.105	1.152	0.110
100	0.996	0.052	1.138	0.081	1.124	0.041
300	0.878	0.000	1.062	0.310	1.086	0.312
1000	0.732	0.151	1.005	0.117	1.002	0.118

Table 3.2: Fracture toughness evaluated in non-stressed specimens, in N/mm.

	CBT		**CBBM**		**J-integral**	
Exposure time, t (h)	AVG	SD	AVG	SD	AVG	SD
0	1.526	0.046	1.481	0.123	1.510	0.099
10	1.894	0.015	1.715	0.070	1.700	0.040
100	1.886	0.041	1.941	0.183	2.042	0.000
300	1.814	0.307	1.837	0.263	1.788	0.277
1000	1.649	0.000	1.714	0.034	1.618	0.113

The effect of an external load is detrimental for bonded joints exposed to temperature and humidity conditions and accelerates the degradation of bonded joints when flexible adhesives are used. According to this, the fracture toughness evaluated through DCB tests decreases with increasing the exposure time (Figure 3.6). Being $G_{IC}]_t$ the fracture toughness at any exposure

time (t) and $G_{IC}]_{t=0}$ the fracture toughness measured in control specimens, a ratio with a value of 1 would represent an undegraded bonded joint. In contrast, the fracture toughness evaluated in non-stressed bonded joints first increases ($t < 100$h) then decreases to the original value although bonded joints have long been exposed to high temperature and humidity conditions (Table 3.2).

Regarding Figure 3.6, however, neither the crack lengths measured in stressed bonded joints through WTs nor the fracture toughness evaluated using the Equation 1.5 show dependence on the time of exposure (Figure 3.7).

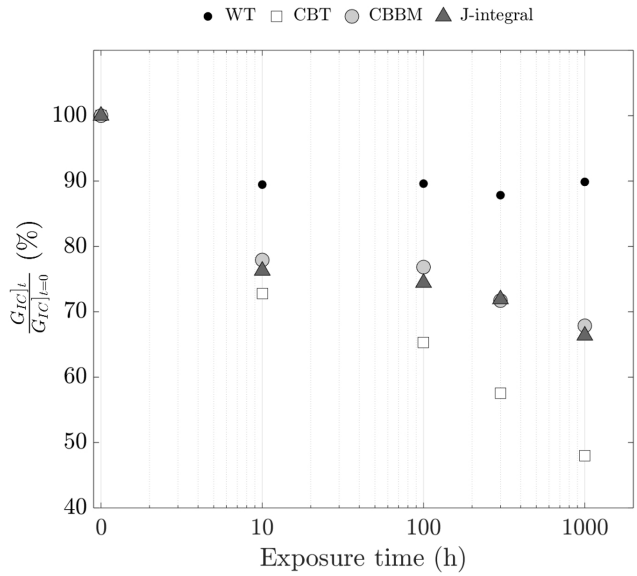

Fig. 3.6: Fracture toughness evaluated in stressed specimens through Wedge Tests and DCB tests, using WT in [46], CBT, CBBM and J-integral data reduction methods.

The adhesive-adherend interface was resistant and moisture diffusion affected the adhesive layer, prevailing cohesive failure as usual in accelerated testing [73]. Regarding stressed bonded joints, the temperature, moisture and sustained load conditions caused a local stress relaxation of the adhesive near the crack tip. This had a negative effect on the stiffness (weakening, Figure 3.8) and the fracture toughness of stressed bonded joints (DCB tests in Figure 3.6).

Regarding non-stressed bonded joints, temperature and moisture conditions also affected the fracture strength and toughness of the bonded joint (Table 3.2). The initial increase in fracture toughness is typically attributed

to a post-cure of the adhesive. The reduction of the fracture toughness, however, may be due to the micro-cracking of the adhesive in the interior of the bonded joint (Figure 6 in the Appendix C). This reduction is lower than in stressed bonded joints since the absence of the sustained load during the environmental exposure avoided the coalescence and growth of voids.

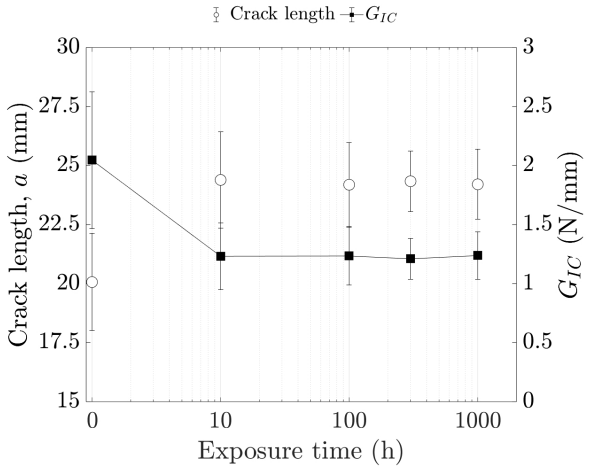

Fig. 3.7: Measured crack length in stressed bonded joints through Wedge Tests and the fracture toughness evaluated using Equation 1.5.

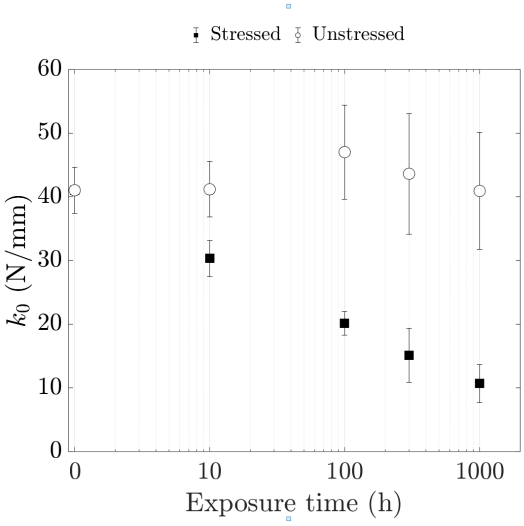

Fig. 3.8: Variation of the initial stiffness with exposure time in stressed bonded joints.

3.3.2 The FPZ and data reduction methods to evaluate G_{IC}

R-curves in Figure 3.9 were obtained from DCB tests using the CBT method [42]. Figure 3.9a shows that the length of the area in which the adhesive is weakened due to the sustained load grows approximately from 20 mm (t = 10h) to 50 mm (t = 1000h) in stressed bonded joints. This results in an enlargement of the FPZ, and lower load and fracture toughness values are evaluated. Thus, the damaged area in the adhesive layer grows in stressed bonded joints with increased exposure time.

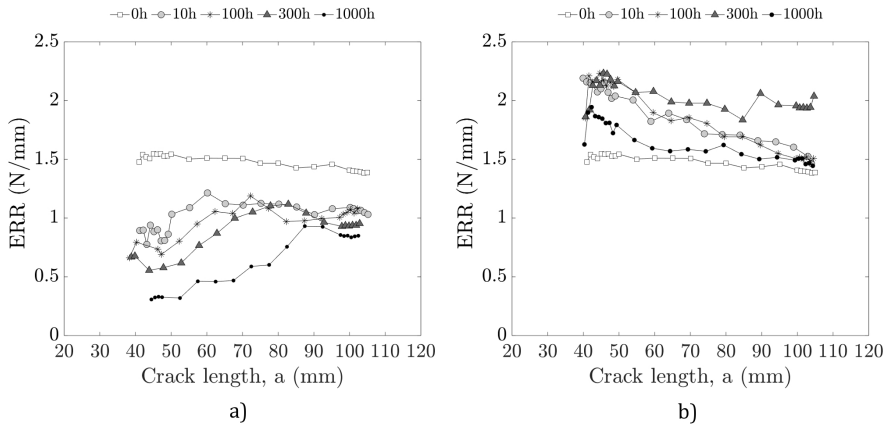

Fig. 3.9: R-curves evaluated through DCB tests using CBT [42] data reduction method in a) stressed and b) non-stressed bonded joints.

But although the FPZ grows, the crack does not, and the damage induced in the adhesive layer is not externally visible in stressed bonded joints. Then, a significant lag is produced between the external location of the crack tip and its effective location accounting for the extension of the FPZ. This difference has an important impact on the evaluation of the fracture toughness specially when methods that require a visual measurement of the crack length are used. In the case of stressed bonded joints, the loss of stiffness is such (Figure 3.8) that when a certain ageing condition is reached (t = 10h) the adhesive relaxes and the opening displacement is not large enough to propagate the crack (Figure 3.7). Then, the crack stops growing and, although the adhesive is more and more damaged with increasing the exposure time, the fracture toughness evaluated through Equation 1.5 keeps constant (Figure 3.7). Thus, the data reduction method in Equation 1.5 [46] is not valid to calculate the fracture toughness when durability studies are carried out in flexible bonded joints sustaining an external load. Nor is the procedure proposed in [43] appropriate to evaluate the durability of bonded joints when

flexible adhesives are used, which supports the recent withdrawal with no replacement of the standard ASTM D3762(2010).

Regarding DCB tests in stressed bonded joints (Figure 3.6), inaccurate values of the fracture toughness are evaluated through the CBT method since deviations grow up approximately to 20% with respect to CBBM and J-integral results. This is attributed to the fact that, unlike CBBM and J-integral methods, the CBT data reduction method depends on the visual measurement of the crack length. Then, the CBT method understimates the calculated fracture toughness and deviations are incremented with the increase of the exposure time. CBBM and J-integral methods may provide reliable values of fracture toughness since the extension of the FPZ is accounted through the specimen compliance and the rotation of adherends, respectively.

In contrast, the fracture toughness evaluated in non-stressed bonded joints matches using either the CBT, the CBBM or the J-integral data reduction methods (Table 3.2). Moreover, R-curves in Figure 3.9b show that the fracture strength of non-stressed bonded joints fluctuates around a constant value. Unlike in stressed specimens, the FPZ of non-stressed specimens did not increase due to environmental exposure and the deviation between the external and internal location of the crack tip is negligible.

3.4 Evaluation of G_{IC} using WDT+

The proposed WDT+ method attempts to solve the weaknesses evidenced in Section 3.3 regarding the suitability of existing experimental methods to perform a durability study. The following subsections show the results of an experimental campaign aimed to validate the applicability of the WDT+ method to evaluate the fracture toughness of bonded joints.

3.4.1 Assessment of the test procedure

Regarding WDT+ tests, the rotation of adherends was measured to avoid either crack length measurement or the estimation of the equivalent COF to evaluate the fracture toughness of bonded joints (Figure 3.10). The evolution of θ measured through the inclinometers was much more stable than the evolution of the equivalent COF or the F_{push}, which was measured with the load cell during the test. The evolution of the contact angles and the average value are shown in Figure 3.10a and Figure 3.10b for rigid and flexible bonded joints respectively, while the evolution of F_{push} and the equivalent COF are given in Figure 3.10c and Figure 3.10d. In addition, it is observed that the COF fluctuates during the test and strongly depends on the adherend surface, test speed and interfacial friction coefficient among other variables [82].

Therefore, the data reduction method proposed in Equation 2.10 is shown to be more robust than the proposed in Equation 1.9, which depends on the average value of the equivalent COF to calculate the ERR [26].

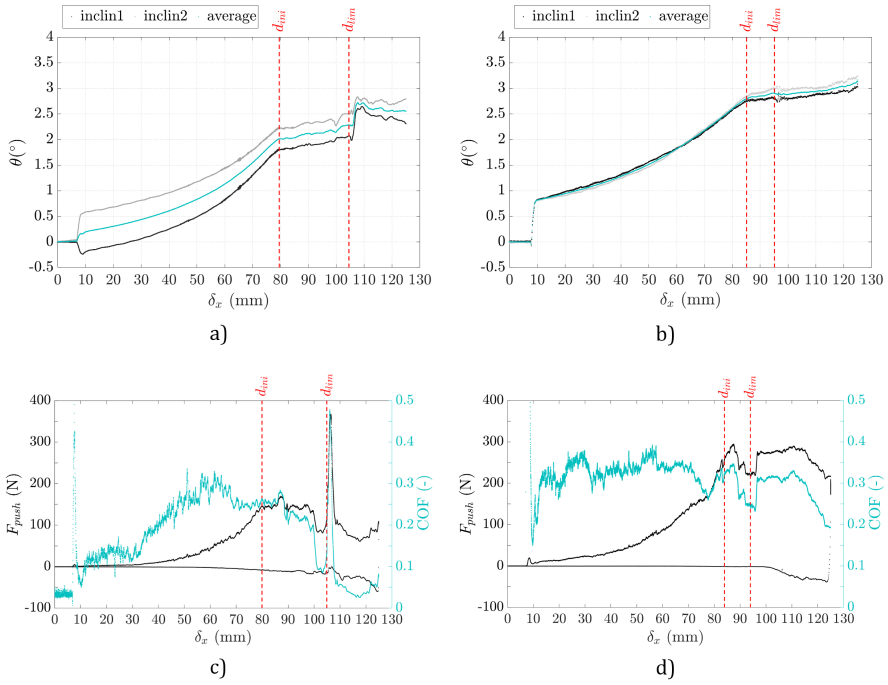

Fig. 3.10: Adherend rotation measured with inclinometers in a) rigid adhesive samples and b) flexible adhesive samples; and load-displacement (left axis) and equivalent COF-displacement (right axis) curves for c) rigid and d) flexible adhesive samples, tested following WDT+ method.

Experimental data recorded before the wedge was inserted in the adhesive layer was of interest. Thus, the values of θ recorded between d_{ini} and d_{lim} were considered to evaluate the fracture toughness in WDT+ tests. Moreover, fracture toughness results evaluated through DCB and WDT+ methods at quasi-static conditions are compared in Table 3.3. G_{IC} values obtained from DCB tests following J-integral method and WDT+ tests are similar in both rigid and flexible bonded joints.

It is observed that the WDT+ is stable, robust and valid for rigid and flexible bonded joints. For further details of the descriptions of load-displacement curves and equivalent COF-displacement curves in Figure 3.10 the reader may refer to the Appendix D.

Table 3.3: G_{IC} results from DCB tests and WDT+, in N/mm.

Method	Adhesive	AVG	SD
DCB	Rigid	1.193	0.143
	Flexible	1.503	0.055
WDT+	Rigid	1.128	0.071
	Flexible	1.440	0.082

3.4.2 Effect of test speed for quasi-static characterisation

Figure 3.11 compares load cell and inclinometer output data to analyse the effect of the displacement rate on the parameters used for the data reduction process. For both displacement rates considered, it can be observed through θ and F_{push} that the inclinometers exhibited a smoother response than the load cell. As in Equation 2.10 the ERR only depends on the arm rotation angle and not the force, it almost does not vary with the increase of the displacement rate, having quasi-static values of the fracture toughness.

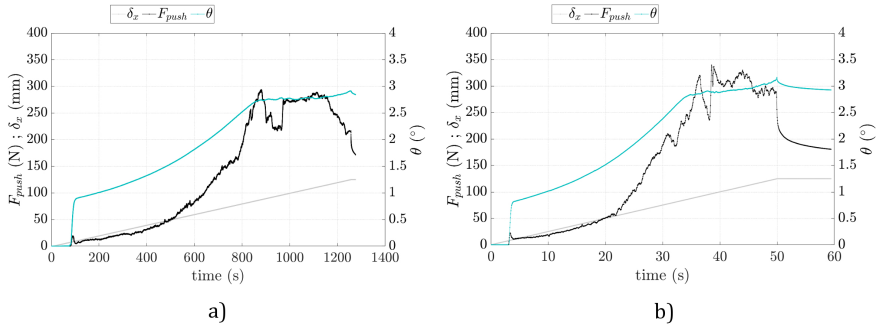

Fig. 3.11: Evolution of θ and F_{push} in flexible bonded joints tested at a) 6 mm/min and b) 150 mm/min with the WDT+.

This is an important advantage when compared to the DCB test, presenting the possibility to test at higher displacement rates, reducing the testing time but obtaining the same quasi-static value of fracture toughness (Figure 3.12). An increase of the fracture toughness was expected with the increase of the displacement rate beyond the quasi-static conditions suggested in ISO-25217, as evidenced in DCB tests for flexible bonded joints. However, while wedge driven tests keep an almost constant distance a during crack propagation, the data reduction method proposed in Equation 2.10 is load- and crack-length-independent. Thus, dynamic effects are minimised for the eval-

uation of G_{IC} and the range of test velocities at which quasi-static conditions are met is increased. In support of the proposed method, a similar strategy was followed in [49, 83, 84] but for high rates of testing. Studies in [83] identified strong dynamic effects on the characterisation of G_{IC} in bonded joints and, to avoid so, a load- and crack-length-independent data reduction method were suggested in [84] and [49], respectively. Then, the results in Figure 3.11 clearly demonstrate that the effect of the displacement rate on θ is almost negligible at slow displacement rates, but not the force applied.

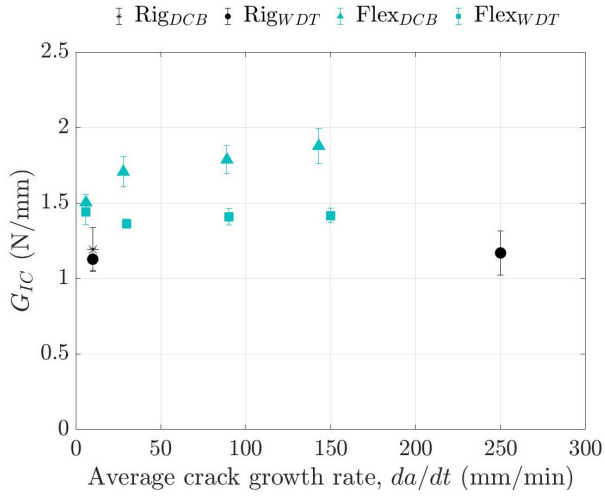

Fig. 3.12: Fracture toughness obtained in DCB tests and WDT+ tests for rigid and flexible bonded joints. The average crack growth rate is used for comparison.

3.4.3 Influence of the wedge diameter

With regards to the wedge dimension, thick wedges anticipate the crack initiation and increase the crack length (Figure 3.13).

If the wedge diameter increases the evaluated fracture toughness is less influenced by the bondline thickness, which is beneficial to get a more robust data reduction method. However, the thicker the wedge the greater the error in the results produced due to the assumption of the simplified contact point between the rounded wedge and adherends. Therefore, when D_w/t_a approaches 1, the error between the exact and simplified formulation asymptotically goes to infinite (Figure 3.14a). This occurs because the thickness of the adhesive layer is neglected in the analytical derivations of the classic WT (Equation 1.5) and therefore, there is a wrong estimation of the fracture toughness (Figure 3.14b). The error also increases if D_w/t_a increases for a given t_a, i.e. wedges with larger diameters have larger differences in the con-

tact points as also observed in [26]. These effects are more pronounced for smaller crack lengths and thicker adhesives because both cases involve larger wedge diameters, and thus larger differences in the contact points and, ultimately, large errors in the estimation of fracture toughness.

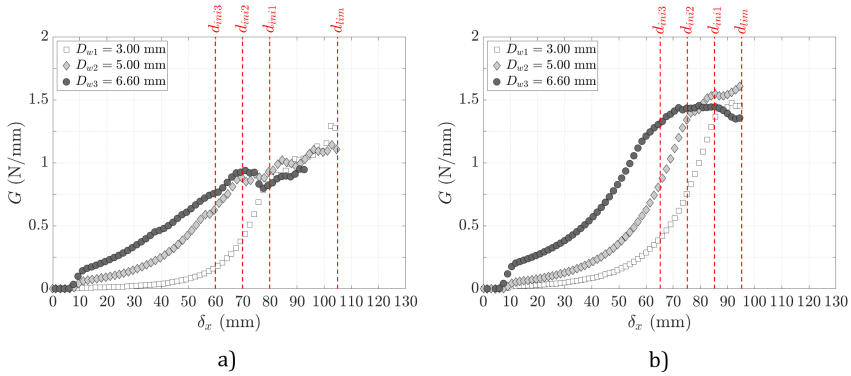

Fig. 3.13: ERR-displacement curves for a) rigid and b) flexible bonded joints tested with different wedge thicknesses. Distances d_{ini1}, d_{ini2} and d_{ini3} correspond to the test cases associated with D_{w1}, D_{w2} and D_{w3}, respectively.

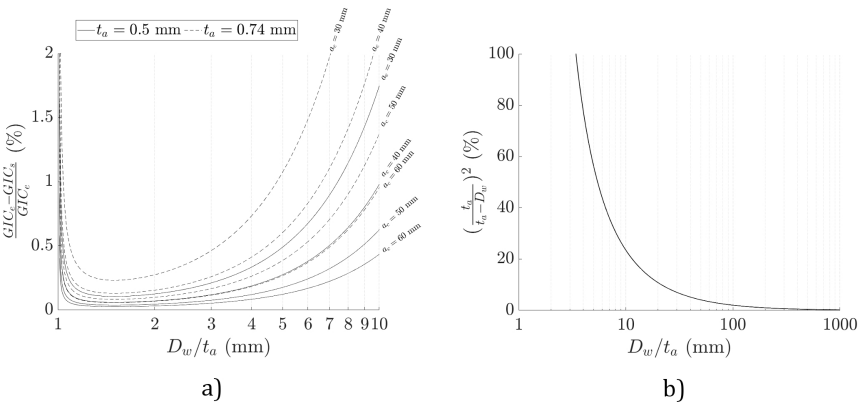

Fig. 3.14: Relative error in the measurement of the fracture toughness: a) between the exact and simplified formulations in function of the ratio D_w/t_a (in logarithmic scale) for different crack lengths and adhesive thicknesses and, b) through the simplified formulation in function of the ratio D_w/t_a taking into account the bondline thickness ($G_{IC_s}(t_a)$) or neglecting it ($G_{IC_s}(t_a = 0)$).

In any case, the wedge configuration and the WDT+ data reduction method provide relative errors in the calculation of fracture toughness that were lower than 1% in all tests, as can be seen in Table 6 of the Appendix D. However,

if the formulation in [26], which does not consider the bondline thickness, is used, significant errors may be encountered in the evaluation of the fracture toughness, which depends on the bondline thickness, the wedge diameter and the contact point.

In accordance with [27, 85], the data reduction method must consider the bondline thickness, which is included in Equation 2.9. Otherwise, strong deviations in the evaluation of the fracture toughness will be obtained. Therefore, the WDT+ is valid for any adhesive type, bondline thickness and friction between the wedge and adherends, which improves the classic WT in [43].

3.5 Summary and discussion

The analysis of the fracture behaviour of flexible bonded joints and the development of new experimental methods to characterise the fracture toughness of bonded joints are the main contributions and their scope of application is varied, intended mostly for industrial needs and applications.

The analytical model developed to relate the fracture toughness of different bonded joints is valid for rigid and flexible adhesives and it captures the elastic behaviour of the adhesive layer. Its application in thick adhesive layers within 0.5 mm and 2.0 mm is validated in joints bonded with an almost incompressible adhesive ($\nu_a = 0.4977$), whose fracture behaviour evidences a strong dependence on the elasticity of the adhesive layer.

Aimed at large structural components, AE technique is valid for either rigid or flexible bonded joints to locate the crack growth when fracture occurs and to estimate its FPZ's size. The study is focused on bonded joints with metal adherends and thus, care must be taken when using this method to analyse bonded joints with different adherend materials such as composites. In those cases, AE-events may origin in adherends and the location of the crack growth in the adhesive may be difficult. Moreover, failure mode identification capabilities are needed to understand the nature of AE-events and to distinguish the origin of each AE-event for location purposes.

Regarding the durability of structural components, the new experimental method to evaluate the durability of bonded joints exposed to load and environmental conditions proposes an improved alternative to the recently withdrawn ASTM D3762 test standard. It allows a quantitative evaluation of the durability by monitoring the evolution of the ERR in real-time with controlled load and environmental conditions. Unlike the data reduction method WDT+, the durability test has not been fully experimentally validated yet. However, it is expected to be valid for any type of adhesive and bondline thickness as it has been demonstrated with the WDT+ method. In addition to increasing the scope of the WDT method in [26] towards large adhesive

thicknesses and flexible adhesives, the WDT+ becomes essential for the characterisation of bonded joints subjected to ageing, as described in Subsection 2.3.3 and proposed in the patent request.

Chapter 4

Concluding remarks

4.1 Conclusions

New analytical and experimental procedures have been developed for the structural characterisation of flexible bonded joints. The analytical model aims to describe the fracture behaviour of flexible bonded joints while the experimental methods solve some of the current challenges in adhesively bonded joint characterisation, such as crack growth monitoring, testing efficiency and durability assessment. Although the analytical model is focused on flexible bonded joints, the experimental methods are feasible for either rigid or flexible bonded joints. They provide reliable alternatives to the existing fracture characterisation methods to evaluate the fracture toughness of adhesively bonded joints.

4.1.1 The dependence of fracture toughness on the stress state

The proposed analytical model in Equation 2.5 considers the stress state to predict the fracture toughness of flexible bonded joints. Since the width-to-thickness ratio describes the stress state of a bonded joint, it is proved that the effective width shortens due to the elastic behaviour of the adhesive, i.e. Poisson effect, and that the shortening is independent on the bondline thickness.

A new method is suggested herein, the main advantage of which is that only the experimental result of a bonded joint with a specific B/t_a is needed to predict the fracture toughness of bonded joints of any width but with the same bondline thickness as the joint being tested.

4.1.2 Direct real-time location of the crack growth

AE technique is valid to locate the crack tip when fracture occurs in rigid and flexible bonded joints and to estimate its FPZ's size. Unlike other conventional SHM techniques, AE provides continuous real-time information about bonded joints no matter the composition or manufacture of the constituent parts. AE events in DCB tests are related to the crack growth along the bonded path and their location corresponds to the point of maximum normal stress induced in the adhesive layer under fracture conditions. While AE events in rigid bonded joints originate just ahead of the crack tip, AE events in flexible joints are located in the interior of the bonded area which demonstrates that FPZs are larger in flexible bonded joints than in rigid bonded joints.

Crack growth monitoring using AE technique removes the dependency on unreliable visual crack length measuring, increasing the scope of application towards inspections of fracture processes of bonded joints, even flexible adhesives, using non-fungible sensors.

4.1.3 Potential test to evaluate the durability of bonded joints

The effect of a sustained load is detrimental and accelerates the degradation in flexible bonded joints, being of particular concern in primary structures. However, the Wedge Test described in ASTM D3762 is not suitable for flexible bonded joints because the crack does not grow during the exposure period due to adhesive relaxation. Thus, experimental procedures are lacking to evaluate the durability of bonded joints, mainly when external load and environmental exposure are combined.

Due to the lack of experimental procedures, DCB tests can be carried out once the exposure period is completed. However, large deviations in the calculated fracture toughness are produced when crack length dependent data reduction methods are used. Crack length measuring should be avoided when durability in bonded joints is studied. Moreover, this characterisation method consumes many resources since many specimens are tested to characterise the curve of the evolution of the fracture toughness.

The proposed experimental method attempts to solve the difficulties experienced when the durability of stressed bonded joints is evaluated. The new test procedure named WDT+ monitors continuously the ERR of the bonded joint avoiding crack length measurement and allows the application of a constant G_I by controlling the load during the test. The proposed test rig neither depends on a tensile testing machine nor a coupled climate chamber. Moreover, the growth of the damage in the bonded joint is captured through inclinometers without altering the evaluation of the ERR, even if adhesive relaxation occurs during ageing. Moreover, it is valid for any combination

of adhesive-adherend material and thicknesses. The proposed test rig can be adapted to mode II or mixed-mode failure modes and fatigue tests. It also allows to perform different tests in parallel, being the only limitation the space inside the climate chamber.

4.1.4 Reduction in test time and sensitivity

The proposed data reduction method named Wedge Driven Test Plus (WDT+), unlike similar test procedures in the literature, avoids crack length measurement, load tracking or equivalent COF estimation to evaluate mode I fracture toughness in bonded joints. Then, the test procedure is fully-objective and simple, while human intervention is not necessary.

The test procedure is stable, robust and less sensitive to test speed, increasing accuracy and the range of test velocities established by the ISO-25217 at which quasi-static test conditions are met. Moreover, the WDT+ is valid for any type of adhesives and bondline thicknesses, improving the classic WT available in the literature. Then, the proposed method is appropriate for rigid and flexible adhesives and its simplicity makes it fast and reliable for carrying out large experimental test campaigns. The scope of the test method is increased towards large adhesive thicknesses, flexible adhesives and even to the characterise the durability of bonded joints subjected to service conditions.

4.2 Future work

The analytical and experimental procedures developed in the current thesis pave the way for new research in methods to characterise the fracture behaviour of flexible bonded joints. In fact, focusing future work on addressing technical challenges with high degree of applicability in industry, such as the fracture behaviour of bonded joints or the characterisation of service conditions, indirectly contributes to solve societal challenges such as climate change. Considering the results of the current research, the following works are suggested.

4.2.1 Continue with the analysis of the fracture behaviour

– ***Effect of additional fracture mechanisms:***

Owing to the method only having been validated for flexible adhesives, future work should focus on the analysis of additional mechanisms involved in the fracture of joints bonded with rigid adhesives or small bondline thicknesses since fracture could be attributed e.g. to adhesive plasticisation or flaws in the adhesive layer. Moreover, the study of the influence of the stress

state on these fracture mechanisms may converge in new analytical models which could complement the proposed analytical approach, increasing the scope towards rigid bonded joints and new bonded joint configurations. Mode II and mixed-mode (I+II) failure modes may be also analysed, in which new failure mechanisms to those analysed in mode I may be found.

4.2.2 On the use of acoustic emissions

– ***Damage detection and failure mode identification using AE:***

In the present work, AE technique is used to localize fracture events in bonded joints subjected to mode I loading. However, AE monitoring can be also applied for failure mode identification. For this purpose, new experimental campaigns may be performed, and recorded AE data should be analysed following either a parametric, e.g. number of hits and counts or peak amplitude, or a frequential analysis to find correlations between experimental data and physical evidences before and during fracture occurs.

– ***Crack growth monitoring in additional failure modes:***

Crack growth monitoring can be extended to other failure modes in which the visual observation of the crack growth is even more difficult, such as mode II and mixed-mode (I+II) failure modes. Further, the evolution of the FPZ may be analysed in such a way that the mode mixity ratio could be determined when opening, sliding and tearing loads work together.

– ***Damage evolution in bonded joints exposed to service conditions:***

As studied, bonded joints are often exposed to environmental ageing and external loads when they work in service conditions. Under these conditions, the FPZ in the adhesive layer grows but the damage may not be visually detectable and thus, a sudden failure of the bonded joint may occur. To avoid such a catastrophic scenario, AE technology may contribute on damage quantification in bonded joints subjected to service conditions so that the bonded joint failure is prevented.

– ***Validation of the proposed method in large structures:***

The applicability of the proposed method in large structural components may be evaluated through a real scale demonstrator of a structural component of interest. External loads and even specific temperature and humidity conditions may be applied to create cracks inside the bonded structure, "invisible" for visual detection but detectable for the acoustic emissions technique to compare the results with the location provided by alternative methods such as ultrasonics.

4.2.3 Next steps with the new durability test

– ***Validate the new experimental set-up:***

The proposed test method is patent pending but it is still located in a low level in the technology readiness level (TRL) scale and, for the concept to mature, experimental validations must be performed. Thus, next steps must be focused on the manufacture of the test rig and the development of an experimental campaign to obtain useful data to determine the durability of stressed bonded joints exposed to service environment.

– ***Implementation of the experimental data in FE models:***

FE models are commonly used to represent the structural behaviour of complex geometries. To make calculations, specific software requires input data which can be obtained through experimental procedures to get more representative simulations. In particular, cohesive elements are used to model the fracture behaviour of bonded joints and a traction-separation law must be defined using experimental evidence of the bonded interface to reproduce the real behaviour of the bonded joint. Using these simulation tools, the proposed experimental method could be useful to obtain input data for the lifetime reproduction of structures with stressed bonded joints exposed to environmental ageing. In addition, experiments may be complemented by AE to validate the FPZ length.

– ***Adapt the test set-up for additional failure modes and fatigue tests:***

As demonstrated, the WDT+ is an efficient test procedure to characterise the mode I fracture toughness of either rigid or flexible bonded joints. After the validation of its applicability for durability tests, the scope of the experimental method can be expanded to mode II (Figure 4.1) and mixed-mode (I+II) failure modes, and fatigue tests combined with service load and environmental conditions. For this purpose, new test procedures based on the WDT+ method should be developed and new equations should be formulated to evaluate the ERR. This leads to a robust test package that may be of industrial interest due to the simplicity, the reliability and the time saving of the test method. Moreover, the test package is modular and innovative, since, for the first time, static or fatigue loading and environmental conditions are considered in the same test frame to evaluate the durability of bonded joints.

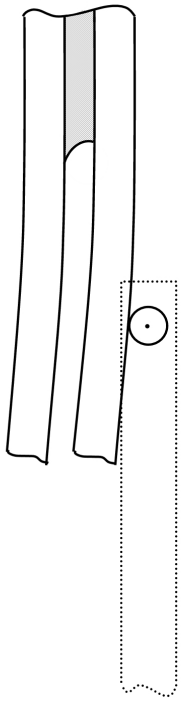

Fig. 4.1: Concept: WDT+ applied for mode II failure.

References

[1] "Paris Agreement," *Official Journal*, vol. L282, pp. 1–3, 2016.

[2] "Regulation (EU) 2019/631 of the European Parliament and of the Council setting CO2 emission performance standards for new passenger cars and for new light commercial vehicles and repealing Regulations (EC) No 443/2009 and (EU) No 510/2011," *Official Journal*, vol. L111, pp. 13–53, 2019.

[3] "Proposal for a Regulation of the European Parliament and of the Council on type-approval requirements for motor vehicles and their trailers, and systems, components and separate technical units intended for such vehicles, as regards their general safety a," *Official Journal*, vol. COM/2018/2, 2018.

[4] "Regulation (EC) No 661/2009 of the European Parliament and of the Council concerning type-approval requirements for the general safety of motor vehicles, their trailers and systems, components and separate technical units intended therefor," *Official Journal*, vol. L200, pp. 1–24, 2009.

[5] European Commission, *Flightpath 2050 - Europe's vision for aviation. Report of the High-level Group on Aviation Research.* 2012.

[6] Advisory Council for Aviation Research and Innovation in Europe, *Strategic Research & Innovation Agenda. Volume 1.* 2017.

[7] "Communication from the Commission to the European Parliament, the Council, the European Economic and Social Committee and the Committee of the Regions, A policy framework for climate and energy in the period from 2020 to 2030," *Official Journal*, vol. COM/2014/0, 2014.

[8] "Directive (EU) 2018/2001 of the European Parliament and of the Council on the promotion of the use of energy from renewable sources," *Official Journal*, vol. L328, pp. 82–209, 2018.

[9] European Investment Bank, *The future of the European space sector – How to leverage Europe's technological leadership and boost investments for space ventures*. 2019.

[10] S. Watson, A. Moro, V. Reis, C. Baniotopoulos, S. Barth, G. Bartoli, ..., and R. Wiser, "Future emerging technologies in the wind power sector: A European perspective," *Renewable and Sustainable Energy Reviews*, vol. 113, 109270, 2019.

[11] L. F. M. da Silva, A. Öchsner, and R. D. Adams, *Handbook of Adhesion Technology*. Springer Berlin Heidelberg, 2 ed., 2018.

[12] K. Dilger, B. Burchardt, and M. Frauenhofer, "Automotive industry," in *Handbook of Adhesion Technology* (L. F. M. da Silva, A. Öchsner, and R. D. Adams, eds.), pp. 1333–1366, Springer Berlin Heidelberg, 2 ed., 2018.

[13] S. Dagras, J. Eck, C. Tonon, and D. Lavielle, "Adhesives in space environment," in *Handbook of Adhesion Technology* (L. F. M. da Silva, A. Öchsner, and R. D. Adams, eds.), pp. 915–940, Springer Berlin Heidelberg, 2 ed., 2018.

[14] L. Hart-Smith, "Adhesively bonded joints in aircraft structures," in *Handbook of Adhesion Technology* (L. F. M. da Silva, A. Öchsner, and R. D. Adams, eds.), pp. 1235–1284, Heidelberg: Springer Berlin Heidelberg, 2 ed., 2018.

[15] P. Davies, "Marine Industry," in *Handbook of Adhesion Technology* (L. F. M. da Silva, A. Öchsner, and R. D. Adams, eds.), pp. 1391–1417, Springer Berlin Heidelberg, 2 ed., 2018.

[16] C. Désagulier, P. Pérés, and G. Larnac, "Aerospace industry," in *Handbook of Adhesion Technology* (L. F. M. da Silva, A. Öchsner, and R. D. Adams, eds.), pp. 1285–1331, Springer Berlin Heidelberg, 2 ed., 2018.

[17] D. B. Lee, T. Ikeda, N. Miyazaki, and N. S. Choi, "Effect of bond thickness on the fracture toughness of adhesive joints," *Journal of Engineering Materials and Technology, Transactions of the ASME*, vol. 126, no. 1, pp. 14–18, 2004.

[18] T. Pardoen, T. Ferracin, C. M. Landis, and F. Delannay, "Constraint effects in adhesive joint fracture," *Journal of the Mechanics and Physics of Solids*, vol. 53, no. 9, pp. 1951–1983, 2005.

[19] A. J. Kinloch and S. J. Shaw, "The fracture resistance of a toughened epoxy adhesive," *The Journal of Adhesion*, vol. 12, no. 1, pp. 59–77, 1981.

[20] A. Crawford, M. G. Droubi, and N. H. Faisal, "Analysis of acoustic emission propagation in metal-to-metal adhesively bonded joints," *Journal of Nondestructive Evaluation*, vol. 37, no. 2, 2018.

[21] A. Crawford, M. G. Droubi, and N. H. Faisal, "Modal Acoustic Emission Analysis of Mode-I and Mode-II Fracture of Adhesively-Bonded Joints," in *33rd European Conference on Acoustic Emission testing*, (Senlis), 2018.

[22] M. F. S. F. de Moura, R. D. S. G. Campilho, and J. P. M. Gonçalves, "Crack equivalent concept applied to the fracture characterization of bonded joints under pure mode I loading," *Composites Science and Technology*, vol. 68, no. 10-11, pp. 2224–2230, 2008.

[23] A. J. Paris and P. C. Paris, "Instantaneous evaluation of J and C*," *International Journal of Fracture*, vol. 38, no. 1, 1988.

[24] C. Sarrado, A. Turon, J. Costa, and J. Renart, "An experimental analysis of the fracture behavior of composite bonded joints in terms of cohesive laws," *Composites Part A: Applied Science and Manufacturing*, vol. 90, pp. 234–242, 2016.

[25] J. G. Williams, "Friction and plasticity effects in wedge splitting and cutting fracture tests," *Journal of Materials Science*, vol. 33, no. 22, pp. 5351–5357, 1998.

[26] J. Renart, J. Costa, G. Santacruz, S. Lazcano, and E. González, "Measuring fracture toughness of interfaces under mode I loading with the wedge driven test," *under submission*, 2020.

[27] R. D. Adams, J. W. Cowap, G. Farquharson, G. M. Margary, and D. Vaughn, "The relative merits of the Boeing wedge test and the double cantilever beam test for assessing the durability of adhesively bonded joints, with particular reference to the use of fracture mechanics," *International Journal of Adhesion and Adhesives*, vol. 29, no. 6, pp. 609–620, 2009.

[28] M. Brede, A. Sondag, O. Hesebeck, and B. Schneider, "On the energy release rate of aged adhesive joints," in *Adhesive Joints: Ageing and Durability of Epoxies and Polyurethanes* (W. Possart and M. Brede, eds.), pp. 375–404, Wiley, 2019.

[29] G. Viana, M. Costa, M. D. Banea, and L. F. M. da Silva, "A review on the temperature and moisture degradation of adhesive joints," *Proceedings of the Institution of Mechanical Engineers, Part L: Journal of Materials: Design and Applications*, vol. 231, no. 5, pp. 488–501, 2017.

[30] G. Viana, M. Costa, M. D. Banea, and L. F. M. da Silva, "Moisture and temperature degradation of double cantilever beam adhesive joints," *Journal of Adhesion Science and Technology*, vol. 31, no. 16, pp. 1824–1838, 2017.

[31] D. O. Adams, H. M. McCartin, and Z. Sievert, "Development of environmental durability test methods for composite bonded joints," in *JAMS Technical Review Meeting*, (Long Beach), 2018.

[32] S. Fevery, H. Hallez, D. Vandepitte, and S. Debruyne, "Lifetime assessment of structural adhesive joints by combining effects of mechanical load, humidity, moisture and UV: design of a test rig," *The Journal of Adhesion*, 2019.

[33] H. M. McCartin, D. M. Ricsi, N. C. Brown, D. O. Adams, and K. L. DeVries, "Environmental durability assessment of composite bonded joints using the wedge test," in *Composites and Advanced Materials Expo*, (Anaheim), 2016.

[34] J. P. Sargent, "Durability studies for aerospace applications using peel and wedge tests," *International Journal of Adhesion and Adhesives*, vol. 25, no. 3, pp. 247–256, 2005.

[35] D. O. Adams, K. L. DeVries, and C. Child, "Durability of adhesively bonded joints for aircraft structures," in *JAMS Technical Review Meeting*, (Baltimore), 2012.

[36] D. O. Adams, K. L. DeVries, C. Child, and N. C. Brown, "Test method development for environmental durability of bonded joints," in *JAMS Technical Review Meeting*, (Everett), 2013.

[37] D. O. Adams, K. L. DeVries, N. C. Brown, D. M. Ricsi, and K. Gillette, "Test method development for environmental durability of composite bonded joints," in *JAMS Technical Review Meeting*, (Seattle), 2014.

[38] G. Jhin, S. Azari, A. Ameli, N. V. Datla, M. Papini, and J. K. Spelt, "Crack growth rate and crack path in adhesively bonded joints: Comparison of creep, fatigue and fracture," *International Journal of Adhesion and Adhesives*, vol. 46, pp. 74–84, 2013.

[39] M. Cabello, A. Turon, J. Zurbitu, J. Renart, C. Sarrado, and F. Martínez, "Progressive failure analysis of DCB bonded joints using a new elastic foundation coupled with a cohesive damage model," *European Journal of Mechanics, A/Solids*, vol. 63, pp. 22–35, 2017.

[40] M. Cabello, J. Zurbitu, A. Turon, C. Sarrado, J. Renart, and F. Martínez, "Influence of the specimen width on the experimental measurement of the cohesive law using the J-Integral approach," in *17th European Conference on Composite Materials*, (Munich), 2016.

[41] M. Cabello, J. Zurbitu, J. Renart, A. Turon, and F. Martínez, "A general analytical model based on elastic foundation beam theory for adhesively bonded DCB joints either with flexible or rigid adhesives," *International Journal of Solids and Structures*, vol. 94-95, pp. 21–34, 2016.

[42] ISO 25217:2009, "Determination of the mode I adhesive fracture energy, GIC, of structural adhesives using the double cantilever beam (DCB) and tapered double cantilever beam (TDCB) specimens," *International Organization for Standardization*, 2009.

[43] ASTM D3762-03(2010), "Standard test method for adhesive-bonded surface durability of aluminium (Wedge Test)," *ASTM International*, 2010.

[44] J. G. Williams, "End corrections for orthotropic DCB specimens," *Composites Science and Technology*, vol. 35, no. 4, pp. 367–376, 1989.

[45] J. Cognard, "The mechanics of the wedge test," *The Journal of Adhesion*, vol. 20, no. 1, pp. 1–13, 1986.

[46] D. Plausinis and J. K. Spelt, "Designing for time-dependent crack growth in adhesive joints," *International Journal of Adhesion and Adhesives*, vol. 15, no. 3, pp. 143–154, 1995.

[47] J. Jumel and M. E. R. Shanahan, "Crack front curvature in the wedge test," *The Journal of Adhesion*, vol. 84, no. 9, pp. 788–804, 2008.

[48] R. D. Adams and B. W. Drinkwater, "Nondestructive testing of adhesively-bonded joints," *NDT and E International*, vol. 30, no. 2, pp. 93–98, 1997.

[49] D. A. Dillard, D. J. Pohlit, G. C. Jacob, J. M. Starbuck, and R. K. Kapania, "On the use of a driven wedge test to acquire dynamic fracture energies of bonded beam specimens," *The Journal of Adhesion*, vol. 87, no. 4, pp. 395–423, 2011.

[50] R. Lacroix, J. Monatte, A. Lens, G. Kermouche, J. M. Bergheau, and H. Klöcker, "Spot weld strength determination using the wedge test: In-situ observations and coupled simulations," in *Applied Mechanics and Materials*, vol. 24-25, pp. 299–304, 2010.

[51] E. Z. Kordatos, D. G. Aggelis, and T. E. Matikas, "Monitoring mechanical damage in structural materials using complimentary NDE techniques based on thermography and acoustic emission," in *Composites Part B: Engineering*, vol. 43, pp. 2676–2686, 2012.

[52] C. Barile, C. Casavola, G. Pappalettera, and C. Pappalettere, "Analysis of crack propagation in stainless steel by comparing acoustic emissions and infrared thermography data," *Engineering Failure Analysis*, vol. 69, pp. 35–42, 2015.

[53] D. Sans, S. Stutz, J. Renart, J. A. Mayugo, and J. Botsis, "Crack tip identification with long FBG sensors in mixed-mode delamination," *Composite Structures*, vol. 94, no. 9, pp. 2879–2887, 2012.

[54] H. Y. Ling, K. T. Lau, Z. Su, and E. T. T. Wong, "Monitoring mode II fracture behaviour of composite laminates using embedded fiber-optic sensors," *Composites Part B: Engineering*, vol. 38, no. 4, pp. 488–497, 2007.

[55] J. Xavier, J. R. A. Fernandes, O. Frazão, and J. J. L. Morais, "Measuring mode I cohesive law of wood bonded joints based on digital image correlation and fibre Bragg grating sensors," *Composite Structures*, vol. 121, pp. 83–89, 2015.

[56] X. Ning, H. Murayama, K. Kageyama, D. Wada, M. Kanai, I. Ohsawa, and H. Igawa, "Dynamic strain distribution measurement and crack detection of an adhesive-bonded single-lap joint under cyclic loading using embedded FBG," *Smart Materials and Structures*, vol. 23, no. 10, 2014.

[57] Y. Li, Y. Liao, and Z. Su, "Graphene-functionalized polymer composites for self-sensing of ultrasonic waves: An initiative towards "sensor-free" structural health monitoring," *Composites Science and Technology*, vol. 168, pp. 203–213, 2018.

[58] M. Budzik, J. Jumel, K. Imielińska, and M. E. R. Shanahan, "Accurate and continuous adhesive fracture energy determination using an instrumented wedge test," *International Journal of Adhesion and Adhesives*, vol. 29, no. 7, pp. 694–701, 2009.

[59] A. Bernasconi, M. Kharshiduzzaman, and L. Comolli, "Strain profile measurement for structural health monitoring of woven carbon-fiber reinforced polymer composite bonded joints by fiber optic sensing using an optical backscatter reflectometer," *The Journal of Adhesion*, vol. 92, no. 6, pp. 440–458, 2016.

[60] A. Bernasconi, M. Carboni, L. Comolli, R. Galeazzi, A. Gianneo, and M. Kharshiduzzaman, "Fatigue crack growth monitoring in composite bonded lap joints by a distributed fibre optic sensing system and comparison with ultrasonic testing," *The Journal of Adhesion*, vol. 92, no. 7-9, pp. 739–757, 2016.

[61] B. Masserey, C. Raemy, and P. Fromme, "High-frequency guided ultrasonic waves for hidden defect detection in multi-layer aircraft structures," *Ultrasonics*, vol. 54, no. 7, pp. 1720–1728, 2014.

[62] H. Chan, B. Masserey, and P. Fromme, "High frequency guided ultrasonic waves for hidden fatigue crack growth monitoring in multi-layer model aerospace structures," *Smart Materials and Structures*, vol. 24, no. 2, 025037, 2015.

[63] K. Zhang and Z. Zhou, "Quantitative characterization of disbonds in multilayered bonded composites using laser ultrasonic guided waves," *NDT and E International*, vol. 97, pp. 42–50, 2018.

[64] M. Diakhate, E. Bastidas-Arteaga, R. M. Pitti, and F. Schoefs, "Cluster analysis of acoustic emission activity within wood material: Towards a real-time monitoring of crack tip propagation," *Engineering Fracture Mechanics*, vol. 180, pp. 254–267, 2017.

[65] M. Fotouhi, M. Saeedifar, S. Sadeghi, M. A. Najafabadi, and G. Minak, "Investigation of the damage mechanisms for mode I delamination growth in foam core sandwich composites using acoustic emission," *Structural Health Monitoring: An International Journal*, vol. 14, no. 3, pp. 265–280, 2015.

[66] E. H. Saidane, D. Scida, M. J. Pac, and R. Ayad, "Mode-I interlaminar fracture toughness of flax, glass and hybrid flax-glass fibre woven composites: Failure mechanism evaluation using acoustic emission analysis," *Polymer Testing*, vol. 75, pp. 246–253, 2019.

[67] C. Barile, C. Casavola, and G. Pappalettera, "Acoustic emission waveform analysis in CFRP under Mode I test," *Engineering Fracture Mechanics*, vol. 210, pp. 408–413, 2019.

[68] A. Carpinteri, G. Lacidogna, G. Niccolini, and S. Puzzi, "Morphological fractal dimension versus power-law exponent in the scaling of damaged media," *International Journal of Damage Mechanics*, vol. 18, no. 3, pp. 259–282, 2009.

[69] A. Anzani, L. Binda, A. Carpinteri, G. Lacidogna, and A. Manuello, "Evaluation of the repair on multiple leaf stone masonry by acoustic emission," *Materials and Structures/Materiaux et Constructions*, vol. 41, no. 6, pp. 1169–1189, 2008.

[70] A. Carpinteri, G. Lacidogna, and M. Paggi, "Acoustic emission monitoring and numerical modeling of FRP delamination in RC beams with non-rectangular cross-section," *Materials and Structures/Materiaux et Constructions*, vol. 40, no. 6, pp. 553–566, 2007.

[71] A. L. Glessner, M. T. Takemori, M. A. Vallance, and S. K. Gifford, "Mode I interlaminar fracture toughness of unidirectional carbon fiber composites using a novel wedge-driven delamination design," in *Composite Materials: Fatigue and Fracture, Second Volume*, pp. 181–200, ASTM International, 1989.

[72] I. A. Ashcroft, J. Comyn, and A. Mubashar, "Effect of water and mechanical stress on durability," in *Handbook of Adhesion Technology* (L. F. M. da Silva, A. Öchsner, and R. Adams, eds.), pp. 879–914, Springer Berlin Heidelberg, 2 ed., 2018.

[73] S. Ebnesajjad and A. H. Landrock, *Adhesives Technology Handbook*. William Andrew, 3 ed., 2015.

[74] ASTM D1151-00(2013), "Standard practice for effect of moisture and temperature on adhesive bonds," *ASTM International*, 2013.

[75] ASTM D1183-03(2019), "Standard practice for resistance of adhesives to cyclic laboratory ageing conditions," *ASTM International*, 2019.

[76] L. Zhang, L. Zhou, J. Zhang, Z. Wang, S. Lu, and X. Wang, "Influence of high temperature on the flexural properties of GF/pCBT laminates and their fusion-bonded joints," *Composites Part B: Engineering*, vol. 110, pp. 124–131, 2017.

[77] S. Budhe, M. D. Banea, S. de Barros, and L. F. M. da Silva, "An updated review of adhesively bonded joints in composite materials," *International Journal of Adhesion and Adhesives*, vol. 72, pp. 30–42, 2017.

[78] L. Carreras, B. L. Bak, A. Turon, J. Renart, and E. Lindgaard, "Point-wise evaluation of the growth driving direction for arbitrarily shaped delamination fronts using cohesive elements," *European Journal of Mechanics, A/Solids*, vol. 72, pp. 464–482, nov 2018.

[79] H. Vallen, "Acoustic emission testing: fundamentals, equipment, applications," in *Informative booklets for non-destructive testing, NDT. Compact and understandable*, Kaarst: Castell Publication Inc., 2006.

[80] ASTM E976-15, "Standard guide for determining the reproducibility of acoustic emission sensor response," *ASTM International*, 2015.

[81] J. A. Pascoe, D. S. Zarouchas, R. C. Alderliesten, and R. Benedictus, "Using acoustic emission to understand fatigue crack growth within a single load cycle," *Engineering Fracture Mechanics*, vol. 194, pp. 281–300, 2018.

[82] X. Shi, Y. Pan, and X. Ma, "Modeling and analysis of the rope-sheave interaction at traction interface," *Journal of Applied Mechanics*, vol. 84, no. 3, 2017.

[83] B. R. K. Blackman, J. P. Dear, A. J. Kinloch, H. Macgillivray, Y. Wang, J. G. Williams, and P. Yayla, "The failure of fibre composites and adhesively bonded fibre composites under high rates of test. Part I Mode I loading-experimental studies," *Journal of Materials Science*, vol. 30, no. 23, pp. 5885–5900, 1995.

[84] B. R. K. Blackman, A. J. Kinloch, F. S. Rodriguez Sanchez, W. S. Teo, and J. G. Williams, "The fracture behaviour of structural adhesives under high rates of testing," *Engineering Fracture Mechanics*, vol. 76, no. 18, pp. 2868–2889, 2009.

[85] J. Y. Sener, T. Ferracin, L. Caussin, and F. Delannay, "On the precision of the wedge-opened double cantilever beam method for measuring the debonding toughness of adhesively bonded plates," *International Journal of Adhesion and Adhesives*, vol. 22, no. 2, pp. 129–137, 2002.

Appendix
Publications

Paper A

Effect of the width-to-thickness ratio on the mode I fracture toughness of flexible bonded joints

J. Manterola[a], M. Cabello[a], J. Zurbitu[a], J. Renart[b], A. Turon[b], J. Jumel[c], I. Urresti[a]

[a]Ikerlan Technology Research Centre, Applied Mechanics Area, Mondragón, Spain

[b]AMADE, Polytechnic School, Universitat de Girona, Girona, Spain

[c]Université de Bordeaux, I2M, Talence, France

The paper has been published in
Engineering Fracture Mechanics Vol. 218, 106584, 2019.

Engineering Fracture Mechanics 218 (2019) 106584

Contents lists available at ScienceDirect

Engineering Fracture Mechanics

journal homepage: www.elsevier.com/locate/engfracmech

Effect of the width-to-thickness ratio on the mode I fracture toughness of flexible bonded joints

J. Manterola[a,*], M. Cabello[a], J. Zurbitu[a], J. Renart[b,d], A. Turon[b], J. Jumel[c], I. Urresti[a]

[a] Applied Mechanics Area, Ikerlan Technology Research Centre, P°.J.M°. Arizmendiarrieta, 2, 20500 Arrasate-Mondragón, Spain
[b] AMADE, Polytechnic School, University of Girona, Campus Montilivi, s/n, 17071 Girona, Spain
[c] Université de Bordeaux, I2M, UMR 5295, F-33400 Talence, France
[d] Serra Húnter Fellow, Generalitat de Catalunya, Spain

ARTICLE INFO

Keywords:
Flexible adhesive
Fracture toughness
Double cantilever beam (DCB)
Bondline deformation

ABSTRACT

The stiffness and strength of a bonded joint mainly depend on the geometry of the assembly and the constitutive behaviour of its constituent parts (adherends, adhesives and interfaces). The adhesive itself may sustain a significant hydrostatic contribution to fluctuation along the bonded area, strongly influencing the local joint stiffness and strength. A considerable amount of work has been undertaken to independently evaluate the effect of the width and thickness of bonded specimens on strength or toughness. However, experimental results are lacking, especially when dealing with thick low modulus/hyperelastic adhesives. In the present work, the influence of the width-to-thickness ratio on the equivalent mode I fracture toughness of a flexible bonded joint is evaluated. Thus, an analytical model capable of predicting the fracture toughness of double cantilever beam (DCB) flexible bonded joints for a given thickness and any width has been developed. The analysis is supported through an experimental testing regime with DCB specimens made by bonding two aluminium adherends with a thick silicon-based adhesive layer, proving that the fracture behaviour of flexible bonded joints is dominated by the elastic behaviour of the adhesive layer.

1. Introduction

The evaluation of the mechanical performance of a bonded joint is a complex process which is often based on a simplified description of its geometry and on the simple mechanical properties of the bonding interface such as its strength and toughness. However, these properties are determined using standard procedures and they evidence a strong dependence on specimen dimensions such as the thickness (t_a) and width (B) of the adhesive layer. Indeed, the stress and strain distribution along the interface (stress gradients, the contribution from hydrostatic pressure etc.) is known to be highly dependent on these geometrical parameters, as evidenced by previous studies [1–12].

The critical strain energy release rate (critical SERR, G_{IC}) is a property which characterizes the capacity of a material to sustain mechanical loadings in the presence of flaws [13]. It is known from the literature that this property exhibits strong bondline thickness dependence. This effect is the result of a complex phenomenon, but also shows two main trends, as illustrated in Fig. 1. In the case of Type-A adhesives, a monotonic increase in the fracture energy with the bondline thickness is observed until an asymptotic value is reached [1–5]. In the case of Type-B adhesives, the fracture energy first reaches an optimum (peak) value, then decreases slowly,

* Corresponding author.
E-mail address: jmanterola@ikerlan.es (J. Manterola).

https://doi.org/10.1016/j.engfracmech.2019.106584
Received 8 February 2019; Received in revised form 1 July 2019; Accepted 27 July 2019
Available online 31 July 2019

Nomenclature

a_0	initial crack length
B	total width of the specimen
B^*	effective width before fracture occurs
E_a	adhesive's Young's modulus
$E_a^{'(eng)}$	apparent Young's modulus for the adhesive interface
G_{IC}	fracture energy, Critical Strain Energy Release Rate
J	fracture energy, following J-integral method
J^{ext}	fracture energy measured on a specific zone under plane-stress
$J^{(eq)}$	equivalent fracture energy of a specific bonded joint
$J_{PE}^{(eq)}$	equivalent fracture energy of a bonded joint under plane-strain state
$J_{PS}^{(eq)}$	equivalent fracture energy of a bonded joint under plane-stress state
$J_{(B/t_a)}^{(eq)}$	equivalent fracture energy of bonded joints with a given B/t_a configuration
$J_{(B/t_a)}$	fracture energy measured experimentally for a given B/t_a configuration
P	applied load at the load application point
r_p	plastic zone radius
t_a	bondline thickness
$\hat{u}$	strain energy density
$\mathbb{U}$	elastic potential energy
V	volume
x	longitudinal displacement of the crack tip associated with Poisson's effect
δ_y	opening displacement
Δ_c	maximum longitudinal deformation of the crack tip due to the shear effect
$\boldsymbol{\varepsilon}$	strain tensor
ε_{xx}, ε_{yy},ε_{zz}	normal strains in the x-y-z local coordinate system
ε_{xy}	shear strain in the x-y local plane
θ_P	relative rotation between adherends
λ, μ	Lamé constants
ν_a	adhesive's Poisson's ratio
$\xi_{(B/t_a)}^{(eq)}$	equivalent correction factor for a given B/t_a configuration
$\boldsymbol{\sigma}$	stress tensor
σ_{zz}	normal stress in z direction, according to the local coordinate system
ψ_x	correction function
B/t_a	width-to-thickness ratio
$B/t_a]_{PE}$	width-to-thickness ratio for a plane-strain configured joint
$B^*(\Delta_c)/B$	stretch ratio due to lateral contraction
DCB	double cantilever beam
DIC	digital image correlation
FE	finite element
MSE	mean squared error
SERR	strain energy release rate

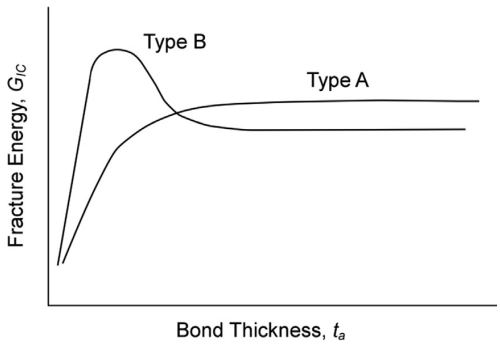

Fig. 1. Main typical types of bond-thickness effects on the fracture energy of adhesive joints [6].

finally reaching an asymptotic value [6–9].

The bondline–thickness dependence could be attributed to the confinement of the plastically deformed area near the crack tip [6]. In fact, the extension is constrained by the adherends and the size of the plastic zone along the bondline is increased.

This may explain the increase in the fracture energy following an increase in the bondline thickness. The *plateau* value is reached when the plastic zone size, as estimated via Irwin's model ($2r_p$), matches the bondline thickness ($t_a = 2r_p$) (Type A). From this point on ($t_a > 2r_p$), the fracture energy corresponds to the intrinsic adhesive's critical SERR. However, failure could also be attributed to flaws in the adhesive whose characteristic size increases with the bondline thickness. This may explain the reduction in the fracture energy after the peak value in case B [9,10].

Additionally, the parametric study carried out in [11] shows that the total bond toughness not only depends on the adhesive layer's thickness but is also significantly affected by the adherend's thickness. Thus, the differences between Type-A and Type-B curves may also derive from the adhesive–adherend thickness configuration.

For a given bondline thickness, the measured critical SERR varies with the width of the test specimen (Fig. 2). The fracture energy is almost constant for wide specimens and drops when the width decreases. This is because the stress state near the crack tip varies

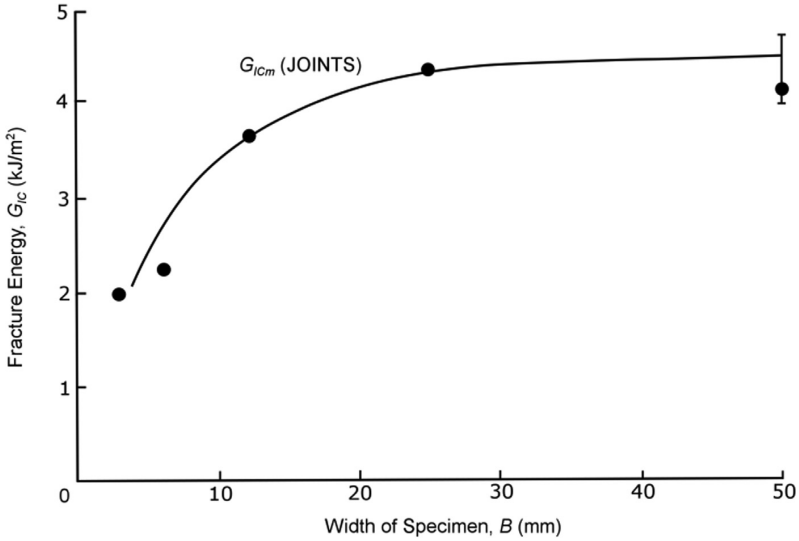

Fig. 2. Width effect over the fracture energy in a bonded joint [12] made with mild steel adherends with a toughened epoxy adhesive. The points represent specimens with a similar bondline thickness (within 0.65 mm and 0.85 mm) but with different widths.

from plane stress in a very thin specimen to plane strain near the centre of a wide plate and, consequently, the degree of plasticity that develops at the crack tip varies [12]. For wide specimens, the plane-stress to plane-strain zone transition remains small enough in comparison with the total width of the adhesive layer so that it has little influence on the overall performance of the specimen.

However, all the previous works are based on studies with rigid bonded joints and experimental research is lacking for flexible bonded joints.

In relation to flexible adhesives, the influence of the stress distribution along the specimen width on the fracture behaviour of a bonded joint has been analysed in double cantilever beam (DCB) specimens [14,15]. The authors obtain a relationship between the equivalent fracture energy of the whole bonded joint ($J^{(eq)}$) and the fracture energy measured for a specific zone in the adhesive layer (the same bonded joint) that is purely under the plane-stress state, i.e. the external face of the bonded joint (J^{ext}):

$$J^{(eq)} = \xi^{(eq)}_{(B/t_a)} J^{ext} \tag{1}$$

where $\xi^{(eq)}_{(B/t_a)}$ is a correction factor that depends on the specimen width, B, and the bondline thickness, t_a, and where the adhesive's Poisson's ratio is ν_a. Thus, it is valid for any type of adhesive joint:

$$\xi^{(eq)}_{(B/t_a)} = 1 - \frac{\nu_a^2}{(1-\nu_a)} + \frac{6\nu_a^3}{(1-\nu_a)} \frac{[1 - e^{-(1/6\nu_a)(B/t_a)}]}{B/t_a} \tag{2}$$

In addition, in [14], the dimensionless parameter B/t_a is used to identify the stress state of an adhesive layer. Although the stress distribution in an adhesive layer is fully influenced by the Poisson ratio, the B/t_a ratio may define the equivalent stress state of the adhesive layer in a bonded joint. Low values for the B/t_a ratio may indicate a plane-stress-prevailing stress state and large values of B/t_a may indicate a plane-strain-dominated stress state.

Despite the simple approach in Eq. (1) being experimentally and numerically validated in [15] as a way to describe the stress state and its effect on the fracture toughness in a specific bonded joint, there is a lack of experimental work not only on a more general validation but also in terms of gaining a deeper understanding of the mechanisms explaining the dependence of the fracture energy on the specimen dimensions.

Following the recent analytical work in [15], the present contribution will focus on the analysis of the effect of the width-to-thickness ratio on the equivalent fracture energy of bonded joints with the same materials but with different widths and bondline thicknesses. Consequently, the present work has been structured as follows: First, Section 2 describes an analytical model developed to predict the fracture behaviour of bonded joints. Second, an experimental regime is enacted to validate the analytical model (Section 3). Then, the experimental results are shown in Section 4 and, finally, the suitability of the analytical model is discussed in Section 5.

2. Analytical model

Broadening the relation in Eq. (1) to relate the equivalent fracture toughness of bonded joints to different width-to-thickness configurations, the ($J^{(eq)}_{(B/t_a)}$) expression (1) is modified, resulting in:

$$J^{(eq)}_{(B/t_a)} = \xi^{(eq)}_{(B/t_a)} J^{(eq)}_{PS} \tag{3}$$

where $J^{(eq)}_{PS}$ is defined as the fracture toughness of a bonded joint whose B/t_a tends to zero, being purely under a plane-stress-prevailing stress state. However, $J^{(eq)}_{PS}$ is immeasurable due to its unrealistic configuration ($B/t_a \to 0$), whereas $J^{(eq)}_{(B/t_a)}$ might be obtained experimentally for any B/t_a-configured specimen. Since $J^{(eq)}_{PS}$ can be related to the fracture toughness of the bonded joint under plane-strain conditions as $J^{(eq)}_{PS} = J^{(eq)}_{PE} \big/ \xi^{(eq)}_{(B/ta\to\infty)}$, Eq. (3) is rewritten as follows:

$$J^{(eq)}_{(B/t_a)} = \frac{\xi^{(eq)}_{(B/t_a)}}{\xi^{(eq)}_{(B/t_a\to\infty)}} J^{(eq)}_{PE} \tag{4}$$

where according to Eq. (2) in the limit case:

$$\xi^{(eq)}_{(B/t_a\to\infty)} = 1 - \frac{\nu_a^2}{(1-\nu_a)} \tag{5}$$

Then, the equivalent fracture toughness under plane-strain conditions ($J^{(eq)}_{PE}$) is experimentally measurable by testing a large B/t_a-configured bonded joint and Eq. (4) can be solved.

Due to the almost incompressible nature of elastomeric flexible adhesives ($\nu_a \approx 0.5$), very pronounced lateral contractions are observed along the specimen sides near the crack tip (Fig. 3). As a consequence, the effective bondline width is shortened.

To link the effect of the stretch-shortening phenomenon to the fracture toughness, a geometrical relation $B^*(x)/t_a$ is defined in [14], which allows us to evaluate the effective bondline width $B^*(x)$ as a function of the adhesive bondline thickness t_a and adhesive Poisson ratio ν_a:

$$\frac{B^*(x)}{t_a} = \frac{B}{t_a} - \ln\left[\left(\frac{1-\nu_a-\nu_a^2+\psi_x}{(1+\nu_a)(1-2\nu_a)+\psi_x+\psi_{(B/2)}}\right)^{6\nu_a}\right] \tag{6}$$

where B is the apparent width of the underformed adhesive and ψ_x is a correction function that reads:

$$\psi_x = \nu_a^2 e^{\left(-\frac{x}{3\nu_a t_a}\right)} \tag{7}$$

The correction function $\psi_{(B/2)}$ in Eq. (6) is obtained by setting $x = B/2$ in Eq. (7). If Eq. (6) is written as a function of the $B^*(x)/B$ ratio,

$$\frac{B^*(x)}{B} = 1 - \frac{t_a}{B}\ln\left[\left(\frac{1-\nu_a-\nu_a^2+\psi_x}{(1+\nu_a)(1-2\nu_a)+\psi_x+\psi_{(B/2)}}\right)^{6\nu_a}\right] \tag{8}$$

then we have an analytical expression for the stretch ratio that depends on the measurable geometrical parameters B, t_a, and the Poisson ratio of the adhesive ν_a and x, where x is defined as the longitudinal displacement of the crack tip associated with the constitutive behaviour of the adhesive (the Poisson effect). When a DCB specimen with a flexible adhesive is subjected to an opening load, shear deformations appear in the adhesive layer and a concave-shaped crack front is produced. As shown in Fig. 4, the

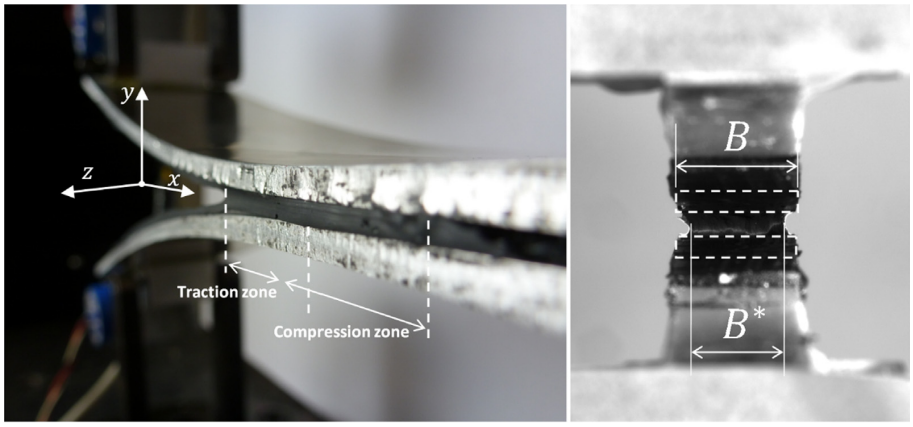

Fig. 3. Out-of-plane deformation of the adhesive layer in (a) the traction and compression zones, and (b) the total width of the specimen, where B is the total width of the specimen and B* is the effective width before fracture occurs.

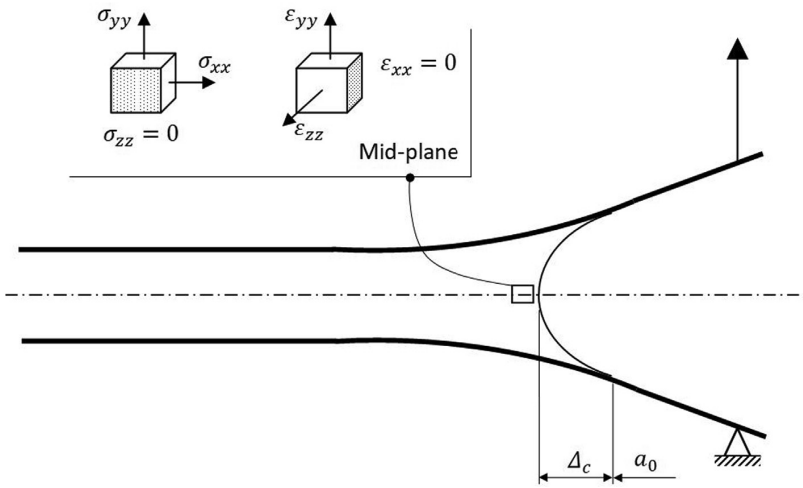

Fig. 4. Scheme of the strain and stress fields in the adhesive layer.

maximum longitudinal deformation due to the shear effect is located in the mid-plane of the adhesive layer (Δ_c), where, theoretically, the crack tip is located. Thus, it is considered that $x = \Delta_c$.

As the fracture energy measured during the tests depends on B^* and not on B, the measured value can be related to $J_{\mathrm{PE}}^{(eq)}$ by taking into account the $B^*(\Delta_c)/B$ ratio,

$$J_{(B/t_a)} = \frac{B^*(\Delta_c)}{B} J_{(B/t_a)}^{(eq)} = \frac{B^*(\Delta_c)}{B} \frac{\xi_{(B/t_a)}^{(eq)}}{1 - \frac{\nu_a^2}{(1-\nu_a)}} J_{\mathrm{PE}}^{(eq)} \tag{9}$$

where $J_{(B/t_a)}$ is the fracture energy measured during the test, as specified in equation (20) (Section 3.3).

2.1. Longitudinal displacement of the crack tip (Δ_c)

Since the previous development is based on the equivalent behaviour of bonded joints with different width-to-thickness configurations, the study of the longitudinal displacement Δ_c is also based on this statement. Thus, a transversal plane-stress-prevailing stress state ($\sigma_{zz} = 0$) and a longitudinal plane-strain-prevailing stress state ($\varepsilon_{xx} = 0$) are assumed for the following analysis (Fig. 4).

The strain tensor is defined in local terms:

$$\boldsymbol{\varepsilon} = \begin{pmatrix} 0 & \varepsilon_{xy} & 0 \\ \varepsilon_{xy} & \varepsilon_{yy} & 0 \\ 0 & 0 & \varepsilon_{zz} \end{pmatrix} \tag{10}$$

Using the constitutive equations for an isotropic linear elastic material, the stress tensor reads,

$$\boldsymbol{\sigma} = \lambda tr(\boldsymbol{\varepsilon})\mathbf{1} + 2\mu\boldsymbol{\varepsilon} \tag{11}$$

where the Lamé constants are $\lambda = E_a\nu_a/((1+\nu_a)(1-2\nu_a))$ and $\mu = E_a/(2(1+\nu_a))$. Thus, the following relation can be obtained:

$$\varepsilon_{zz} = \frac{\nu_a}{\nu_a - 1}\varepsilon_{yy}. \tag{12}$$

When the bonded joint is externally loaded, the adhesive layer accumulates some potential energy due to strains induced in it. This internal energy is denominated as elastic potential energy and reads,

$$\mathbb{U} = \int_V \hat{u}(\boldsymbol{\varepsilon}(\mathbf{u}))\mathrm{d}V \tag{13}$$

By considering a linear elastic analysis, the strain energy density can be written as follows:

$$\hat{u}(\boldsymbol{\varepsilon}) = \frac{1}{2}\boldsymbol{\varepsilon}\colon\boldsymbol{\sigma} \tag{14}$$

Then, following the expression in Eq. (14) and considering the strain and stress tensors in Eqs. (10) and (11), respectively, the strain energy density subjected to the internal elastic potential energy of the adhesive layer is obtained:

$$\hat{u}(\boldsymbol{\varepsilon}) = \frac{E_a}{2(1-\nu_a^2)}\varepsilon_{yy}^2 + \frac{E_a}{(1+\nu_a)}\varepsilon_{xy}^2 \tag{15}$$

The elastic potential energy reaches a maximum in the crack tip when a fracture occurs and, following the principle of minimum potential energy, the equilibrium condition is conformed as follows:

$$\frac{d\mathbb{U}}{dV} = \frac{E_a}{2(1-\nu_a^2)}\varepsilon_{yy}^2 + \frac{E_a}{(1+\nu_a)}\varepsilon_{xy}^2 = 0 \tag{16}$$

If Eq. (16) is solved, a relationship between the normal (ε_{yy}) and shear (ε_{xy}) strains is obtained:

$$\varepsilon_{xy} = \sqrt{\frac{1}{2(1-\nu_a)}}\varepsilon_{yy} \tag{17}$$

Finally, using Eq. (17), Δ_c can be expressed as a function of the opening displacement, since $\varepsilon_{xy} = \Delta_c/t_a$:

$$\Delta_c = \sqrt{\frac{1}{2(1-\nu_a)}}\delta_y \tag{18}$$

If Eq. (18) is introduced into Eq. (7), the expression for ψ_x is completed. However, note that the correction function still depends on the opening displacement, δ_y, and the thickness of the adhesive layer, t_a. From experimental evidence, as will be shown in the results section, it is observed that for a given flexible adhesive (with a specific ν_a), the $B^*(\Delta_c)/B$ ratio only depends on the B/t_a ratio. Thus, the effect of the lateral contraction is independent of the thickness of the adhesive layer, so $\delta_y = t_a$ is proposed. Thus, the final expression for the correction function is given as:

$$\psi_x = \nu_a^2 e^{\left(-\frac{1}{3\nu_a}\sqrt{\frac{1}{2(1-\nu_a)}}\right)} \tag{19}$$

As a result, the lateral contraction $B^*(\Delta_c)/B$ now depends on the width-to-thickness ratio and the Poisson ratio of the adhesive and, at the same time, integrates the shear effect through equation (17) (Fig. 5). Note that for an incompressible adhesive ($\nu_a = 0.5$), the $\varepsilon_{xy}/\varepsilon_{yy}$ ratio is 1.

3. Methodology

To evaluate the effect of the width-to-thickness ratio on the mode I fracture energy of a bonded joint, DCB tests were performed. Different specimens having different width-to-thickness ratios were manufactured to load the interface under the mode I condition. In addition, the elastic properties of the adhesive were determined by performing tensile tests on bulk adhesive dumbbell specimens and butt-squared joints. As demonstrated in [14], the apparent elastic behaviour of a joint bonded with an elastomeric adhesive is very sensitive to the Youngś modulus and Poisson's ratio. Thus, an accurate Young's modulus was obtained through the dumbbell tensile tests and, since the Poisson's ratio was very sensitive to this test, butt-squared joints were also tested. From these tests, the apparent Young's modulus was obtained, and an accurate Poisson's ratio was fitted, numerically reproducing the butt-squared joint tests with a finite element (FE) model. This procedure was successfully implemented in [14].

3.1. Determination of the elastic properties of the adhesive

A silicone-based type of adhesive, SIKASIL SG-500, supplied by SIKA, was used for this study. This two-component, high-

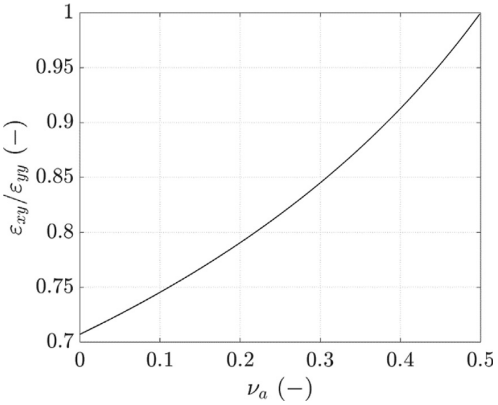

Fig. 5. Relationship between shear-normal strains and the Poisson ratio.

performance structural silicone-based adhesive was handled and cured under room temperature conditions for 72 h before testing. To determine the Young's modulus of the adhesive (Table 1), three dumbbell specimens were manufactured and tested following the ISO-37 standard procedure [16] (Fig. 6). In addition, the digital image correlation (DIC) technique was used to determine the Poisson's ratio.

According to the test results presented in Fig. 7, the Young's modulus and the Poisson's ratio varied with the increase in the measured engineering strain, which is consistent with the expected behaviour of an elastomeric material.

However, the Poisson's ratio was too sensitive to the dumbbell tensile tests and the procedure detailed in [17] was followed to validate an accurate Poisson's ratio (up to the 4th decimal). Therefore, two additional tensile tests were performed on butt joints with a squared section of 50 mm width and 2 mm thick bondline thickness. The adherends' relative displacement normal to the interface was measured using the DIC technique (Fig. 6b). Later, the apparent Young's modulus ($E_a^{'(eng)} = P/(B^2\varepsilon_y)$) for the interface was evaluated iteratively with numerical simulations of the butt-squared joint test using the commercial software ANSYS-Inc and by varying the adhesive's Poisson's ratio until the numerical results fitted the experimental data accurately (Table 1). The initial linear elastic regime of the test results (E_0, Fig. 7) was considered for the analysis.

3.2. Material and specimen design

DCB specimens were manufactured by bonding two aluminium adherends with a thickness of 3 mm and a length of 200 mm with the SIKASIL adhesive. High-strength aluminium alloy (type Al 7075-T6) with a yield strength of 550 MPa was used to prevent any plastic deformation during the test. A 71 GPa Young's modulus and a Poisson's ratio value of 0.33 are considered in the following. The aluminium substrates were first sanded then cleaned with acetone to remove the native metal oxide. Prior to bonding, the substrates were cleaned again with isopropyl alcohol to improve adhesion. Once the adhesive was applied and the adherends bonded, the specimens were left under ambient room temperature conditions to allow the crosslinking of the adhesive to occur.

Teflon-calibrated spacers were placed in between the adherends to guarantee a constant thickness of the adhesive layer throughout the whole specimen and also to specify a bondline edge. The bondline was thick enough to allow for a sharp initial crack to be produced by cutting the adhesive with a knife. The initial crack length was set to $a_0 = 40$ mm.

Several specimens having different bondline width-to-thickness ratios were manufactured within the range of $5 \leq B/t_a \leq 40$. For this purpose, two thicknesses were selected ($t_a = 0.5$ mm and $t_a = 2.0$ mm) with the width being varied within the interval of $5 \leq B \leq 50$.

3.3. DCB tests: Set-up and execution

The fracture energy was obtained via experimentation on DCB specimens. ISO-25217 [18] is the most widespread standardized method employed to measure fracture energy in structural adhesives, but it is not applicable to elastomeric adhesives since linear elastic fracture mechanic (LEFM) conditions may not be met during the tests due to the flexible behaviour of the adhesive and the large fracture process regions expected. Thus, a data reduction method independent of the crack length measurement was applied, the J-integral method, since it was successfully implemented in [19,20]. Following the set-up recommended in ISO-25217 and the data reduction procedure of the J-integral method, two NA3-30 capacitive inclinometers from SEIKA Mikrosystemtechnik GmbH were fixed to each adherend at each load application position to measure the rotation of the adherends, with this data being used to calculate the J-integral evolution during the test (Fig. 8) with the relation given by [21]:

$$J = \frac{P}{B}\theta_P, \tag{20}$$

where θ_P is the relative rotation between adherends at the applied load position with respect to the bondline of the DCB specimen, P is the applied load and B is the total specimen width, which is equal to the width of the adhesive layer according to the type of specimen tested. End blocks were bonded to the adherend to allow for the separation load application and special care was taken to align the loading points to minimize shear effects in mode I loading. Note that equation (20) is used to then apply equation (9).

All tests were carried out on a Zwick/Roell universal tensile testing machine under room temperature and 50% relative humidity conditions. They were run under a 2-mm/min constant displacement rate condition to ensure quasi-static crack growth according to the standard [18].

Eight different specimen batches were produced (T1 to T8): four batches with 2-mm-thick specimens (T1 to T4) and four more batches with 0.5-mm-thick specimens (T5 to T8). The main geometrical parameters are summarized in Table 2 as well as the number of specimens tested for each batch. The thickness assigned to each batch of specimens was related to the average thickness measured

Table 1
Mechanical properties of the adhesive. Average and standard deviation.

	SIKASIL SG-500
Young's modulus (MPa)	2.06 ± 0.54
Poisson's ratio (–)	0.4977 ± 0.0005

Fig. 6. (a) The prepared dumbbell specimens for the application of the DIC technique and (b) the DIC analysis on the butt-squared joint tensile tests.

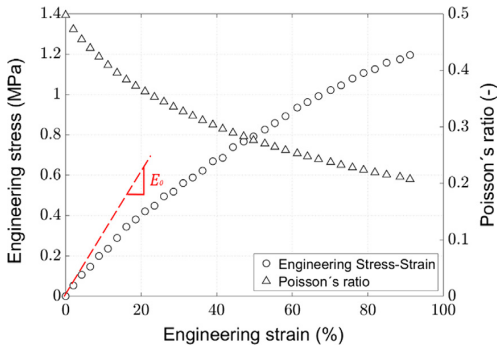

Fig. 7. Dumbbell tensile test results with the bulk SIKASIL SG-500 adhesive.

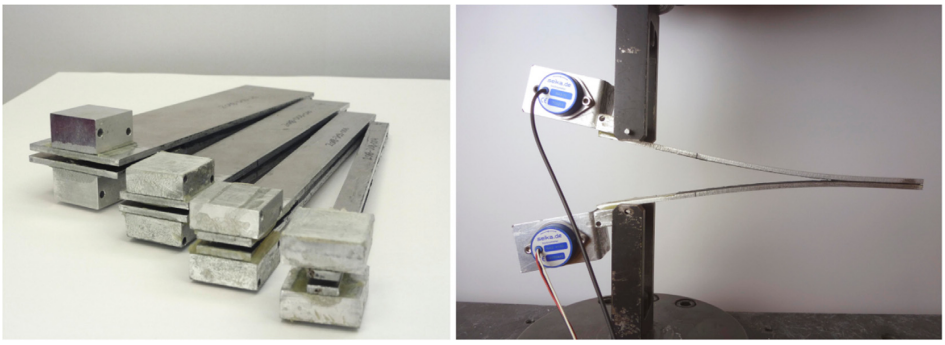

Fig. 8. (a) The manufactured specimens and (b) the DCB test in progress.

for each batch of specimens and the range between the maximum and minimum of these average values.

The test results for the 24 specimens are presented in Section 4. The analysis and discussion of the results are provided in Section 5.

4. Results

In the following subsections, the load-displacement curves and the results for the fracture toughness are explained. The code used

Table 2
Configuration of the specimens tested.

Batch	B/t_a	B (mm)	t_a (mm)	No. of specimens
T1	4.33	10	2.31 ± 0.24	4
T2	8.89	20	2.25 ± 0.21	3
T3	13.70	30	2.19 ± 0.10	3
T4	22.42	50	2.23 ± 0.12	4
T5	9.09	5	0.55 ± 0.00	2
T6	16.95	10	0.59 ± 0.03	3
T7	23.15	12.5	0.54 ± 0.03	3
T8	37.04	20	0.54 ± 0.03	2

to identify the test specimens is defined as no. batch (TX) followed by a 3-digit number (XXX) to ensure traceability between figures and specimens.

4.1. The fracture toughness's dependency on the width-to-thickness ratio

The load-displacement curves are presented in Figs. 9 and 10 for the T1 to T4 batch and the T5 to T8 batch, respectively. Cohesive failure predominated in most of the tests that were carried out. However, traces of adhesive failure were detected in some specimens, as follows:

- T2-005 and T2-006: at the beginning of the crack propagation.
- T5-016 and T7-022: at the end of the test.
- T7-024: in the middle of the crack-propagation process.

When some degree of adhesive failure did occur, lower values for the load and fracture toughness were obtained. However, these isolated events did not unduly affect the performance of the tests, since good repeatability was achieved. Cohesive failure was also present in large regions and the fracture path was long enough to stabilize. These zones, where full cohesive failure was not achieved (thus, having some eventual adhesive failure), were removed from the analysis. The curves that were obtained had the characteristic shape of a DCB test with non-linear behaviour due to the elasto-plastic behaviour of the adhesive.

Figs. 11 and 12 show the results of the J-integral versus the displacement. The J-integral was calculated using Eq. (20). Two regions can be distinguished in these curves: the first one is associated with loading up to the peak force value and the second one is associated with stable crack propagation. During the initial loading phase, the J-integral increases and a *plateau* value is reached when the crack propagation is initiated. Then, the J-integral stops increasing and fluctuates around the *plateau* value.

A fully cohesive and stable crack growth was observed from 25 mm and 15 mm of displacement (for the 2.0-mm- and 0.5-mm-thick specimens, respectively) and, from this point on, the fracture toughness was determined as the average value of the calculated J-integral over the next 20 mm. Good repeatability was also achieved for the J-integral results.

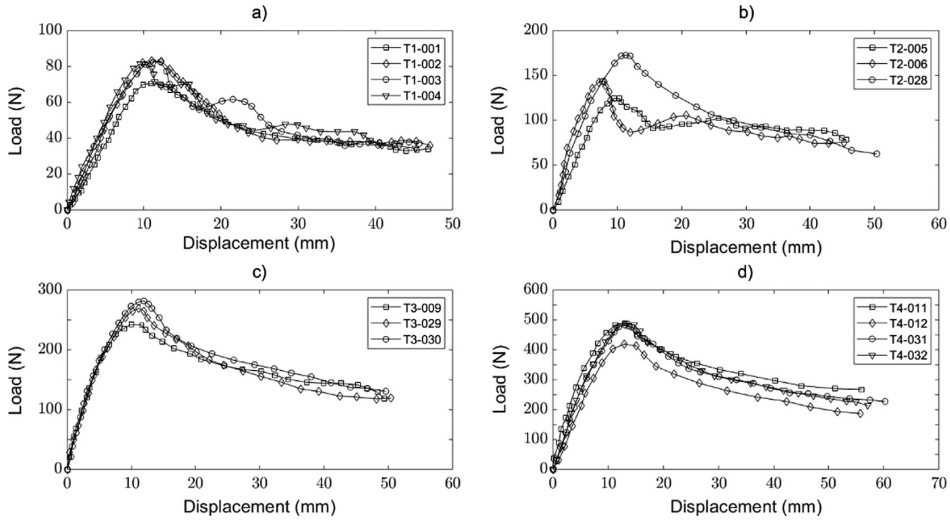

Fig. 9. Load-displacement curves for the 2-mm bondline thickness samples.

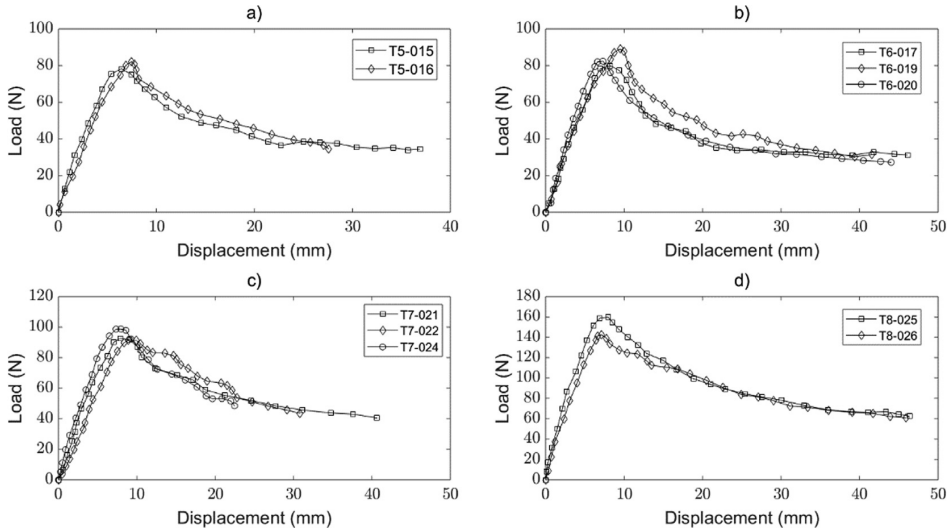

Fig. 10. Load-displacement curves for the 0.5-mm bondline thickness samples.

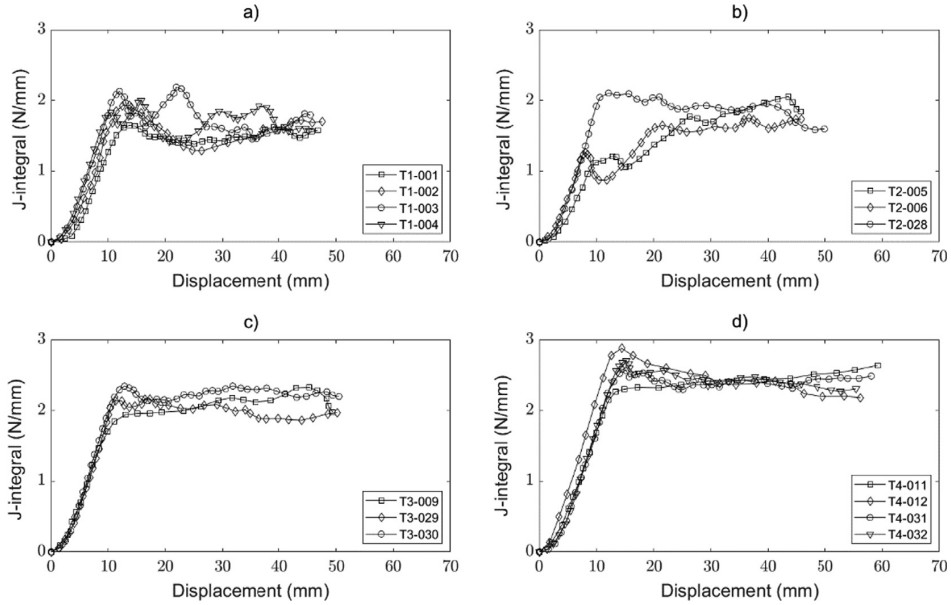

Fig. 11. J-integral displacement curves for the 2-mm bondline thickness samples.

In Fig. 13, the experimental results are compared with the analytical description in Eq. (9): First, for the experimental validation of the proposed analytical model and second, to explore the implementation of the analytical model for other adhesives.

To evaluate the accuracy of the correction proposed for the effect of the lateral contraction, the mean squared error (MSE) was estimated between the experimental data $J_{(B/t_a)}/J^{(eq)}_{(B/t_a)}$ and the analytical approach $B^*(\Delta_c)/B$ for different $B/t_a]_{PE}$ values (Fig. 14). The estimated MSE errors were 0.05 and 0.04 for t_a = 2.0mm and t_a = 0.5mm, respectively.

The fracture toughness predicted by the analytical curves in Eq. (4) and Eq. (9) is shown alongside the experimental results (average and standard deviation) in Fig. 15.

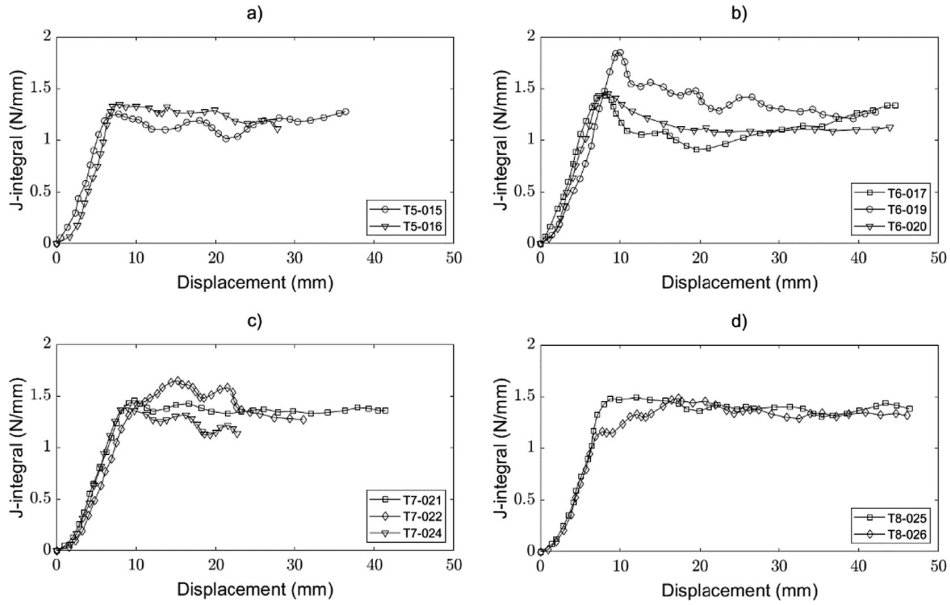

Fig. 12. J-integral displacement curves for the 0.5-mm bondline thickness samples.

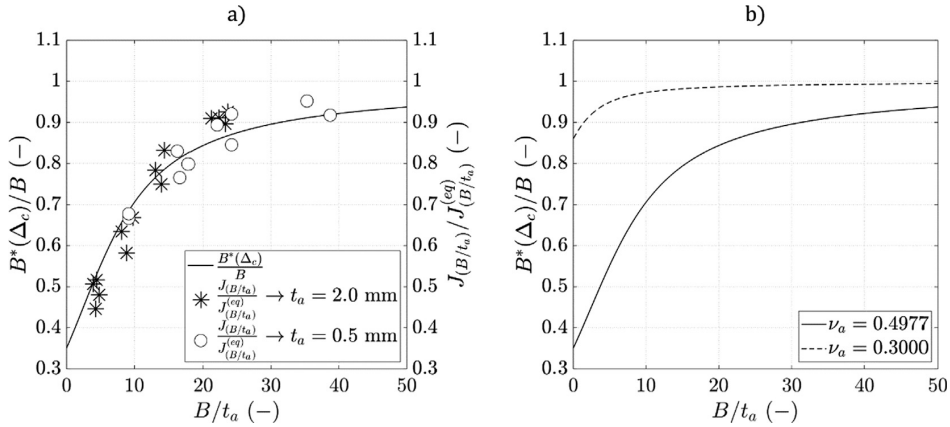

Fig. 13. (a) Experimental validation of the lateral contraction and (b) the lateral contraction for a rigid ($\nu_a = 0.3$) and an almost incompressible adhesive ($\nu_a = 0.4977$).

5. Discussion

The lateral contraction is independent of the bondline thickness, as demonstrated with the experimental data in Fig. 13a. If we assume that $\delta_y = t_a$ in Eq. (9), then this enables the correction $B^*(\Delta_c)/B$ to be independent of t_a, confirming that the fracture behaviour of a bonded joint is completely dominated by the stress state and emphasizing the need to consider the B/t_a ratio as a whole. Thus, the analytical curve given by $B^*(\Delta_c)/B$ for the lateral contraction accurately predicts the stretch-shortening phenomenon, as determined by the MSE analysis (Fig. 14).

The analytical model is valid for rigid and flexible adhesives, although it has not been experimentally validated for rigid adhesives (Fig. 13b). For flexible adhesives, the effective width may shorten by up to 65% when $B/t_a \rightarrow 0$, with the consequent effect on the prediction of the fracture toughness. In the case of rigid adhesives, the curve of the effective width is almost constant and drops by 13% when $B/t_a \rightarrow 0$. This means that the effect of the adhesive layer's elastic behaviour on the fracture toughness is much lower in the case of rigid adhesives than for flexible adhesives and this confirms the findings mentioned in [12] whereby there is an effect from the stress state in addition to the effect from plasticity.

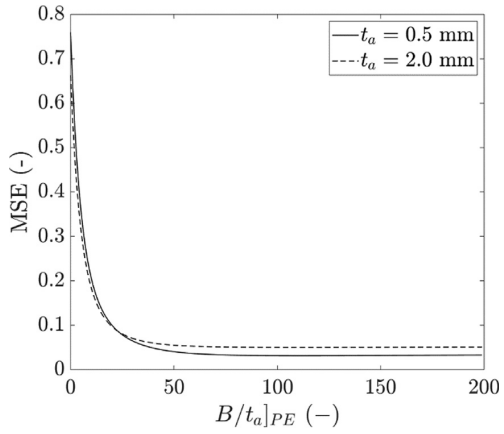

Fig. 14. Mean squared error for different plane-strain B/t_a ratios.

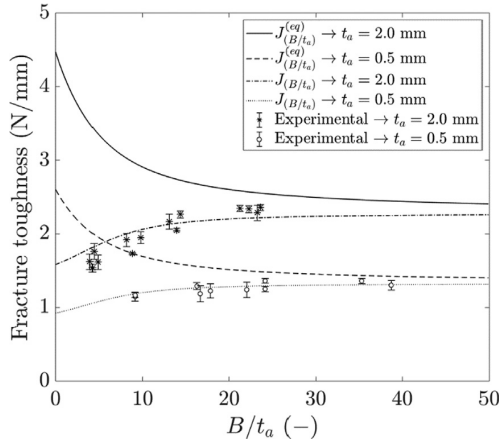

Fig. 15. Validation of the analytical prediction curves with experimental data in terms of fracture toughness.

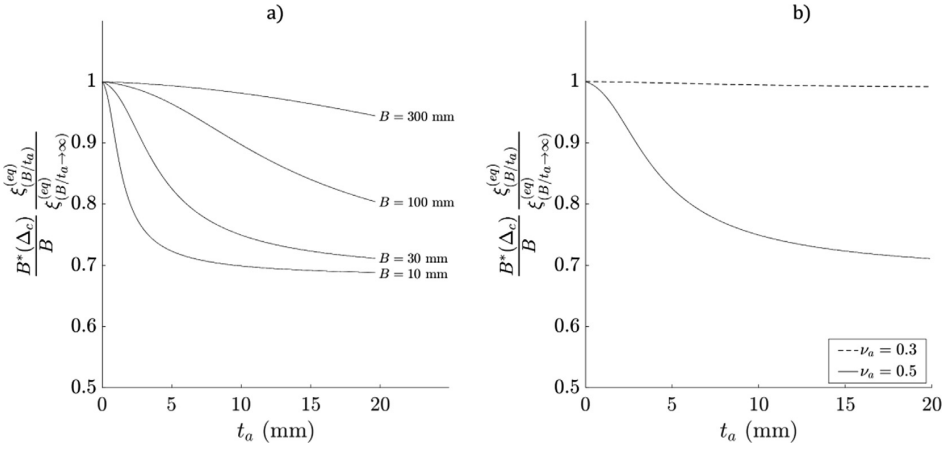

Fig. 16. Effect of the bondline thickness on the fracture toughness: (a) for different widths of a flexible adhesive, and (b) for 30-mm-wide rigid and flexible adhesives.

Therefore, since the analytical model in Eq. (4) does not capture the shortening of the effective width generated due to the elastic behaviour of the adhesive (Fig. 15), the correction in Eq. (8) needs to be added, as proposed in Eq. (9).

The experimental findings result in two curves being drawn (one for each bondline thickness), and these curves are also superposed by two different analytical curves, since $J_{\mathrm{PE}}^{(eq)}$ is different for each bondline thickness. Thus, the corrected analytical model accurately predicts the experimental data whatever the stress state is: Under plane-stress conditions, the curves drop in a non-parallel manner, and in plane-strain conditions, the fracture toughness is asymptotic and does not increase even though the total width increases.

The advantage of this method is that only the experimental results of a bonded joint with a specific B/t_{a} are needed to predict the fracture toughness of bonded joints of any width but with the same bondline thickness as the joint being tested. If the bondline thickness is changed, the $J_{\mathrm{PE}}^{(eq)}$ also changes and new tests must be performed.

Additionally, although the corrected analytical model is valid for rigid and flexible adhesives, the experimental evidence for rigid adhesives in [12] (Fig. 2) shows that other failure mechanisms may be involved in the fracture behaviour of rigid bonded joints, apart from the effect of the adhesive layer's elastic behaviour. In these cases, a new correction factor should be added to capture the additional failure mechanism, yet this aspect is out of the scope of the current article.

Different curves such as Type-A and Type-B curves (Fig. 1) are also obtained if the effect of the bondline thickness on the fracture toughness is analysed. This arises due to the effect of the stress state and the elastic behaviour of the adhesive. If Eq. (9) is analysed according to the effect of the bondline thickness, we get:

$$\frac{J_{(B/t_{\mathrm{a}})}}{J_{\mathrm{PE}}^{(eq)}} = \frac{B^*(\Delta_c)}{B} \frac{\xi_{(B/t_{\mathrm{a}})}^{(eq)}}{\xi_{(B/t_{\mathrm{a}}\to\infty)}^{(eq)}} \tag{21}$$

Thus, the effect of the bondline thickness on the fracture toughness can be evaluated merely by fixing the rest of the variables in Eq. (21) (Fig. 16).

Small total-width values may represent the Type-B curve since large values of the total width may be closer to a Type-A behaviour (Fig. 16a). A similar trend is captured with the variation in the Poisson's ratio. The curve for a flexible adhesive ($\nu_{\mathrm{a}} = 0.5$) may represent the Type-B curve, and for rigid adhesives ($\nu_{\mathrm{a}} = 0.3$), Type A might be closer (Fig. 16b).

However, note that in the case of very small bondline thicknesses ($t_{\mathrm{a}} \to 0$), the curves do not decrease as anticipated in [6] for rigid adhesives. In these cases, additional failure mechanisms such as plasticity may be involved, which are not captured by the proposed correction.

6. Conclusions

A new method is proposed to evaluate the fracture toughness of bonded joints according to the type of adhesive used and the geometrical parameters of the width and bondline thickness. Unlike the analytical models proposed in the literature (which do not reproduce the experimental results when plane-strain conditions are not satisfied), the current article proves that the width-to-thickness ratio must be considered as a whole since the fracture behaviour of a bonded joint is influenced by its stress state. Consequently, the elastic behaviour of bonded joints was analysed and its effect on the fracture toughness was evaluated. However, it has only been validated for flexible adhesives and additional failure mechanisms such as plasticity may be involved in the case of rigid adhesives.

Since the mismatch between the analytical predictions and the experimental results may have been produced due to the flexible behaviour of the adhesive layer, a constitutive analysis of the adhesive layer was carried out. Additionally, observations during the experimental stage confirmed that there were lateral contractions of the adhesive layer and that the effective width was shortened due to the Poisson's effect. Thus, the correction $B^*(\Delta_c)/B$ was proposed and its independent behaviour on the bondline thickness was identified.

Hence, a new method is suggested herein, the main advantage of which is that only the experimental results of a bonded joint with a specific B/t_{a} are needed to predict the fracture toughness of bonded joints of any width but with the same bondline thickness as the joint being tested. Owing to the method only having been validated for flexible adhesives, future work should focus on the analysis of additional failure mechanisms of joints bonded with rigid adhesives or small bondline thicknesses.

Acknowledgements

The authors gratefully acknowledge the financial support of the Spanish government through the "Ministerio de Economía y Competitividad" under the contract TRA2015-71491-R.

References

[1] Carlberger T, Stigh U. Influence of layer thickness on cohesive properties of an epoxy-based adhesive – An experimental study. J Adhes 2010;86:816–35. https://doi.org/10.1080/00218464.2010.498718.

[2] Azari S, Papini M, Spelt JK. Effect of adhesive thickness on fatigue and fracture toughened epoxy joints – Part I: Experiments. Eng Fract Mech 2011;78:153–62. https://doi.org/10.1016/j.engfracmech.2010.06.025.

[3] Cooper V, Ivankovic A, Karac A, McAuliffe D, Murphy N. Effects of bond gap thickness on the fracture of nano-toughened epoxy adhesive joints. Polymer 2012;53:5540–53. https://doi.org/10.1016/j.polymer.2012.09.049.

[4] Campilho RDSG, Moura DC, Banea MD, da Silva LFM. Adhesive thickness effects of a ductile adhesive by optical measurement techniques. Int J Adhes Adhes 2015;57:125–32. https://doi.org/10.1016/j.ijadhadh.2014.12.004.
[5] Quan D, Murphy N, Ivankovic A. Fracture behaviour of a rubber nano-modified structural epoxy adhesive: Bond gap effects and fracture damage zone. Int J Adhes Adhes 2017;77:138–50. https://doi.org/10.1016/j.ijadhadh.2017.05.001.
[6] Lee D, Ikeda T, Miyazaki N, Choi N. Effect of bond thickness on the fracture toughness of adhesive joints. J Eng Mater Technol 2004;126:14–8. https://doi.org/10.1115/1.1631433.
[7] Khoo TTR, Kim H. Effect of bondline thickness on mixed-mode fracture of adhesively bonded joints. J Adhes 2011;87:989–1019. https://doi.org/10.1080/00218464.2011.600668.
[8] Marzi S, Biel A, Stigh U. On experimental methods to investigate the effect of layer thickness on the fracture behavior of adhesively bonded joints. Int J Adhes Adhes 2011;31:840–50. https://doi.org/10.1016/j.ijadhadh.2011.08.004.
[9] Boutar Y, Naïmi S, Mezlini S, da Silva LFM, Ben M. Sik Ali, Characterization of aluminium one-component polyurethane adhesive joints as a function of bond thickness for the automotive industry: Fracture analysis and behavior. Eng Fract Mech 2017;177:45–60. https://doi.org/10.1016/j.engfracmech.2017.03.044.
[10] Kinloch AJ, Shaw SJ, Tod A, Hunston DL. Deformation and fracture behaviour of rubber-toughened epoxy: 1. Microstructure and fracture studies. Polymer 1983;24:1341–54. https://doi.org/10.1016/0032-3861(83)90070-8.
[11] Pardoen T, Ferracin T, Landis CM, Delannay F. Constraint effects in adhesive joint fracture. J Mech Phys Solids 2005;53:1951–83. https://doi.org/10.1016/j.jmps.2005.04.009.
[12] Kinloch AJ, Shaw SJ. The fracture resistance of a toughened epoxy adhesive. J Adhes 1981;12:59–77. https://doi.org/10.1080/00218468108071189.
[13] da Silva LFM, Dillard DA, Blackman B, Adams RD. Testing adhesive joints. Best practices: Wiley; 2012.
[14] Cabello M, Zurbitu J, Renart J, Turon A, Martínez F. A general analytical model based on elastic foundation beam theory for adhesively bonded DCB joints either with flexible or rigid adhesives. Int J Solids Struct 2016;94–95:21–34. https://doi.org/10.1016/j.ijsolstr.2016.05.011.
[15] Cabello M, Zurbitu J, Turon A, Sarrado C, Renart J, Martínez F. Influence of the specimen width on the experimental measurement of the cohesive law using the J-Integral approach. In: 17th Eur. Conf. Compos. Mat.; 2016.
[16] ISO-37. Rubber, vulcanized or thermoplastic – Determination of tensile stress-strain properties, Tech. Rep., Int. Org. Stdzn.; 2017.
[17] Cabello M, Zurbitu J, Renart J, Turon A, Martínez F. A non-linear hyperelastic foundation beam theory model for double cantilever beam tests with thick flexible adhesive. Int J Solids Struct 2016;80:19–27. https://doi.org/10.1016/j.ijsolstr.2015.10.017.
[18] ISO-25217. Determination of the Mode I Adhesive Fracture Energy of Structural Adhesive Joints Using Double Cantilever Beam and Tapered Double Cantilever Beam Specimens, Tech. rep., Rep., Int. Org. Stdzn.; 2009.
[19] Cabello M, Turon A, Zurbitu J, Renart J, Martínez F. Progressive failure analysis of DCB bonded joints using a new elastic foundation coupled with a cohesive damage model. Eur J Mech A-Solids 2017;63:22–35. https://doi.org/10.1016/j.euromechsol.2016.12.004.
[20] Sarrado C, Turon A, Renart J, Costa J. An experimental analysis of the fracture behaviour of composite bonded joints in terms of cohesive laws. Compos Pt A-Appl Sci Manuf 2016;90:234–42. https://doi.org/10.1016/j.compositesa.2016.07.004.
[21] Paris AJ, Paris PC. Instantaneous evaluation of J and O-star. Int J Fract 1988;38:19–112.

Paper B

Using acoustic emissions (AE) to monitor mode I crack growth in bonded joints

J. Manterola[a], M. Aguirre[a], J. Zurbitu[a], J. Renart[b], A. Turon[b], I. Urresti[a]

[a]Ikerlan Technology Research Centre, Applied Mechanics Area, Mondragón, Spain

[b]AMADE, Polytechnic School, Universitat de Girona, Girona, Spain

The paper has been published in
Engineering Fracture Mechanics Vol. 224, 106778, 2020.

Engineering Fracture Mechanics 224 (2020) 106778

Contents lists available at ScienceDirect

Engineering Fracture Mechanics

journal homepage: www.elsevier.com/locate/engfracmech

Using acoustic emissions (AE) to monitor mode I crack growth in bonded joints

J. Manterola[a,*], M. Aguirre[a], J. Zurbitu[a], J. Renart[b,c], A. Turon[b], I. Urresti[a]

[a] Applied Mechanics Area, Ikerlan Technology Research Centre, P°.J.M°. Arizmendiarrieta, 2, 20500 Arrasate-Mondragón, Spain
[b] AMADE, Polytechnic School, University of Girona, Campus Montilivi, s/n, 17071 Girona, Spain
[c] Serra Húnter Fellow, Generalitat de Catalunya, Spain

ARTICLE INFO

Keywords:
Bonded joint
Mode I
Fracture testing
Acoustic Emissions (AE)
Crack monitoring

ABSTRACT

The usual way to evaluate the fracture toughness of bonded joints is via experimental characterization of the critical strain energy release rate. Different test procedures and data reduction methods for mode I fracture characterization can be found in the literature, such as ISO-25217, where crack length measurement is required. However, obtaining an accurate visual determination of crack length is often a challenge due to large fracture process zones (FPZ) and difficulties in reaching the bonded path. To compensate, structural health monitoring (SHM) techniques such as embedded Fiber Bragg Grating (FBG), digital image correlation (DIC), backface strain gauges and ultrasonic inspection are used as crack length monitoring. However, experimental work demonstrates the need for experimentation with non-intrusive methods. In the present work, acoustic emission (AE) testing is proposed to measure mode I crack growth in bonded joints. This is valid both for rigid adhesives with a small FPZ ahead of the crack tip and for flexible adhesives in which a correlation between AE event location and external analytical and numerical models confirm that a large FPZ is behind the crack tip. A correlation between the AE source location, visual location and numerical models determines the nature of AE events during the fracture process.

1. Introduction

Damage tolerance to a mode I fracture determines the quality of a bonded joint. The quality is evaluated by fracture strength and toughness, and experimental tests are needed to determine the critical strain energy release rate (critical SERR). According to Griffith, the critical SERR or energy required to create new surfaces during fracture must be balanced by a decrease in stored elastic energy in the material [1]. The test procedures and data reduction methods available in the literature, such as in ISO-25217 [2], to characterize mode I fractures in bonded joints strongly depend on crack length measurement. This is because small errors or subjectivity in crack length measurement can result in large variances in fracture energy calculations. Moreover, an accurate visual determination of crack length is often difficult to obtain due to large fracture process zones (FPZ), barely visible crack propagations (typical in mode II cracking) and obstacles to reaching the bonded path. As shown in [3] on double cantilever beam (DCB) bonded specimens, large FPZs can develop ahead of the crack tip as a consequence of the elasto-plastic behaviour of the adhesive; when dealing with flexible adhesives, this FPZ may extend several millimetres [4]. Further, bonded joints in real structures are hidden, and visual crack length measuring is not always possible.

* Corresponding author.
E-mail address: jmanterola@ikerlan.es (J. Manterola).

https://doi.org/10.1016/j.engfracmech.2019.106778
Received 24 July 2019; Received in revised form 4 October 2019; Accepted 8 November 2019
Available online 07 December 2019

Nomenclature

A_{th}	signal peak amplitude threshold
a	visual crack length
a_c	corrected crack length
B	total width of the specimen
C	compliance
D	distance between sensors
d	distance from first hit sensor
F	large-displacement correction
G_{IC}	mode I fracture toughness
l_1	distance from the centre of the loading pin to the mid-plane of the adherend
l_2	distance from the loading-pin centre to the edge of the block
N	load-block correction
P	opening load
V	velocity of dispersion of waves
Δ	crack length correction factor
$\Delta_{\text{AE}-a}$	distance between visual crack length (a) and AE source.
ΔT	arrival time delay
δ	opening displacement
$\sigma_y^{\max}$	maximum normal stress
AE	acoustic emission
AVG	average
CBBM	compliance-based beam method
CBT	corrected beam theory
CCD	charge-coupled device
CFRP	carbon fibre reinforced polymer
CHAN	channel
DCB	double cantilever beam
DIC	digital image correlation
FBG	Fiber Bragg Grating
FE	finite element
FPZ	fracture process zone
LUCY	location uncertainty
NDT	non-destructive techniques
OBR	optical backscatter reflectometer
PLB	pencil lead break
SD	standard deviation
SERR	strain energy release rate
SHM	structural health monitoring

For laboratory purposes, alternative data reduction methods which do not require crack length measurement, as well as an equivalent crack length estimate technique, are available in the literature (e.g. the J-integral method [5] and the compliance-based beam method (CBBM) [6], respectively). However, these methods lack applicability in real structures. For structural health monitoring (SHM) purposes, non-destructive techniques (NDT) are of great interest due to their capacity to examine materials and components without changing or destroying their usefulness. NDTs comprise different crack length monitoring techniques [7], such as strain measurement techniques, ultrasonics and acoustic emissions (AE). They can be classified in three different groups: non-contacting techniques, embedded sensors and backface techniques.

Non-contacting techniques such as high-speed photography help during image processing to reduce subjectivity in the visual measurement of the crack tip, even when monitoring high crack growth rates [8]. Alternatively, [9] demonstrates how digital image correlation (DIC) software can be used to analyse displacements in successive images recorded during fracture tests. This allows the zero-vertical displacement of the adherends in mode I to be identified continuously, provided the crack tip is located at this point because the DIC signal will be lost on the edge of the adherends. Despite the increased accuracy afforded by this technique, crack length measurement is still subjective because the location of the crack tip is determined by observation and assumptions. Further, differentiation between elastic deformation and breakage is not evident. Advanced thermographic methods are also used to monitor the crack growth by analysing external surfaces [10,11]. Despite its accuracy even in cases when cracking is not visible [10], thermography only works when the rise of temperature around the crack tip is high enough [11]. However, scanning is not required and the access to measure is just from one side of the specimen.

Sensors can be also embedded in bonded joints, be they in the adherends when composite laminates are used [12,13], in the adhesive layer [14] or in the interface between the adherend and the adhesive [15]. The most commonly used sensor is the Fiber Bragg Grating (FBG), which provides strain distribution measurements along the bonded joint. The crack tip and FPZ are detected by interpreting variations in the longitudinal strain distribution. As a further step, in [16] a sensor-free SHM is observed to form a built-in sensing network with graphene nanoparticles diffused in fibre-reinforced polymers. Using this network, guided ultrasonic waves are transmitted at any site of the composite component, and there is no need to attach any conventional ultrasonic transducer. However, embedding sensors complicates the composite manufacturing, and monitoring strategy must be foreseen before the manufacturing process.

Backface techniques consist of attaching sensors to the outer surface of adherends so as to monitor the behaviour of the bonded joint during testing. Different techniques with different levels of sophistication exist to characterize the crack length of a bonded joint. For example, in [17], a simple micrometre is used to find the zero-vertical displacement of the adherends (assuming the crack tip is located at this point). Alternatively, in [18] strain gauges are bonded along the central line of a thin adherend to perform an asymmetric test. Longitudinal strains on the thin adherend are measured and, to estimate the crack length, strain gauge measurements are interpreted using simple beam theory. More sophisticatedly, optical fibres can bond to the outer face of the adherend to yield a higher spatial resolution using such technologies as an optical backscatter reflectometer (OBR) [19,20]. The ability to characterize crack length in bonded joints tested in static [19] and fatigue [20] conditions makes the fibre optic a versatile technology. However, these technologies use fungible components and produce only external information of the bonded joint.

In ultrasonic analysis, ultrasonic waves are transmitted into materials to detect internal flaws or for characterization purposes. Ultrasonic devices are widely used for the local inspection of aerospace structures composed of multi-layer, adhesively bonded metallic and composite components that are difficult to access. In multi-layer metallic components, wave propagation [21] and the

localization of hidden defects such as fatigue cracks and localized disbonds [22] are analysed using high-frequency guided ultrasounds. In [23], defect sizes created in multi-layer composite bonded structures are evaluated. Nevertheless, continuous information about the evolution of components condition is lacking when using ultrasonic technology.

AE testing provides continuous real-time information about structures. Some literature exists about detecting, locating and identifying damage events to predict failure in early stages—such as [24]'s reference to timber structures. These damage events may be produced by deformations, crack formation, corrosion or defects, and AE can be deployed within a wide range of applications (e.g. fabrication processes, pressure equipment, aerial structures, aerospace structures, bonded joints and composite structures). Regarding composite structures, different types of damage mechanisms such as fibre breakage, core failure, matrix cracking or debonding are studied using AE techniques in delamination of sandwich structures [25] and woven composites [26]. Moreover, in [27], the delamination damage evolution is monitored using AE in unidirectional CFRP specimens and acoustic activity is analysed to identify the delamination onset and crack propagation. The fracture process of concrete and masonry structures is also analysed with AE testing [28–30]. In [28], the spatial distribution of damage is characterized using AE signals emerging from the growing of cracks in a concrete specimen. Further, the crack propagation is localized using AE in a repaired multiple leaf stone masonry [29] and in an FRP-concrete beam [30], proving the effectiveness of the AE technique in bi-material structural components. Regarding bonded structures, [31] shows how AE events are produced following the pencil lead break (PLB) test procedure, and wave propagation on a present adhesive layer is analysed in bonded large aluminium sheets at different distances and source orientations. The study provides guidance for locating and identifying AE events occurring within adhesive joints, but neither fracture tests nor adhesive cracking are examined. In [32], a modal AE analysis of mode I and mode II fractures is carried out. AE source events are analysed, and location and identification guidance is provided. A correlation between AE source location and the visually observed crack front is suggested, but there lacks experimental evidence for any rigorous conclusions, especially since the presence of an FPZ ahead of the crack tip also denotes damage [4].

These studies exemplify the lack of experimental data on techniques such as AE that do not use fungible sensors to detect, locate and identify cracks when obtaining the fracture properties of bonded joints with metallic adherends. In the present study, AE's applicability for continuous real-time crack growth monitoring in bonded joints is studied as an alternative to visual crack length measurement. Rigid and flexible bonded joints are tested, and AE sensors are attached to produce AE events for identification and location purposes. A correlation between AE source location, visual location and finite element (FE) models determines the nature of AE events during the fracture process. The present work is structured as follows: Section 2 describes the methodology for AE application and numerical analysis. Experimental and numerical results are discussed in Section 3.

2. Methodology

DCB specimens bonded with a rigid and a flexible adhesive were manufactured to analyse the suitability of the AE monitoring technique to any bonded joint. The DCB test protocol was applied per the ISO-25217 standard to generate mode I fracture paths in the bonded joints. Acoustic sensors were coupled to the specimens to process the acoustic events generated during crack growth. The location results of the acoustic events were compared with the visually tracked crack propagation, a, and other estimations of the crack length (such as the corrected crack length, a_c) or the fracture toughness (G_{IC}) were evaluated following the corrected beam theory (CBT) data reduction [2]. FE simulations were carried out to correlate the experimental evidence to the fracture process.

2.1. Experimental campaign

DCB specimens were manufactured by bonding two aluminium adherends 3 mm thick and 200 mm long. High-strength aluminium alloy (type Al 7075-T6) adherends with a Young's modulus of 71 GPa and a yield strength of 550 MPa were used to prevent plastic deformation during the test. Two bicomponent high-strength structural adhesives were selected: Araldite 2021 (A2021), a methacrylate rigid adhesive, and Sikasil SG500 (SG500), a silicone-based flexible adhesive. Six specimens were manufactured in total, three for each type of adhesive.

Aluminium substrates were first roughly filed (rigid adhesive) or sanded (flexible adhesive), then cleaned with acetone to remove the native metal oxide. Prior to bonding, the substrates were cleaned again with isopropyl alcohol to improve adhesion. Teflon calibrated spacers of 0.5 mm were placed between the adherends to guarantee constant thickness of the adhesive layer throughout the whole specimen and to delimit an edge in the crack front. The specimens were cured for 72 h under ambient room temperature conditions to allow for adhesive crosslinking, as per the cure time specifications given by the manufacturer. A sharp artificial crack was produced by cutting the adhesive with a sharp edge, and the initial crack length was measured. All manufactured specimens had a total width of 25 mm and an average bondline thickness of 0.80 mm and 0.86 mm for the rigid and flexible bonded joints, respectively. Two specimens were manufactured with each type of adhesive, making four specimens in total.

Finally, end blocks were bonded to the adherends to apply the load for the DCB tests. The specimens were painted with white spray, and a ruler was marked on the lateral side of the joint to allow visual measurement of the crack's length during testing, as suggested by the ISO-25217 test standard.

2.1.1. Fracture tests

DCB tests were run on a Zwick/Roell universal tensile testing machine at a constant displacement rate of 2 mm/min to ensure quasi-static crack growth. The tests were run at room temperature and under 50% relative humidity conditions per the ISO-25217 test standard. The mode I crack position was recorded using a high-performance optical system: a CCD camera (Manta G-917, ALLIED

Vision Technologies GmbH) and a high-resolution, high-speed optical lens (Xenoplan 2.8/50, Schneider Kreuznach). Per the ISO-25217 test standard, 65 mm of crack propagation was allowed in all tests, and the crack length on the external face of the adhesive layer was tracked visually from the initiation of the crack with a resolution of 0.0198 mm per pixel; then every 1 mm in the first 10 mm of crack propagation; subsequently every 5 mm in the next 50 mm; and finally, every 1 mm in the last 5 mm. The CBT data reduction method proposed in ISO-25217 was applied to evaluate the crack length by correcting the visual crack length as follows:

$$a_c = a + |\Delta|, \tag{1}$$

where Δ is the crack length correction factor. Δ was found by plotting the cube root of the normalized compliance, $y = (C/N)^{1/3}$, as a function of crack length a. The compliance ($C = \delta/P$) was normalized considering the load-block correction N since load blocks were used to apply the opening load (P) and displacement (δ) on the bonded joint. Then, a linear fit was extrapolated through the data in the plot $y - a$ to yield Δ as the x-intercept of the function $y = 0$.

According to CBT data reduction method, the fracture toughness was evaluated using the following equation:

$$G_{IC} = \frac{3P\delta}{2B(a + |\Delta|)}\frac{F}{N}, \tag{2}$$

where B is the total width of the bonded area and F is the large-displacement correction.

Corrections F and N were calculated following Eqs. (3) and (4), respectively:

$$F = 1 - \frac{3}{10}\left(\frac{\delta}{a}\right)^2 - \frac{3}{2}\left(\frac{l_1\delta}{a^2}\right), \tag{3}$$

$$N = 1 - \left(\frac{l_2}{a}\right)^3 - \frac{9}{8}\left[1 - \left(\frac{l_2}{a}\right)^2\right]\frac{l_1\delta}{a^2} - \frac{9}{35}\left(\frac{\delta}{a}\right)^2, \tag{4}$$

where l_1 is the distance from the centre of the loading pin to the mid-plane of the adherend to which the load-block is attached and l_2 is the distance from the loading-pin centre to the edge of the block in the longitudinal direction.

2.1.2. Acoustic emissions technique

AE monitoring, defined in ASTM E1316 as 'the class of phenomena whereby transient elastic waves are generated by the rapid release of energy from localized sources within a material' [33], involves measuring the mechanical vibration energy (acoustic emissions) emitted by bonded joints after a sudden change or movement during testing (e.g. cracking or plastic deformation). These acoustic waves propagate from the source throughout the structure in an omni-directional manner with a velocity of dispersion (V in Fig. 1). An AE sensor in contact with the material being monitored detects the mechanical shock wave and converts the low-displacement, high-frequency mechanical wave into an electric signal, amplified by a pre-amplifier and processed by the AE instrument [34]. Recorded data can then be used to determine the location of the AE event (d in Fig. 1) between two sensors at a known distance (D in Fig. 1) by processing the arrival time delay in each sensor (ΔT in Fig. 1).

For location purposes, four AE piezoelectric sensors (VS45-H, Vallen Systeme GmbH) were coupled to the adherends with an external 34 dB pre-amplifier. An elastic sticky band was used to produce hold-down pressure on the contact surface between the AE sensors and the aluminium adherends while measurements were being taken, and a viscous gel was used to ensure continuity of the AE between the sensors and adherend surface (Fig. 2). The AE device used to process the acoustic signal was a 4-channel AE system

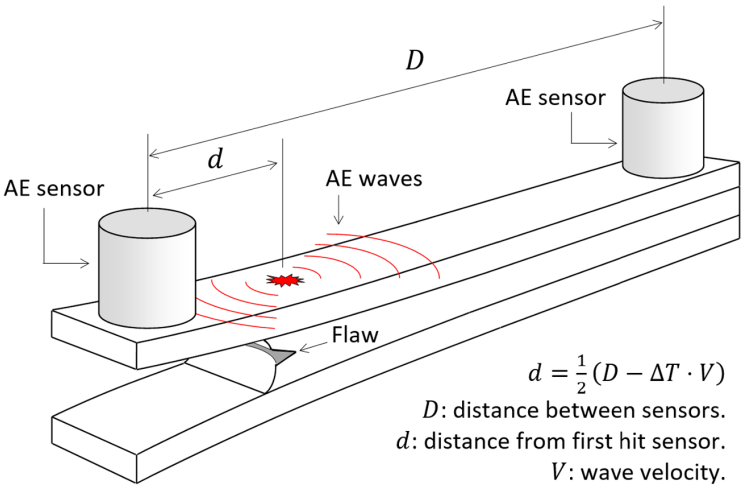

Fig. 1. Scheme of acoustic emissions (AE) principle.

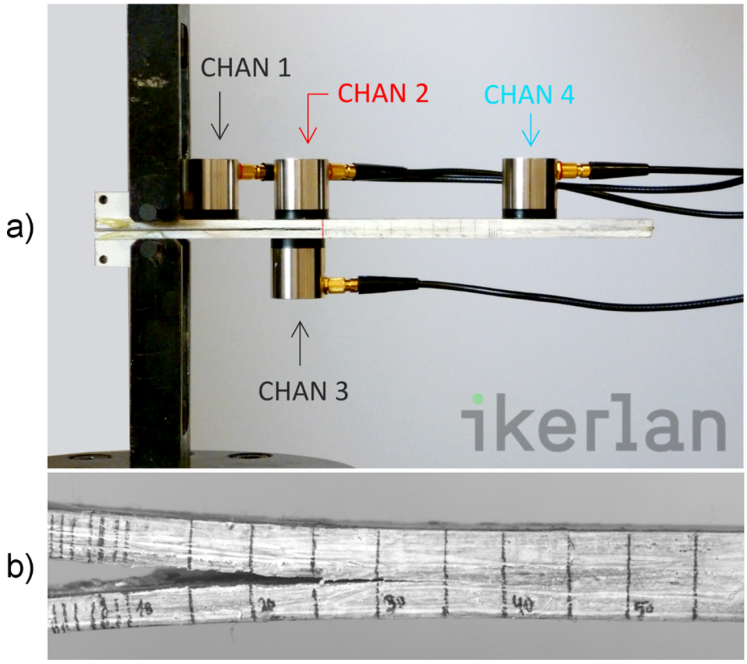

Fig. 2. (a) Test set-up with fastened AE sensors. (b) Crack growth tracking.

model (AMSY-6, Vallen Systeme GmbH).

AE sensors were attached to the adherends in a longitudinal direction by measuring the distance from absolute 'zero' to the centre of the sensor with a calliper. The zero reference is located at the left extreme of the specimen's adherend, where adhesive was not applied. Later, the PLB test (also termed Hsu-Nielsen-Source) was applied to check the correct coupling of the AE sensors and to evaluate the acoustic attenuation of the structure. This technique consists of breaking a pencil lead (usually 2H, 0.3 mm) against the structure under a defined angle so that an acoustic event is produced and detected by the AE system. Per the reference system, the locations of these events were calculated using the group velocity of dispersion curves given by Vallen Dispersion software. The group velocity was calculated by setting an aluminium sheet with a thickness of 3 mm for both types of adhesive. AE sensors were able to record AE waves in a frequency range from 40 kHz to 450 kHz. Within these frequency values, the fastest type of Lamb wave was the symmetric wave (S_0) with a group velocity of 5200 m/s, which was quite stable. One output channel (CHAN) was assigned to each AE sensor (Fig. 2): channels 2 and 4 (CHAN2 and CHAN4, respectively) were used for the longitudinal location of the acoustic events; CHAN1 was used to measure location uncertainty (LUCY) by evaluating the time delay between each pair of sensors (triangulation); CHAN3 was assigned as a guard sensor to avoid external noise in measurements (e.g. from test tools). As the minimum sensor quantity for 1D location is two, each pair of sensors estimates a location and the location difference in each acoustic event indicates the LUCY. Furthermore, acoustic events that hit a guard sensor before hitting any normal sensor are rejected. The location module from Vallen VisualAE software was used for the location analysis and, in order to filter out noise, the AE signal peak amplitude threshold (A_{th}) and an admissible LUCY limit were defined following a parametric analysis.

Although the selection of an appropriate A_{th} depends on many parameters such as the sensitivity of sensors or the level of preamplification used, the correct selection of the A_{th} is a relevant point. Setting the threshold too low result in recording noise in addition to the signals generated by crack growth. However, if the threshold is too high, valid AE signals are not recorded. To set an appropriate A_{th} the procedure in [35] was followed; DCB specimens were loaded until crack initiation while the peak amplitude of AE events was monitored. In the initial elastic regime, the peak amplitude of AE events remained mostly below 60 dB while, when crack propagation started, the peak amplitude of AE events raised above 60 dB. Thus, crack growth was associated to AE events with a peak amplitude $\geq$60 dB while AE events $<$ 60 dB were associated to other effects such as adherend or adhesive elastic deformation, which are beyond the scope of the current work.

The LUCY limit was set through PLB test results. Having 5 or 6 measurements depending on the specimen and 33 in total, 90% of PLB tests denoted a LUCY below 3.0 mm. It was considered an admissible limit to get accurate location results.

2.2. Numerical simulations

A 3D numerical model was implemented using the FE method and ANSYS software (ANSYS-Inc, 2019) to reproduce the

experimental DCB tests for the two adhesive types. The adherends and the adhesive layer were modelled using SOLID185 8-node quadrilateral elements, and the elastic properties and ultimate strength of the adhesives were taken from tensile tests given in [3] and [36] for the rigid and flexible adhesives, respectively. A row of cohesive interface elements (INTER205) was added at the mid plane of the adhesive layer. Cohesive law was assumed to be bilinear, as suggested in [3]. The values for the fracture toughness used in the numerical models were taken as the mean value in the crack growth regime, following Eq. (2). The bondline thickness (taken also from the current experiments), the fracture toughness of the bonded joints and the adhesive properties are summarized in Table 1.

Mesh was constructed per the hexahedron meshing algorithms of ANSYS and manual resizing. This resulted in an element size of 0.25 mm in the longitudinal and transversal directions and 0.143 mm in the out-of-plane direction (6 divisions were made in the bondline thickness). The mesh and boundary conditions of the model are illustrated in Fig. 3.

Simulations were used to analyse the size of the FPZ and to correlate the experimental evidence with the observed fracture process.

3. Results and discussion

Load displacement curves and the longitudinal location of the crack tip are reported in Figs. 4 and 5 for the rigid and flexible bonded joints, respectively. The curves for the visual (a) and the corrected (a_c) crack lengths, as well as a point cloud (AE events), were obtained for the longitudinal location of the crack tip. Regarding the procedure in Section 2.1.2, the point cloud of interest was obtained filtering the raw data acquired by the AE system; namely, the channel number (CHAN2 and CHAN4), a LUCY within 0.00 mm and 3.00 mm, and a A_{th} of 60 dB.

A fully cohesive and stable crack growth predominated in all tests, producing continuous load displacement curves with the characteristic shape of a DCB test. Linear behaviour before crack initiation was observed in the rigid adhesive samples, and a non-linear behaviour occurred in the flexible adhesive samples due to the viscoelastic nature of this adhesive. Per testing standard ISO-25217, 65 mm of crack propagation was allowed, commencing in this particular case when the load displacement curves reached the maximum load of the initial region.

Regarding the DCB test results for the rigid bonded joints (Fig. 4), the corrected crack length (a_c) followed the growth of the visual crack length (a) with an average positive offset of 5.92 mm (Table 2), which accounts for the presence of a FPZ developed ahead of the crack tip. The corrected crack length followed the visual crack length at a certain distance in the interior of the bonded area. The average crack growth rate was 9.62 mm/min for the rigid bonded joints. Regarding the AE data, AE event detection began when the visible crack propagation started. The point cloud followed the visually measured crack length, but with some dispersion. A linear regression fit of the point cloud revealed that the AE events followed an average linear slope of 8.47 mm/min with a coefficient of determination (R-square) of 0.8547 for the rigid bonded joints, which was approximate to the visual crack growth rate. The linear function of the AE events showed an average positive offset of 4.98 mm with respect to the visual crack length (Table 2), very close to the corrected crack length. This demonstrates that most of the AE events originated very close to the external crack tip just within the adhesive layer, while the visual method determined the external location of the crack tip.

Regarding the DCB test results of the flexible bonded joints (Fig. 5), the average crack growth rate was 6.37 mm/min. The corrected crack length defined by the correction Δ in Eq. (1) followed the visual crack growth with an average positive offset of 21.78 mm (Table 2) in the interior of the adhesive layer, far away from the visible crack tip. AE event detection began when the visible crack propagation started, having a slope of 6.61 mm/min and a dispersion of 0.9394 (R-square). The AE point cloud followed the crack length measured visually with low dispersion and with an average offset with respect to a of 25.32 mm (Table 2). This showed a clear gap between the visual crack length and the AE data, in which the latter was closer to the corrected crack length. The results demonstrate that for flexible adhesive joints, AE events originate in the interior of the adhesive far from the visually detected external crack tip and in agreement with corrected crack length calculations.

Table 2 compares the corrected crack length (a_c) and AE event data with the visual crack length measurements (a). In the case of AE event data, linear regression was used with the following functions: $\Delta = a_c - a$ for the corrected crack length method, and $\Delta_{\text{AE}-a} = \text{AE} - a$ for the linear regression. Average values and standard deviation were determined for the 65 mm of propagation.

The results indicate that dispersion in AE event point clouds may be caused by the group velocity set in the source location. The group velocity of the S_0 wave modes was assumed to be constant, though there may have been some variance depending on wave frequency. Likewise, the arrival times detected by the AE sensors for location purposes were assumed to be unique to the S_0 wave modes. However, these arrival times may also have corresponded to antisymmetric waves (A_0), or even mixed wave modes ($S_0 + A_0$). This is due to the limited propagation media of the DCB specimen, which may have produced reflections and couplings of different wave modes, as seen in [32]. A modal analysis of such AE events might help differentiate wave mode types, but such analyses are still

Table 1
Elastic and fracture properties of adhesives.

Adhesive	Araldite 2021	Sikasil SG500
Young's modulus (MPa)	1590	2.06
Poisson's modulus (–)	0.35	0.4977
Ultimate strength (MPa)	22.6	1.20
Bondline thickness (mm)	0.80	0.86
Fracture toughness (N/mm)	1.143	1.564

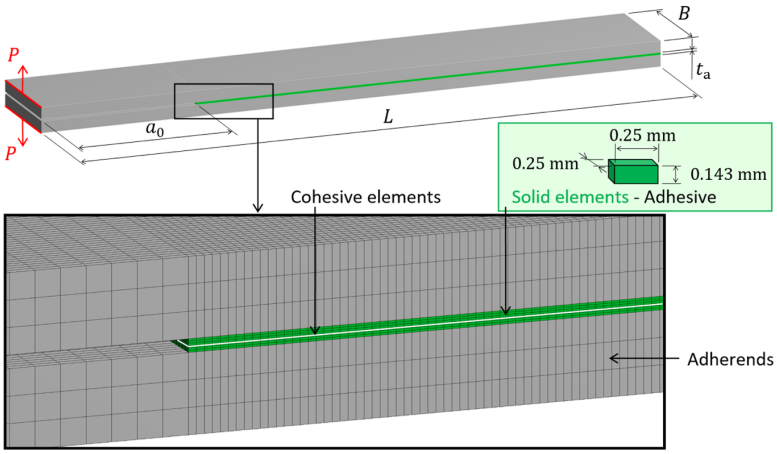

Fig. 3. Mesh and boundary conditions used in the FE model.

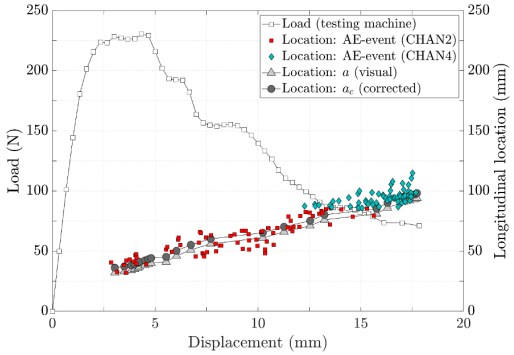

Fig. 4. Load displacement curve and longitudinal location of the crack tip, i.e. crack length, in the rigid adhesive.

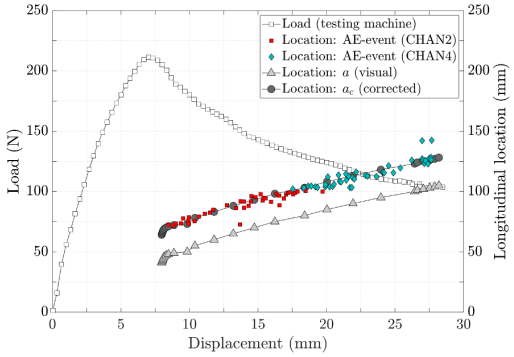

Fig. 5. Load displacement curve and longitudinal location of the crack tip, i.e. crack length, in the flexible adhesive.

the subject of study [32] and thus beyond the scope of the current work.

The AE data in Figs. 4 and 5 show that AE events are located in the interior of the adhesive layer, which is in agreement with [3] and [4] where large FPZs were detected in bonded joints, most notably when tough flexible adhesives were used. The FE models shown in Fig. 6 corroborate the presence of a large FPZ in the interior of the adhesive layer when a crack propagates. Normal stress distribution among the cohesive elements (SSX in Fig. 6) was analysed when the crack was about to propagate. Absolute 'zero' is shown on the rulers in Fig. 6; this determines the visual crack length measured on the external face of the bonded joint. The distance

Table 2
Comparison of crack length estimation methods in mm.

Adhesive		A2021		SG500	
Method		CBT [2]	AE	CBT [2]	AE
		Δ	Δ_{AE-a}	Δ	Δ_{AE-a}
Test 1	AVG	4.17	7.61	23.10	23.39
	SD	–	2.03	–	1.90
Test 2	AVG	8.86	3.89	18.64	24.16
	SD	–	2.82	–	3.25
Test 3	AVG	4.72	2.66	23.60	28.41
	SD	–	2.09	–	5.20
AVG		5.92	4.72	21.78	25.32
SD		2.56	2.58	2.73	2.70

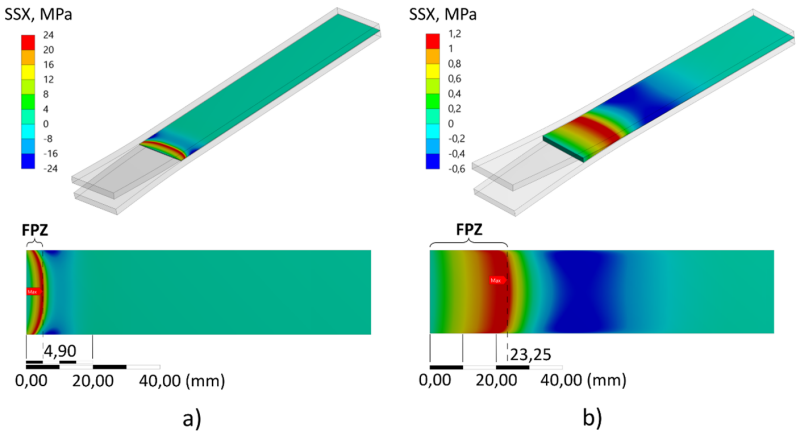

Fig. 6. Stress distribution and maximum stress location on the cohesive interface when crack propagation starts in 0.5 mm-thick (a) rigid and (b) flexible bonded joints.

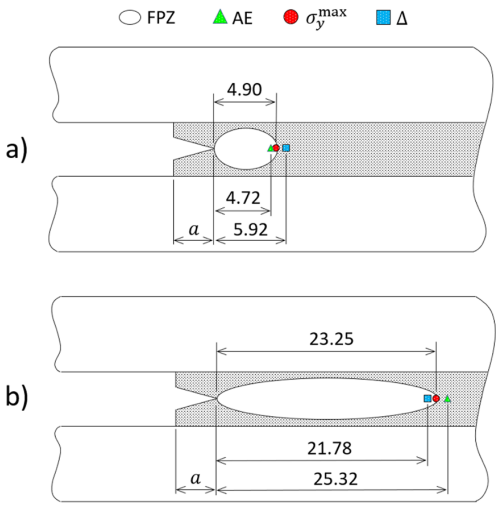

Fig. 7. Extension of the FPZ, AE event location, the point of maximum normal stress (σ_y^{max}) and the crack length correction factor Δ in (a) rigid and (b) flexible bonded joints, in mm.

to the point of maximum stress is represented by the dashed line, i.e. the size of the FPZ.

In the rigid bonded joints (Fig. 6a), the FPZ—the area in which traction forces have overpassed the local maximum strength but still the debonding is not completed—extended approximately 4.90 mm from the crack tip to the interior of the adhesive layer when the crack propagated, the same point where the maximum normal stress (σ_y^{max}) was located; also close to the corrected crack length, situated at 5.92 mm from the crack tip. With flexible bonded joints (Fig. 6b), the FPZ was larger and the maximum normal stress was located approximately 23.25 mm inside the adhesive layer. This was also not far off the 21.78 mm number given by the corrected crack method. Fig. 7 summarises the FPZ, AE event location, maximum normal stress points and the crack length correction factor for both the rigid and flexible bonded joints.

These results confirm that a large damage zone developed inside the adhesive layer under fracture conditions, but this damage was not detected during visual inspection of the crack tip. The CBT data reduction method corrected the visual crack length and thus proposes using the corrected crack length to evaluate fracture energy in bonded joints, which is associated with the FPZ. AE events were produced by real-time physical events, such as cracking or plastic deformation, and a good representation of the real behaviour of a bonded joint was obtained. Unlike [32], where AE source location links to a visually measured crack length, the AE event location observed in this study strongly corresponded to the point of maximum normal stress induced in the adhesive layer under fracture conditions. However, it is easy to confuse AE source location with the crack tip in rigid bonded joints due to dispersion in the AE event point cloud and the small FPZ.

AE monitoring is an alternative method for component testing in a laboratory and for SHM purposes when the location of cracks must be determined. The primary advantage of this method is that it avoids the subjectivity and difficulties of interpreting structural behaviour often experienced when using non-contacting techniques. Unlike techniques that use embedded sensors, this method does not alter the manufacturing process, nor is it necessary to foresee the monitoring strategy before the manufacturing process. In short, AE monitoring facilitates manufacturing, avoids the problematic use of fungible sensors and increases the scope of the SHM towards non-laminated components. Unlike ultrasonic analysis, the method provides continuous real-time monitoring and accurate linear source location measurements in the area enclosed by AE sensors. Further, local analyses extend to larger regions with the consecutive addition of AE sensors. In contrast, AE technique cannot monitor stationary systems where activity is lacking. Moreover, the equipment is expensive, the monitoring process is not user friendly and the post-process is not immediate since a laborious analysis of the data is needed.

4. Conclusions

In the present study, mode I crack growth was monitored using the AE technique. A correlation between AE events and fracture events was found in terms of crack and FPZ locations, thus eliminating dependency on unreliable visual crack length measuring. The location of AE events correlates strongly to the point of maximum normal stress induced in the adhesive layer under fracture conditions. Per the described results, AE events originate just ahead of the crack tip and in the interior of the bonded area in rigid and flexible bonded joints, respectively. The proposed technique demonstrates that FPZs are much larger in flexible bonded joints than in rigid bonded joints. Unlike other conventional SHM techniques, AE provides continuous real-time information about bonded joints no matter the composition or manufacture of the constituent parts. The technology has a broad scope of applicability regarding flexible adhesives and when inspecting the fracture processes of bonded joints using non-fungible sensors.

Declaration of Competing Interest

The authors declare that they have no known competing financial interests or personal relationships that could have appeared to influence the work reported in this paper.

References

[1] da Silva LFM, Dillard DA, Blackman B, Adams RD. Testing adhesive joints. Best practices. Wiley; 2012.
[2] ISO-25217. Determination of the Mode I Adhesive Fracture Energy of Structural Adhesive Joints Using Double Cantilever Beam and Tapered Double Cantilever Beam Specimens. Tech. rep., Rep., Int. Org. Stdzn; 2009.
[3] Cabello M, Zurbitu J, Renart J, Turon A, Martínez F. A general analytical model based on elastic foundation beam theory for adhesively bonded DCB joints either with flexible or rigid adhesives. Int J Solids Struct 2016;94–95:21–34. https://doi.org/10.1016/j.ijsolstr.2016.05.011.
[4] Cabello M, Turon A, Zurbitu J, Renart J, Martínez F. Progressive failure analysis of DCB bonded joints using a new elastic foundation coupled with a cohesive damage model. Eur J Mech A-Solids 2017;63:22–35. https://doi.org/10.1016/j.euromechsol.2016.12.004.
[5] Paris AJ, Paris PC. Instantaneous evaluation of J and O-star. Int J Fract 1988;38:19–112.
[6] De Moura MFSF, Campilho RDSG, Gonçalves JPM. Crack equivalent concept applied to the fracture characterization of bonded joints under pure mode I loading. Compos Sci Technol 2008;68:2224–30. https://doi.org/10.1016/j.compscitech.2008.04.003.
[7] Adams RD, Drinkwater BW. Nondestructive testing of adhesively bonded joints. NDT&E Int 1997;30:93–8. https://doi.org/10.1016/S0963-8695(96)00050-3.
[8] Dillard DA, Pohlit DJ, Jacob GC, Starbuck JM, Kapania RK. On the use of a driven wedge test to acquire dynamic fracture energies of bonded beam specimens. J Adhes 2011;87:395–423. https://doi.org/10.1080/00218464.2011.562125.
[9] Lacroix R, Monatte J, Lens A, Bergheau JM, Klöcker H. Spot weld strength determination using the wedge test: in-situ observations and coupled simulations. Appl Mech Mat 2010;24–25:299–304. https://doi.org/10.4028/www.scientific.net/AMM.24-25.299.
[10] Kordatos EZ, Aggelis DG, Matikas TE. Monitoring mechanical damage in structural materials using complimentary NDE techniques based on thermography and acoustic emission. Compos Pt B-Eng 2012;43(6):2676–86. https://doi.org/10.1016/j.compositesb.2011.12.013.
[11] Barile C, Casavola C, Pappalettera G, Pappalettere C. Analysis of crack propagation in stainless steel by comparing acoustic emissions and infrared thermography data. Engng Fail Anal 2015;69:35–42. https://doi.org/10.1016/j.engfailanal.2016.02.022.
[12] Sans D, Stutz S, Renart J, Mayugo JA, Botsis J. Crack tip identification with long FBG sensors in mixed-mode delamination. Compos Struct 2012;94:2879–87.

https://doi.org/10.1016/j.compstruct.2012.03.032.
[13] Ling HY, Lau KT, Su Z, Wong ETT. Monitoring mode II fracture behaviour of composite laminates using embedded fiber-optic sensors. Compos Pt B-Eng 2007;38:488–97. https://doi.org/10.1016/j.compositesb.2006.07.004.
[14] Xavier J, Fernandes JRA, Frazão O, Morais JJL. Measuring mode I cohesive law of wood bonded joints based on digital image correlation and fibre Bragg grating sensors. Compos Struct 2015;121:83–9. https://doi.org/10.1016/j.compstruct.2014.11.017.
[15] Ning X, Murayama H, Kageyama K, Wada D, Kanai M, Ohsawa I, et al. Dynamic strain distribution measurement and crack detection of an adhesive-bonded single-lap joint under cyclic loading using embedded FBG. Sma Mat Struct 2014;23. https://doi.org/10.1088/0964-1726/23/10/105011.
[16] Li Y, Liao Y, Su Z. Graphene-functionalized polymer composites for self-sensing of ultrasonic waves: an initiative towards “sensor-free” structural health monitoring. Compos Sci Technol 2018;168:203–13. https://doi.org/10.1016/j.compscitech.2018.09.021.
[17] Sargent JP. Durability studies for aerospace applications using peel and wedge tests. Int J Adhes Adhes 2005;25:247–56. https://doi.org/10.1016/j.ijadhadh.2004.07.005.
[18] Budzik M, Jumel J, Imielinska K, Shanahan MER. Accurate and continuous adhesive fracture energy determination using an instrumented wedge test. Int J Adhes Adhes 2009;29:694–701. https://doi.org/10.1016/j.ijadhadh.2008.11.003.
[19] Bernasconi A, Kharshiduzzaman Md, Comolli L. Strain profile measurement for structural health monitoring of woven carbon-fiber reinforced polymer composite bonded joints by fiber optic sensing using an optical backscatter reflectometer. J Adhes 2016;92:440–58. https://doi.org/10.1080/00218464.2015.1043005.
[20] Bernasconi A, Carboni M, Comolli L, Galeazzim R, Gianneo A, Kharshiduzzaman Md. Fatigue crack growth monitoring in composite bonded lap joints by a distributed fiber optic sensing system and comparison with ultrasonic testing. J Adhes 2016;92:739–57. https://doi.org/10.1080/00218464.2015.1123153.
[21] Masserey B, Raemy C, Fromme P. High-frequency guided ultrasonic waves for hidden defect detection in multi-layered aircraft structures. Ultrason 2014;54:1720–8. https://doi.org/10.1016/j.ultras.2014.04.023.
[22] Chan H, Masserey B, Fromme P. High frequency guided ultrasonic waves for hidden fatigue crack growth monitoring in multi-layer model aerospace structures. Sma Mat Struct 2015;24:025037. https://doi.org/10.1088/0964-1726/24/2/025037.
[23] Zhang K, Zhou Z. Quantitative characterization of disbonds in multilayered bonded composites using laser ultrasonic guided waves. NDT&E Int 2018;97:42–50. https://doi.org/10.1016/j.ndteint.2018.03.006.
[24] Diakhate M, Bastidas-Arteaga E, Pitti RM, Schoefs F. Cluster analysis of acoustic emission activity within wood material: towards a real-time monitoring of crack tip propagation. Eng Frac Mech 2017;180:254–67. https://doi.org/10.1016/j.engfracmech.2017.06.006.
[25] Fotouhi M, Saeedifar M, Sadeghi S, Ahmadi Najafabadi M, Minak G. Investigation of the damage mechanisms for mode I delamination growth in foam core sandwich composites using acoustic emission. Struct Health Monit 2015;14(3):265–80. https://doi.org/10.1177/1475921714568403.
[26] Saidane EH, Scida D, Pac M-J, Ayad R. Mode-I interlaminar fracture toughness of flax, glass and hybrid flax-glass fibre woven composites: failure mechanism evaluation using acoustic emission analysis. Polym Test 2019;75:246–53. https://doi.org/10.1016/j.polymertesting.2019.02.022.
[27] Barile C, Casavola C, Pappalettera G. Acoustic emission waveform analysis in CFRP under Mode I test. Engng Fract Mech 2019;210:408–13. https://doi.org/10.1016/j.engfracmech.2018.01.023.
[28] Carpinteri A, Lacidogna G, Niccolini G, Puzzi S. Morphological fractal dimension versus power-law exponent in the scaling of damaged media. Int J Damage Mech 2009;18:259–82. https://doi.org/10.1177/1056789508098700.
[29] Anzani A, Binda L, Carpinteri A, Lacidogna G, Manuello A. Evaluation of the repair on multiple leaf stone masonry by acoustic emission. Mater Struct 2008;41:1169–89. https://doi.org/10.1617/s11527-007-9316-z.
[30] Carpinteri A, Lacidogna G, Paggi M. Acoustic emission monitoring and numerical modeling of FRP delamination in RC beams with non-rectangular cross-section. Mater Struct 2007;40:553–66. https://doi.org/10.1617/s11527-006-9162-4.
[31] Crawford A, Droubi MG, Faisal NH. Analysis of acoustic emission propagation in metal-to-metal adhesively bonded joints. J Nondestruct Eval 2018;37:33. https://doi.org/10.1007/s10921-018-0488-y.
[32] Crawford A, Droubi MG, Faisal NH. Modal acoustic emission analysis of mode-I and mode-II fracture of adhesively bonded joints. In: 33rd Eur. Conf. Acoust. Emiss. Test., Conference paper; 2018.
[33] ASTM E1316-19. Standard Terminology for Nondestructive Examinations. West Conshohocken, PA: ASTM International; 2019. DOI: 10.1520/E1316-19.
[34] Vallen H. Acoustic emission testing: fundamentals, equipment, applications. Informative booklets for non-destructive testing, NDT compact and understandable. Wuppertal (Germany): Castell Publication Inc.; 2006. ISBN: 3-934255-26-4.
[35] Pascoe JA, Zarouchas DS, Alderliesten RC, Benedictus R. Using acoustic emission to understand fatigue crack growth within a single load cycle. Engng Fract Mech 2018;194:281–300. https://doi.org/10.1016/j.engfracmech.2018.03.012.
[36] Manterola J, Cabello M, Zurbitu J, Renart J, Turon A, Jumel J, et al. Effect of the width-to-thickness ratio on the mode I fracture toughness of flexible bonded joints. Engng Fract Mech 2019;218:106584. https://doi.org/10.1016/j.engfracmech.2019.106584.

Paper C

Durability study of flexible bonded joints: the effect of sustained loads in mode I fracture tests

J. Manterola[a], J. Zurbitu[a], J. Renart[b], A. Turon[b], I. Urresti[a]
[a]Ikerlan Technology Research Centre, Applied Mechanics Area, Mondragón, Spain
[b]AMADE, Polytechnic School, Universitat de Girona, Girona, Spain

The paper has been published in
Polymer Testing Vol. 88, 106570, 2020.

Polymer Testing 88 (2020) 106570

Contents lists available at ScienceDirect

Polymer Testing

journal homepage: http://www.elsevier.com/locate/polytest

Test Method

Durability study of flexible bonded joints: The effect of sustained loads in mode I fracture tests

J. Manterola [a,*], J. Zurbitu [a], J. Renart [b,c], A. Turon [b], I. Urresti [a]

[a] Ikerlan Technology Research Centre, Basque Research and Technology Alliance (BRTA), P°.J.M°. Arizmendiarrieta, 2, 20500, Arrasate-Mondragón, Spain
[b] AMADE, Polytechnic School, University of Girona, Campus Montilivi, s/n, 17071, Girona, Spain
[c] Serra Húnter Fellow, Generalitat de Catalunya, Spain

ARTICLE INFO

Keywords:
Durability
Flexible adhesive
Mode I
Relaxation
Wedge test

ABSTRACT

Adhesives in bonded structures are exposed both to external loads and environmental conditions; durability studies are currently needed to assess their service lifetime. Conditioning strategies differ in considering external load conditions (such as stressed or not stressed) for the durability analysis of double cantilever beam (DCB) bonded joints. Different test procedures such as ASTM D3762 (wedge testing) or ISO-25217 (DCB testing) exist to characterise the evolution of the fracture strength and toughness found in bonded joints. These methods depend on crack-length measurements, however, and achieving an accurate visual determination may be difficult due to the large fracture process zones (FPZs) that develop in the adhesive layer, especially in flexible or degraded bonded joints. To compensate, crack-length-independent data-reduction methods such as the compliance-based beam method (CBBM) or the J-integral method can be used, but experimental research is lacking on the suitability of these methods in ageing tests. A lack of consensus also exists in testing methodologies to evaluate the durability of bonded joints, especially when examining flexible bonded joints. The present work evaluates the influence of damage on fracture toughness within flexible bonded joints exposed to service conditions. Wedge tests and DCB tests are conducted using DCB specimens bonded with a flexible structural adhesive, proving that the degradation of flexible bonded joints exposed to environmental conditions is significantly accelerated when external loads act on them. The findings show that crack length estimation is affected due to environmental effects and thus, that crack-length-dependent test methods are not applicable in ageing tests.

1. Introduction

Adhesive bonds must withstand external mechanical loads and the service environment. Studies are currently needed to analyse the strength of bonded joints subjected to many common environments such as temperature, moisture and outdoor weathering. The combination of external loads with the service environment may cause an adhesive bond to degrade at a faster rate than would be caused by temperature and humidity only and thus to fail in early stages [1]. This situation is of particular concern in aircraft structures, in which the durability of bonds under stress must be considered [2].

In applications where bonded joints are not subjected to high loads for prolonged periods (as in non-stressed bonded joints), only the effect of environmental degradation is typically evaluated on element materials and adhesive bonds that are exposed either to simulated service conditions or to accelerated ageing at specified constant conditions, following ASTM D1151-00(2013) [3], or at cyclic service conditions by alternating high and low temperatures and relative humidity (RH), following ASTM D1183-03(2019) [4]. After the completion of exposure, adhesive bonds are tested to evaluate mechanical properties such as mode I fracture strength or failure mechanisms [5], which may be determined following double cantilever beam (DCB) test standard ISO-25217 to measure the fracture toughness (G_{IC}) in structural adhesives [6]. The data-reduction procedures proposed in standard corrected beam theory (CBT), however, require the measurement of the crack length to determine the fracture toughness. Seemingly minor errors or subjectivity in crack-length measurement can result in major deviations in fracture-toughness calculations. Achieving an accurate visual determination of the crack length may be difficult, especially when dealing with elastomeric adhesives [7,8] or degraded bonded joints [9], since large fracture process zones (FPZs) are to be expected.

The compliance-based beam method (CBBM) [10–12] may be used

* Corresponding author.
E-mail address: jmanterola@ikerlan.es (J. Manterola).

https://doi.org/10.1016/j.polymertesting.2020.106570
Received 19 December 2019; Received in revised form 28 February 2020; Accepted 19 April 2020
Available online 28 April 2020

as an alternative. Instead of measuring the crack length, the flexural modulus of the specimen is iteratively adjusted while considering various adherend properties. Although this method is valid for either degraded or undegraded bonded joints, adherend properties may change when composite bonded joints are exposed to environmental conditions [13,14], which may affect fracture-toughness evaluation. Additional tests of degraded composite adherends may be conducted to avoid this problem. The J-integral method does not require crack-length measurement to characterise the fracture toughness in bonded joints [15–18], since the relative rotation between the adherends is measured, for example with inclinometers. Although the J-integral method is valid for characterising the mode I fracture toughness of flexible bonded joints [7,19], experimental research is currently lacking on the suitability of the CBT, CBBM and J-integral data-reduction methods to characterise the fracture toughness of flexible bonded joints in ageing tests.

Specific test setups that control the environment and monitor changes in bonded joint performance are required to assess the service lifetime and durability of bonded joints exposed to external loads, such as stressed bonded joints. The wedge test (WT), standardised in ASTM D3762-03(2010), is the most widely used method to evaluate the environmental durability of adherend-surface preparations in bonded joints with metal adherends [20]. The simple test procedure involves inserting a wedge with the same thickness as the adherends into the bonded joint and then exposing the specimen to a specific temperature/humidity environment. The exposition is prolonged until crack propagation arrests and the crack length is measured; the crack length is related to the toughness of the joint. Crack lengths measured in different bonded joints may then be compared to provide a qualitative study of the performance of the joints.

In addition to the standard, which was withdrawn (with no replacement) in 2019, different formulations have been made available in the literature to obtain quantitative values for fracture toughness, since such toughness is not considered in the test standard. A simple equation was suggested in Ref. [21] to calculate the fracture toughness of bonded joints with a negligible bondline thickness; an improved formulation was then proposed in Ref. [22] that includes the elasticity of the adhesive. Expressions found in Refs. [21,22], however, also depend on crack-length measurements; in accordance with [23], even when using sophisticated equations, the subjectivity of the crack length will make this method of determining the fracture toughness questionable.

Alternative methods to estimate the crack length have been analysed in the literature, for example using strain gauges [9,24], image correlation technologies [25] or acoustic emissions [8], but crack-length measurement is still subjective because its location is determined by interpretations or observation. A state-of-the-art study on the use of the ASTM D3762 test standard to assess the durability of metal bonded joints for aeronautical applications was conducted in Refs. [26,27]. In that study, the effects of several parameters such as surface preparation and bondline thickness on crack propagation were examined during the exposure period in rigid bonded joints. That study [26,27] was continued in Ref. [28] using composite bonded joints, and the authors evaluated the effect of adherend thickness (i.e. flexural stiffness) on crack propagation as well as calculating fracture toughness. Despite this extensive study, low-modulus adhesives or bonded joints with thick bondline thicknesses have been beyond the scope of analysis to date. The applicability of the WT in flexible bonded joints for durability studies has thus yet to be assessed.

In general, few works other than [23,29] have discussed the suitability of different test methods for assessing the durability of bonded joints. While the authors in Ref. [23] concluded that both the DCB test and the WT are valid for assessing the durability of rigid bonded joints, the results obtained through these methods are not comparable. In Ref. [29], test results obtained through constant force loading (i.e. creep tests) and constant deflection/relaxation loading (i.e. wedge test) were compared to analyse the viscoelastic behaviour of bonded joints, emphasizing their good representativeness of in-service conditions even though environmental conditions were not considered. Finally, the effect of environmental exposure on crack growth was investigated in Ref. [30] using the DCB and WT. Although fracture behaviour was analysed in the study, in particular the crack path or the failure mode (cohesive or interfacial), the authors did not discuss fracture toughness in their work.

These studies exemplify the lack of data and consensus on methodologies to evaluate the durability of bonded joints. Durability studies on the combined effect of a sustained load (i.e. stress) and environmental conditions are also lacking on bonded joints, especially when flexible adhesives are used. The present contribution evaluates the effect of the damage induced in the adhesive layer during the evolution of fracture toughness within flexible bonded joints exposed to a service environment. For this purpose, durability studies were conducted among stressed and non-stressed bonded joints, and the evolution of their fracture strength was evaluated by testing bonded joints with different exposure time periods. The fracture toughness was evaluated following the DCB and WT methods using different crack-length dependent/independent data-reduction methods. The results were then compared between stressed and non-stressed bonded joints.

The remainder of this paper is structured as follows: section 2 describes the methodology for the durability analysis, and the experimental results are shown in section 3 and discussed in section 4.

2. Methodology

Durability studies were conducted to evaluate the evolution of the fracture strength of stressed (i.e. subjected to a sustained load) and non-stressed flexible bonded joints while exposed to specific temperature and humidity conditions, which simulated the service environment. For this purpose, DCB specimens were manufactured and conditioned in a climate chamber. From those specimens, some were conditioned and stressed following the WT procedure, and the fracture toughness was measured. All specimens were then tested following the DCB test protocol to analyse their fracture behaviour.

Difficulties in visual crack-length measurement were expected because of adhesive degradation during the condition. Thus, different data-reduction methods were applied to evaluate the fracture toughness of the bonded joints through Wedge and DCB tests: crack-length-dependent data-reduction methods such as the WT [22] and the CBT [6] methods, as well as methods that do not depend on crack length, such as the CBBM [10] and the J-integral method [15].

2.1. Wedge test

Some specimens were stressed following the wedge tests in the ASTM D3762-03(2010) standard [20]. The data-reduction method developed in Ref. [22] was then applied to obtain G_{IC}. A wedge was manually forced into the bondline of the DCB specimen until a small crack propagation was created, thereby producing tensile stress in the region of the resulting crack tip. The position of the crack tip was localized 15', 2 h, 4 h and 24 h after the wedge insertion using a stereoscopic microscope (Nikon, type SMZ645) with two C–W10xA/22 eyepieces that provide 4x to 300x total magnification. To improve vision, a coaxial fibre-optic ring Volpi Intralux 5000-1 light source was attached to the microscope. Cracks in all bonded joints were observed to arrest between the 4^{th} and 24^{th} hour. The distance between the adherend-wedge contact point and the crack tip was later measured by considering the distance as the crack length, a. This value was obtained from the average readings from both sides of the specimen. Stressed specimens were then exposed to environmental conditions, and the resulting crack extension (Δa) with time was evaluated following the same procedure (Fig. 1). Subsection 2.3.1 provides details on the conditioning of the bonded joints.

The mode I fracture energy was obtained with the following equation proposed in Ref. [22], that includes the elasticity of the adhesive:

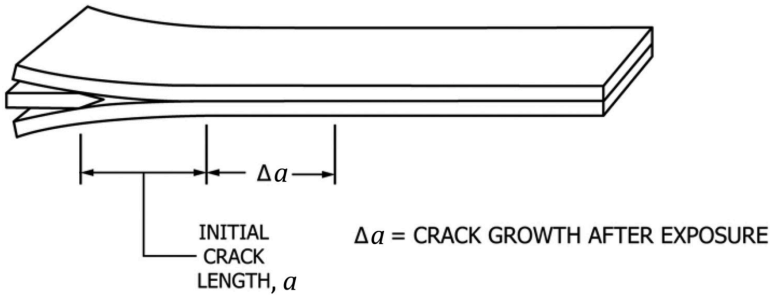

Fig. 1. *Wedge test and crack extension (Δa) due to environmental ageing* [20].

$$G_{IC} = \frac{\delta^2 E_1 \left(h + \frac{t_a}{2}\right)^3 \left(1 - \frac{t_a}{2h+t_a}\right)^3 (a+\beta)^2}{48\left(\frac{a^3}{3} + a^2\beta + a\beta^2\right)^2}, \quad (1)$$

where δ is wedge thickness, E_i is the elastic modulus of the adherend in the i direction, h is the adherend thickness, t_a is the bondline thickness and a is the crack length. In a composite bonded joint, the direction of fibres is $i = 1$. The value of β is expressed as follows:

$$\beta = 0.667\left(h + \frac{t_a}{2}\right)\left\{\left(1 - \frac{t_a}{2h+t_a}\right)^3\left[1 + \frac{t_a}{2h+t_a}\left(\frac{2E_1}{E_a} - 1\right)\right]\right\}^{-4}, \quad (2)$$

where E_a is the elastic modulus of the adhesive.

2.2. DCB test

DCB tests were run on a Zwick/Roell universal tensile testing machine following the DCB test protocol described in the ISO-25217 test standard. The CBT, CBBM and J-integral data-reduction methods were then applied to evaluate G_{IC}. A constant displacement rate of 2 mm/min was applied to ensure quasi-static crack growth. The tests were conducted under room temperature and 50 ± 5% RH conditions. The side-clamped beam (SCB) hinge system [31] was used as a substitute for bonded fixtures, since the specimens were conditioned under severe temperature and humidity conditions (Fig. 2). The SCB hinge system was positioned adequately to obtain the same initial crack length (a_0) in all tests, even in stressed bonded joints in which the location of the crack tip changed during the environmental conditioning because of crack propagation. Table 1 shows the average initial crack lengths.

When using the CBT data-reduction method, the mode I crack position was recorded using a high-performance optical system during the test. A CCD camera-type Manta G-917 from ALLIED Vision technologies GmbH and an optical lens-type Xenoplan 2.8/50 from Schneider Kreuznach were used. According to the ISO-25217 test standard, 65 mm of crack propagation was allowed in all tests, and the fracture energy was evaluated using the following equation:

$$G_{IC} = \frac{3P\delta}{2B(a + |\Delta|)}\frac{F}{N}, \quad (3)$$

where P is the applied load, B is the total width of the bonded area, Δ is a correction factor for the crack length based on the compliance of the bonded joint, F is the large-displacement correction and N is the load-application correction (i.e. the SCB hinges).

The CBBM data-reduction method avoids crack-length measurement; instead, an equivalent crack length, a_e, is evaluated through the compliance of the bonded joint, as follows [10]:

Table 1
Initial crack length after fixing the SCB hinge for DCB tests.

Specimens	Batch	Exposure time t (h)	a_0 (mm)	No. tested specimens
Reference	T1	0	39.76 ± 0.41	3
Stressed	T2	10	39.64 ± 0.76	2
		100	37.01 ± 0.37	2
		300	38.33 ± 0.71	2
		1000	37.74 ± 0.40	2
Non-stressed	T3	10	39.18 ± 0.33	2
		100	39.69 ± 0.14	2
		300	39.85 ± 0.27	2
		1000	39.16 ± 0.23	2

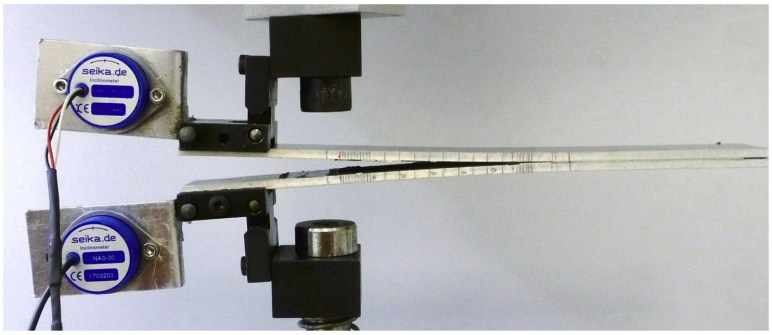

Fig. 2. DCB test with SCB hinge system.

$$C = \frac{8a_e^3}{E_1 B h^3} + \frac{12a_e}{5BhG_{13}}, \tag{4}$$

where C is the compliance $C = \delta/P$, h is the adherend thickness and G_{13} is the out-of-plane shear modulus of the adherend. Only the applied load and the opening displacement are recorded to evaluate the fracture energy:

$$G_{IC} = \frac{6P^2}{B^2 h}\left(\frac{2a_e^2}{h^2 E_f} + \frac{1}{5G_{13}}\right), \tag{5}$$

where E_f is the corrected flexural modulus of the specimen, which can be obtained from equation (4) using the initial compliance (C_0) and the corrected initial crack length ($a_0 + |\Delta|$),

$$E_f = \left(C_0 - \frac{12(a_0 + |\Delta|)}{5BhG_{13}}\right)^{-1} \frac{8(a_0 + |\Delta|)^3}{Bh^3}, \tag{6}$$

The Δ value accounts for the root rotation effect at the crack tip and can be yielded by:

$$\Delta = h\sqrt{\frac{E_f}{11G_{13}}\left[3 - 2\left(\frac{\Gamma}{1+\Gamma}\right)^2\right]}, \tag{7}$$

where

$$\Gamma = 1.18\frac{\sqrt{E_f E_3}}{G_{13}}, \tag{8}$$

Following the iterative procedure described in Ref. [10], equations (6)–(8) were then used to obtain a converged value for E_f.

During the application of the J-integral method, the rotation of adherends at the loading application point and the applied load must be measured. For this purpose, two NA3-30 capacitive inclinometers from SEIKA Mikrosystemtechnik GmbH were fixed to each adherend to measure their rotation. The formulation proposed for the data reduction of the J-integral method [19] is as follows:

$$J_I = \frac{P}{B}\theta, \tag{9}$$

where θ is the relative rotation between adherends at the applied load position with respect to the bondline of the DCB specimen.

In the following, the fracture toughness was determined as the average value of the calculated strain energy release rate (SERR) or J-integral over the 65 mm of crack propagation.

2.3. Experimental campaign

The DCB tests were prepared by bonding two 3 mm thick and 200 mm long aluminium adherends with a structural flexible adhesive. A high-strength aluminium alloy type Al 7075-T6 with a yield strength of 550 MPa was used to prevent any plastic deformation during the DCB tests, as suggested in ASTM D3762(2010). A Young's modulus of 71 GPa and a Poisson's ratio of 0.33 have been considered in the following. The selected adhesive was a bicomponent, high-performance structural silicone-based adhesive named Sikasil SG500.

Aluminium substrates were first sanded with sandpaper and then cleaned with acetone to remove the native metal oxide. Prior to bonding, the substrates were cleaned again with isopropyl alcohol to improve adhesion. Once the adhesive was applied and the adherends had bonded, the specimens were cured under ambient room-temperature conditions for 72 h to allow crosslinking of the adhesive to occur. Teflon-calibrated spacers were placed in between the adherends to guarantee a constant thickness of the adhesive layer throughout the whole specimen and also to delimit an edge in the crack front. Before testing, a small sharp artificial crack was created by cutting the adhesive with a knife. All manufactured specimens had a total width of 25 ± 0.10 mm and an average bondline thickness of 0.59 ± 0.07 mm.

Specimens were painted with white spray, and then a ruler was marked in the lateral side of the joint to measure the crack length, as suggested in the CBT data-reduction method described in ISO-25217 and the WT described in the ASTM D3762-03 standards. For the WT, 3 mm thick and 25 mm wide squared wedges were manufactured. Aluminium (type 7075-T6) was used (as it was for the adherends), and a sharp chamfer was machined in one end of the wedge to facilitate its insertion.

2.3.1. Conditioning

All specimens were preconditioned for two weeks at ambient conditions prior to conditioning (or prior testing in the case of the control specimens). Specimens were then exposed to severe elevated temperature wet (ETW) conditions typical in the aerospace industry [32]. A 1000-h exposure at 85% RH and 82 °C temperature was used as an accelerated fixed time condition. Specimens were introduced in a climate chamber (CLIMATS type EX 5424-HE) with controlled temperature and humidity conditions; the exposure times (t) studied were 0 h, 10 h, 100 h, 300 h and 1000 h.

2.3.2. Stressed versus non-stressed conditioning

Durability studies were conducted in stressed (subjected to a sustained load) and non-stressed bonded joints. Test specimens were separated into three different specimen batches in which control specimens (T1), stressed specimens (T2) and non-stressed specimens (T3) were considered.

Control specimens were tested at ambient conditions immediately after the preconditioning period, following first the WT and then the DCB test protocols. The strength of the T1 specimens was considered to be the original strength of the bonded joints, and that value was compared with the strength after exposure of the T2 and T3 specimens. For the durability analysis, some specimens were stressed following the WT procedure described in subsection 2.1. All stressed (T2) and non-stressed (T3) specimens were then introduced in the climate chamber for conditioning. When any of the exposure times t were reached, four specimens (two for each batch in T2 and T3) were removed from the climate chamber. Immediately afterwards, the crack tip was located in the stressed bonded joints (T2), and the inserted wedge was removed to perform DCB testing. DCB tests were directly run on the non-stressed (T3) specimens after conditioning was complete. Finally, the fracture energy was evaluated following the four different data-reduction methods described in subsections 2.1 and 2.2: the method described in Ref. [22] for the WT, and the CBT [6], CBBM [10] and J-integral [15] methods for DCB testing. In total, 19 specimens were tested: 3 control specimens (T1), 8 stressed specimens (T2) and 8 non-stressed specimens (T3). The average initial crack lengths measured after the SCB hinge was fixed (+/− standard deviation [SD]) and the number of specimens are listed in Table 1.

3. Results

The fracture-toughness evolution of bonded joints subjected to stressed (i.e. sustained loads) and non-stressed conditions were first analysed; the results from the WT and DCB tests were then compared using the different data-reduction methods. For the WT, the crack lengths (a) measured in the control specimens (T1) and in the stressed bonded joints (T2) during the conditioning period and the corresponding fracture-toughness results evaluated using equation (1) are depicted in Fig. 3. Fully cohesive crack growth was obtained in all wedge tests, but the crack growth was arrested in all specimens after 10 h of exposure. The crack tip thus remained the same until the end of the conditioning time was reached. The fracture toughness hence was higher in the control specimens and decreased with increased crack length during the first 10 h of exposure. The cohesive fracturing that occurred after the wedge insertion denotes a strong interface adhesion between the adhesive and the adherends.

For the DCB tests performed after the WT in stressed joints (T2) and

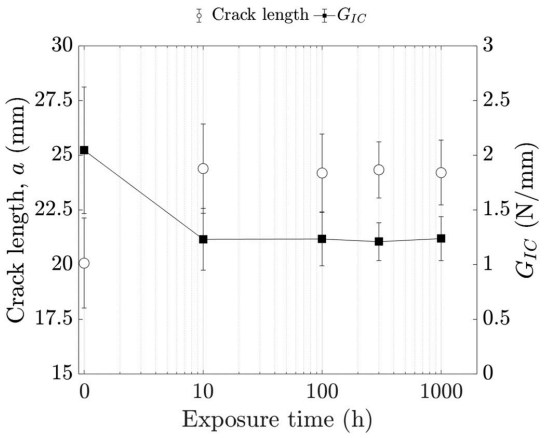

Fig. 3. Measured crack length and evaluated fracture energy during wedge testing. The average value and the SD values are indicated with dots and bars, respectively.

after the conditioning was finished in non-stressed joints (T3), the load-displacement curves from stressed (T2) and non-stressed (T3) specimens are shown in Fig. 4a and Fig. 4b, respectively. The results from the control specimens (T1) are considered as the original strength values, referred to as 0 h-exposure specimens. Fully cohesive and stable crack growth was observed in all tests, which thus showed continuous load-displacement curves. Following the ISO-25217 test standard, 65 mm of crack propagation was allowed in all tests. The curves obtained had the characteristic shape of a DCB test with nonlinear behaviour due to the elasto-plastic behaviour of the adhesive, which became more evident with increased exposure time. The initial stiffness of the specimens in both batches (T2 and T3) also decreased with increased exposure time (which was more prominent in the stressed specimens, as shown in Fig. 4a), and maximum load values and slopes were found to be different between the stressed and non-stressed specimens with the same duration of exposure.

The J-integral versus displacement curves are shown in Fig. 5a and Fig. 5b for the T2 and T3 batches, respectively. The J-integral values were calculated using equation (9), and different curves were obtained, depending on the exposure time and load conditions. Two regions are distinguishable in the J-integral curves: the first showed loading up to the peak value (i.e. crack initiation) and the second to crack propagation, where the J-integral values fluctuated around a constant value. Uniform but slightly decreasing curves were obtained with the control specimens.

Similar behaviour was observed among the curves of specimens in batch T3, which became stable after 15 mm of opening displacement (i.e. 20 mm of crack propagation). The specimens in batch T2, however, exhibited curves that started with low J-integral values and then grew to a plateau value, around which the curves fluctuated. The initial J-integral values of the curves shown in Fig. 5a decreased with increased exposure time, and the opening displacement (i.e. crack propagation) required to reach the plateau value as well as a steady-state crack growth was larger. In all cases, the original J-integral values evaluated in the control specimens were higher than those evaluated in the stressed specimens but lower than those evaluated in the non-stressed specimens. In general, the differences between the J-integral values in the stressed (T2) and non-stressed (T3) specimens were large as a consequence of the different conditioning strategies.

Fig. 6a and Fig. 6b show the results of the J-integral, CBT and CBBM methods versus displacement in stressed and non-stressed specimens, respectively. The figures include the results from specimens exposed during 0 h and 1000 h. The CBT, CBBM and J-integral methods were evaluated using equations (3), (5) and (9), respectively. CBT, CBBM and J-integral curves were found to correspond to the crack initiation and propagation phases. After 1000 h of exposure, the SERR value for crack initiation was much lower in the stressed (T2) than the non-stressed (T3) specimens, in which the evaluated SERR reached a peak value higher than in the control specimens (T1).

For the propagation phase, the SERR of non-stressed specimens (T3) was found to fluctuate around a constant value above the 0 h curves, while in stressed specimens (T2) the curves increased monotonically until a plateau value was reached below the 0 h curve. Similar SERR values were obtained using the CBT, CBBM and J-integral methods in the non-stressed specimens (T3), although the CBT values in the stressed specimens (T1) were much lower than in the CBBM or J-integral values, which are crack-length-independent methods.

The fracture-toughness results, determined as the average value of a calculated SERR or J-integral over the 65 mm of crack propagation, are shown in Table 2, Table 3 and Table 4 for reference (T1), stressed (T2) and non-stressed (T3) specimens respectively. To summarise, the fracture toughness evaluated in the stressed specimens was found to

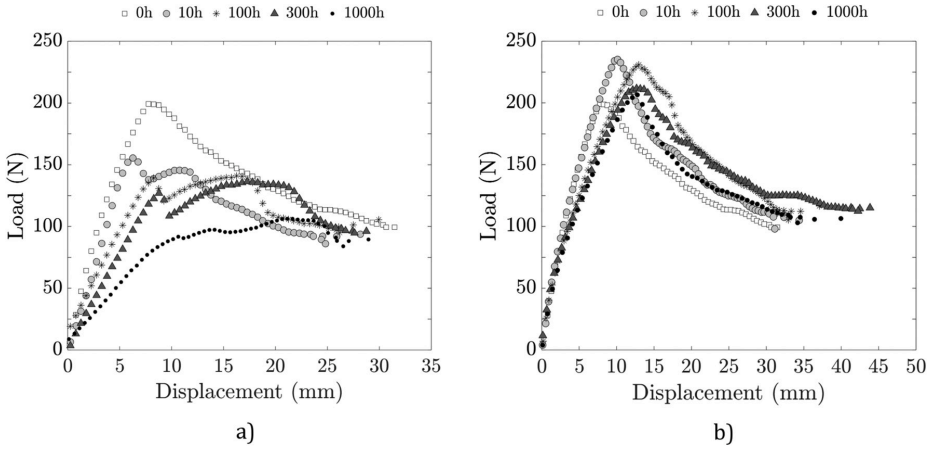

Fig. 4. DCB representative load-displacement curves for a) stressed (T2) and b) non-stressed (T3) specimens.

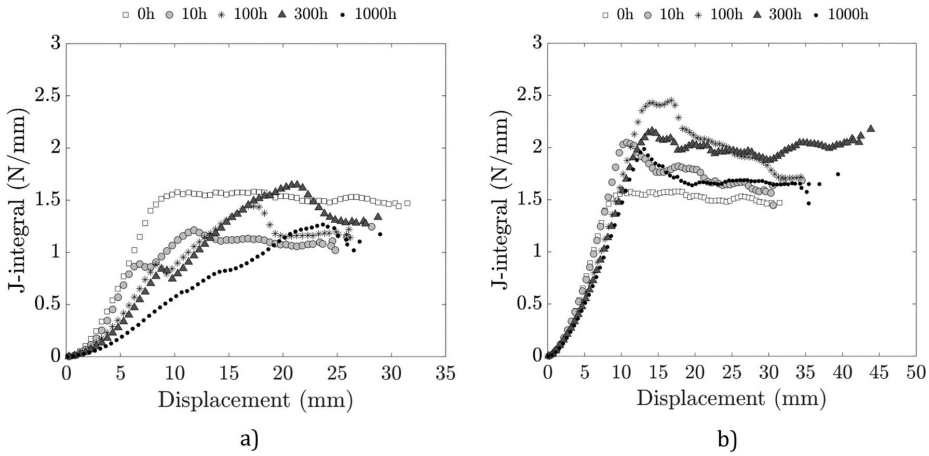

Fig. 5. Representative J-integral versus displacement curves of DCB tests performed on a) stressed (T2) and b) non-stressed (T3) specimens.

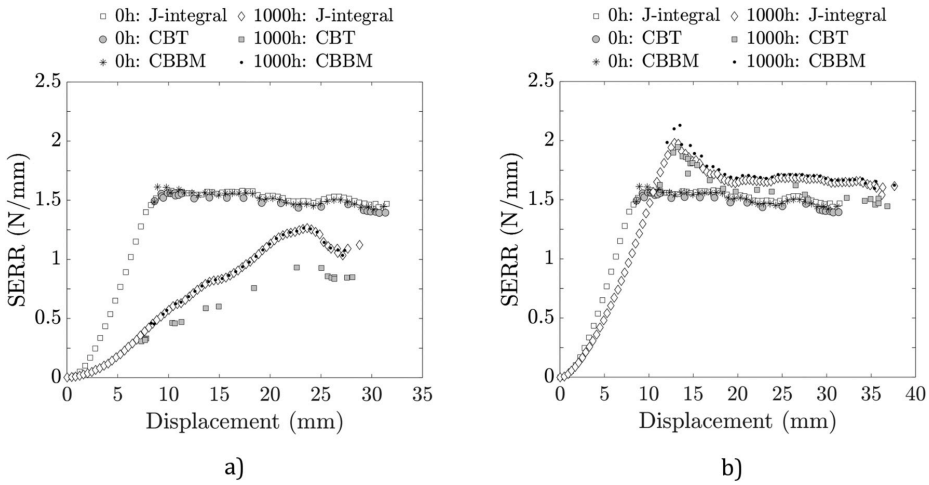

Fig. 6. Effect of exposure time in the evaluation of fracture toughness in stressed bonded joints using the J-integral, CBT and CBBM methods, for a) stressed (T2) and b) non-stressed (T3) specimens.

Table 2
Fracture toughness evaluated in reference specimens (T1), in N/mm.

	CBT		CBBM		J-integral	
Exposure time, *t* (h)	AVG	SD	AVG	SD	AVG	SD
0	1.526	0.046	1.481	0.123	1.510	0.099

Table 3
Fracture toughness evaluated in stressed specimens (T2), in N/mm.

	CBT		CBBM		J-integral	
Exposure time, *t* (h)	AVG	SD	AVG	SD	AVG	SD
10	1.111	0.147	1.154	0.105	1.152	0.110
100	0.996	0.052	1.138	0.081	1.124	0.041
300	0.878	0.000	1.062	0.310	1.086	0.312
1000	0.732	0.151	1.005	0.117	1.002	0.118

decrease with increased exposure time, while in non-stressed specimens the fracture toughness increased during the first 100 h and then decreased again close to the original value.

Fig. 7 shows the evolution of the fracture toughness with exposure time from the different tests and data-reduction methods. The fracture-toughness results obtained using the CBT, CBBM, J-integral and WT methods are compared in Table 3 and Fig. 7 for the stressed specimens (T2) and in Table 4 for non-stressed specimens (T3). As shown in Fig. 7, the fracture-toughness results obtained through DCB testing show that the fracture strength of stressed specimens (T2) decreased monotonically, while the WT results fluctuated around a constant value. The decrement after an exposure of 1000 h was around 33% when using the J-integral or CBBM methods and around 52% when using the CBT method; the mismatch between the results became more pronounced with increased exposure time. The WT showed a decrement of 10%,

Table 4
Fracture toughness evaluated in non-stressed specimens (T3), in N/mm.

	CBT		CBBM		J-integral	
Exposure time, t (h)	AVG	SD	AVG	SD	AVG	SD
10	1.894	0.015	1.715	0.070	1.700	0.040
100	1.886	0.041	1.941	0.183	2.042	0.000
300	1.814	0.307	1.837	0.263	1.788	0.277
1000	1.649	0.000	1.714	0.034	1.618	0.113

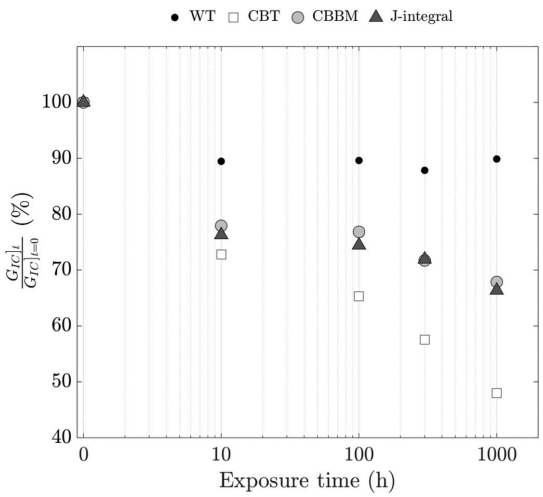

Fig. 7. Fracture toughness evaluated with different test methods in stressed specimens (T2).

however, because of the constant value 10 h of exposure onwards.

The fractured surfaces on the bonded area were also analysed by taking photos of the specimens after the completion of DCB testing. Since the findings described in Ref. [8] have demonstrated that the FPZ in healthy flexible bonded joints is around 25 mm long, the damage generated from this point on was associated with ageing. The photographed area thus is located 25 mm ahead of the crack tip. Fig. 8 shows the evolution of the fractured adhesive surfaces after being exposed to temperature and humidity conditions in stressed (T2) and non-stressed (T3) bonded joints. The failure mechanism identified in stressed bonded joints was ductile, as indicated by the coalescence and growth of voids until failure with time exposure, while brittle adhesive micro-cracking mechanisms were observed in non-stressed bonded joints.

The initial stiffness (k_0) of stressed and non-stressed specimens was evaluated from the load-displacement curves of the DCB tests, as shown in Fig. 4. Fig. 9 shows the evolution of the initial stiffness with time of exposure. Significant differences were observed between the stressed and non-stressed specimens. On the logarithmic time scale, a linear curve of the initial stiffness was observed in the stressed specimens, while in non-stressed specimens, k_0 fluctuated around a constant value. The fractured adhesive surface (Fig. 8) and the measured initial stiffness (Fig. 9) may have been related. In summary, stressed specimens lost 74% of the original stiffness after 1000 h of conditioning, while non-stressed specimens fluctuated around an average value of 42.75 ± 2.63 N/mm.

4. Discussion

Significant differences in the fracture toughness evaluated in stressed (Table 3) and non-stressed (Table 4) bonded joints were observed in this study when exposed to temperature and humidity conditions. In general, the effect of an external load (stress) is detrimental to bonded joints exposed to temperature and humidity conditions and accelerates the degradation of bonded joints when flexible adhesives are used (Fig. 7). The fracture toughness evaluated in non-stressed bonded joints, however, first increased ($t < 100$h) before decreasing to the original value, although bonded joints had long been exposed to high temperature and humidity conditions (Table 4).

In general for joints with metallic adherends, moisture diffusion only

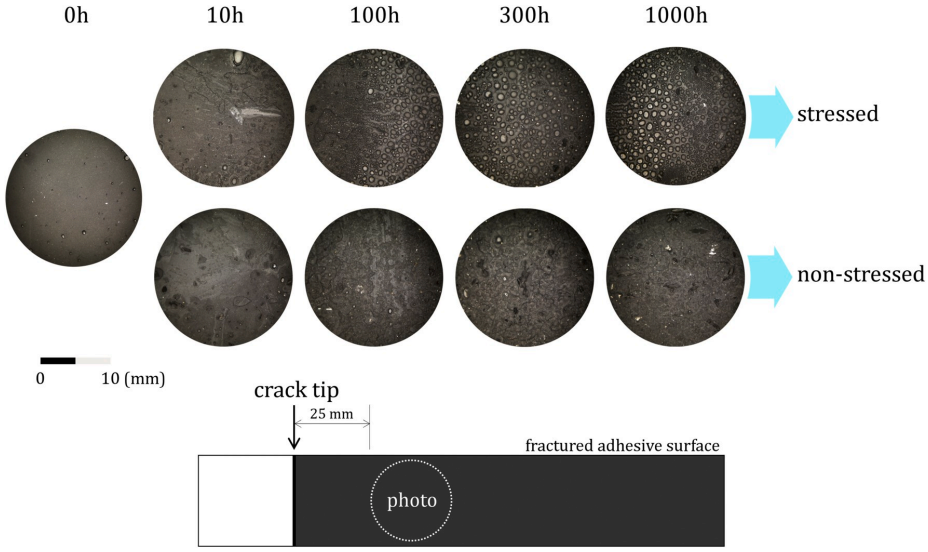

Fig. 8. Evolution of the fractured surfaces in the adhesive layer in stressed (T2) and non-stressed (T3) specimens.

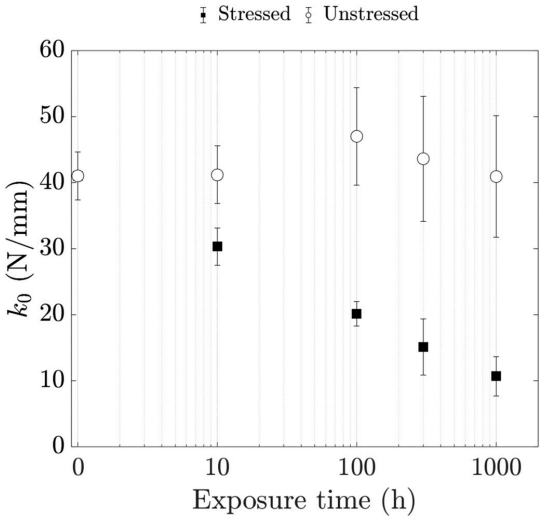

Fig. 9. Variation in initial stiffness with exposure time.

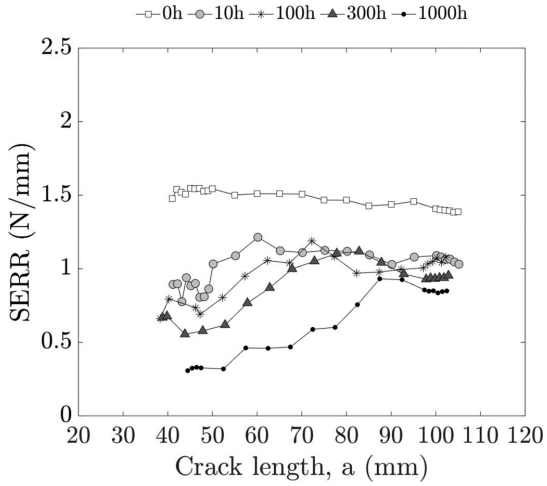

Fig. 10. R-curves evaluated through DCB testing using the CBT data-reduction method with stressed bonded joints.

occurs through the edges of the bond [5,32], and once the moisture enters the joint, the adhesive may weaken (for example by plasticisation) by causing the adhesive to crack, craze or hydrolyse, by attacking the adhesive-adherend interface or by causing the adhesive to swell [23]. As usual in accelerated testing [2], cohesive failure prevailed in all tests. The adhesive-adherend interface was resistant, and moisture diffusion primarily affected the adhesive layer. For stressed bonded joints, the temperature, moisture and sustained load conditions contributed to a viscous flow of the adhesive and the nucleation of voids, which increased in size and density with the prolongation of exposure time (Fig. 8) in agreement with findings in Ref. [29]. This scenario caused a local stress relaxation of the adhesive near the crack tip, which had a negative effect on the stiffness (by weakening, as shown in Fig. 9) and the fracture strength and toughness of the bonded joints (Figs. 4a and 7, respectively).

For non-stressed bonded joints, the temperature and moisture conditions also affected the fracture strength and toughness of the bonded joint (Fig. 4b and Table 4, respectively). The initial increase in fracture toughness is typically attributable to a post-cure of the flexible adhesive, and the reduction in fracture toughness in this study may have been caused by the micro-cracking of the adhesive in the interior of the bonded joint, as observed in Fig. 8. This reduction was lower than in the stressed bonded joints, however, since the absence of the sustained load during the environmental exposure avoided the coalescence and growth of voids.

Another finding from this study is that the area affected by the applied stress grew with increased exposure time, retarding the steady-state crack growth. For the load-displacement curves (Fig. 4a) and R-curves (Fig. 10), the length of the area in which the adhesive was weakened grew from approximately 20 mm (t = 10h) to 50 mm (t = 1000h). In agreement with [9], where changes within the FPZ were tracked in-situ, experimental results evidenced an enlargement of the FPZ that resulted in lower load and SERR values. Due to the unsteady-state crack growth, the DCB test characterisation method may show limitations to evaluate the fracture toughness in $t > 100$ h stressed bonded joints.

But although the FPZ grew, the crack did not (Fig. 3), and the damage induced in the adhesive layer was not externally visible in the stressed bonded joints. A significant lag was then produced between the external location of the crack tip and the internal location of the damage, which affected when the fracture toughness was evaluated, especially when methods that require visual measurement of the crack length were used. In the case of the wedge tests, the loss of stiffness was such that, when a certain ageing condition was reached (t = 10h), the adhesive relaxed and the opening displacement was not large enough to propagate the crack. The crack then stopped growing, and although the adhesive became more and more damaged with increased exposure time (see Table 3), the fracture toughness evaluated through equation (1) remained constant. The data-reduction method proposed in Ref. [22] thus is not valid for calculating fracture toughness when durability studies are conducted in bonded joints with a sustained load, nor is the procedure proposed in Ref. [20] appropriate to evaluate the durability of bonded joints when using flexible adhesives, which supports the recent withdrawal with no replacement of the ASTM D3762(2010) standard.

During DCB testing, large deviations in the calculated value of the fracture toughness (until approximately 20%, as shown in Table 3) were produced when using the CBT data-reduction method in bonded joints with stressed degradation (Fig. 6a), since, unlike the CBBM and J-integral methods, the CBT data-reduction method depends on visual measurement of the crack length. These deviations were found to be higher with increased exposure time (Fig. 7). While the CBT method underestimates the calculated fracture toughness, the CBBM and J-integral methods may provide reliable values of fracture toughness, since the condition of the FPZ is captured through specimen compliance and the rotation of adherends, respectively. Distinctly, in non-stressed bonded joints, the fracture toughness evaluated using the CBT data-reduction method matched the values obtained using the CBBM and J-integral data-reduction methods (Table 4), which means that the deviation between the external and internal location of the crack tip was negligible.

5. Conclusions

The present work studies the feasibility of existing experimental procedures and data-reduction methods to evaluate the evolution of the mode I fracture toughness of flexible bonded joints exposed to service conditions. The degradation of flexible bonded joints exposed to environmental conditions was observed to significantly accelerate when they were acted upon by sustained loads. But the procedure described in the recently withdrawn ASTM D3762-03(2010) standard (the wedge

test) is not suitable for flexible bonded joints, since adhesive relaxation occurs. Crack-length-dependent data-reduction methods are also not recommended when durability studies are performed and large FPZs are expected, such as in flexible bonded joints subjected to a sustained load, since a great lag between the external location of the crack tip and the internal location of the damage may be produced. The use of crack-length-independent data-reduction methods such as the CBBM and J-integral methods is thus recommended. Future efforts may focus on the development of new experimental methods providing a steady-state crack growth and crack-length-independent data-reduction methods to evaluate the evolution of the fracture energy in bonded joints under a service environment and external loads.

Data availability

The raw/processed data required to reproduce these findings cannot be shared at this time due to technical or time limitations.

Declaration of competing interest

The authors declare that they have no known competing financial interests or personal relationships that could have appeared to influence the work reported in this paper.

CRediT authorship contribution statement

J. Manterola: Conceptualization, Methodology, Investigation, Writing - original draft. **J. Zurbitu:** Conceptualization, Supervision, Writing - review & editing. **J. Renart:** Conceptualization, Writing - review & editing. **A. Turon:** Methodology, Writing - review & editing. **I. Urresti:** Resources, Project administration.

Acknowledgements

This research did not receive any specific grant from funding agencies in the public, commercial, or not-for-profit sectors.

References

[1] G. Viana, M. Costa, M.B. Banea, L.F.M. da Silva, A review on the temperature and moisture degradation of adhesive joints, Proc. Inst. Mech. Eng. Pt. L-J. Mater.-Design Appl. (2016) 1–14, https://doi.org/10.1177/1464420716671503, 0.
[2] S. Ebnesajjad, A.H. Landrock, Adhesives Technology Handbook, third ed., William Andrew, Norwich, 2015.
[3] ASTM D1151-00(2013), Standard Practice for Effect of Moisture and Temperature on Adhesive Bonds, ASTM International, West Conshohocken, PA, 2013, https://doi.org/10.1520/D1151-00R13.
[4] ASTM D1183-03(2019), Standard Practice for Resistance of Adhesives to Cyclic Laboratory Ageing Conditions, ASTM International, West Conshohocken, PA, 2019, https://doi.org/10.1520/D1183-03R19.
[5] S. Xu, D.A. Dillard, J.G. Dillard, Environmental aging effects on the durability of electrically conductive adhesive joints, Int. J. Adhesion Adhes. 23 (3) (2003) 235–250, https://doi.org/10.1016/S0143-7496(03)00027-7.
[6] ISO-25217, Determination of the mode I adhesive fracture energy of structural adhesive joints using double cantilever beam and tapered double cantilever beam specimens, Tech. rep., Rep., Int. Org. Stdzn. (2009).
[7] M. Cabello, A. Turon, J. Zurbitu, J. Renart, F. Martínez, Progressive failure analysis of DCB bonded joints using a new elastic foundation coupled with a cohesive damage model, Eur. J. Mech. Solid. 63 (2017) 22–35, https://doi.org/10.1016/j.euromechsol.2016.12.004.
[8] J. Manterola, M. Aguirre, J. Zurbitu, J. Renart, A. Turon, I. Urresti, Using acoustic emissions (AE) to monitor mode I crack growth in bonded joints, Eng. Fract. Mech. 224 (2020), 106778, https://doi.org/10.1016/j.engfracmech.2019.106778.
[9] M.K. Budzik, J. Jumel, M.E.R. Shanahan, An in situ technique for the assessment of adhesive properties of a joint under load, Int. J. Fract. 171 (2) (2011) 111–124, https://doi.org/10.1007/s10704-011-9630-x.
[10] M.F.S.F. de Moura, J.J.L. Morais, N. Dourado, A new data reduction scheme for mode I wood fracture characterization using the double cantilever beam test, Eng. Fract. Mech. 75 (2008) 3852–3865, https://doi.org/10.1016/j.engfracmech.2008.02.006.
[11] G. Viana, M. Costa, M.D. Banea, L.F.M. da Silva, Moisture and temperature degradation of double cantilever beam adhesive joints, J. Adhes. Sci. Technol. 31 (2017) 1824–1838, https://doi.org/10.1080/01694243.2017.1284640.
[12] Z. Jia, G. Yuan, D. Hui, X. Feng, Y. Zou, Effect of high strain rate and low temperature on mode II fracture toughness of ductile adhesive, Int. J. Adhesion Adhes. 86 (2018) 105–112, https://doi.org/10.1016/j.ijadhadh.2018.09.003.
[13] L. Zhang, L. Zhou, J. Zhang, Z. Wang, S. Lu, Influence of high temperature on the flexural properties of GF/pCBT laminates and their fusion-bonded joints, Compos. Pt. B 110 (2017) 124–131, https://doi.org/10.1016/j.compositesb.2016.11.020.
[14] S. Budhe, M.D. Banea, S. de Barros, L.F.M. da Silva, An updated review of adhesively bonded joints in composite materials, Int. J. Adhesion Adhes. 72 (2017) 30–42, https://doi.org/10.1016/j.ijadhadh.2016.10.010.
[15] A.J. Paris, P.C. Paris, Instantaneous evaluation of J and C-star, Int. J. Fract. 38 (1988), https://doi.org/10.1007/BF00034281, 19-21.
[16] M. Pérez-Galmés, J. Renart, C. Sarrado, A. Rodríguez-Bellido, J. Costa, A data reduction method based on the J-integral to obtain the interlaminar fracture toughness in a mode II end-loaded split (ELS) test, Compos. Pt. A 90 (2016) 670–677, https://doi.org/10.1016/j.compositesa.2016.08.020.
[17] U. Stigh, K.S. Alfredsson, A. Biel, Measurement of cohesive laws and related problems, Proc. ASME Int. Mech. Eng. Congre. Expo. (IMECE) 11 (2009) 293–298, https://doi.org/10.1115/IMECE2009-10474.
[18] C. Sarrado, A. Turon, J. Renart, J. Costa, An experimental data reduction method for the Mixed Mode Bending test based on the J-integral approach, Compos. Sci. Technol. 117 (2015) 85–91, https://doi.org/10.1016/j.compscitech.2015.05.021.
[19] J. Manterola, M. Cabello, J. Zurbitu, J. Renart, A. Turon, J. Jumel, I. Urresti, Effect of the width-to-thickness ratio on the mode I fracture toughness of flexible bonded joints, Eng. Fract. Mech. 218 (2019), 106584, https://doi.org/10.1016/j.engfracmech.2019.106584.
[20] ASTM D3762-03(2010), Standard Test Method for Adhesive-Bonded Surface Durability of Aluminium (Wedge Test), ASTM International, West Conshohocken, PA, 2010, https://doi.org/10.1520/D3762-03R10.
[21] J. Cognard, The mechanics of the wedge test, J. Adhes. 20 (1986) 1–13, https://doi.org/10.1080/00218468608073236, 1.
[22] D. Plausinis, J.K. Spelt, Designing for time-dependent crack growth in adhesive joints, Int. J. Adhesion Adhes. 15 (1995) 143–154, https://doi.org/10.1016/0143-7496(95)91625-G.
[23] R.D. Adams, J.W. Cowap, G. Farquharson, G.M. Margary, D. Vaughn, The relative merits of the Boeing wedge test and the double cantilever beam test for assessing the durability of adhesively bonded joints, with particular reference to the use of fracture mechanics, Int. J. Adhesion Adhes. 29 (2009) 609–620, https://doi.org/10.1016/j.ijadhadh.2009.02.010.
[24] M. Budzik, J. Jumel, K. Imielinska, M.E.R. Shanahan, Accurate and continuous adhesive fracture energy determination using an instrumented wedge test, Int. J. Adhesion Adhes. 29 (2009) 694–701, https://doi.org/10.1016/j.ijadhadh.2008.11.003.
[25] J.P. Sargent, Durability studies for aerospace applications using peel and wedge tests, Int. J. Adhesion Adhes. 25 (2005) 247–256, https://doi.org/10.1016/j.ijadhadh.2004.07.005.
[26] D.O. Adams, K.L. DeVries, C. Child, Durability of adhesively bonded joints for aircraft structures, Proc. Fed. Aviat. Adm. JAMS Tech. Rev. Meet. (2012). Baltimore, MD.
[27] D.O. Adams, K.L. DeVries, C. Child, N. Brown, Test method development for environmental durability of bonded joints, Proc. Fed. Aviat. Adm. JAMS Tech. Rev. Meet. (2013). Everett, WA.
[28] D.O. Adams, K.L. DeVries, N. Brown, D. Ricsi, K. Gillette, Test method development for environmental durability of composite bonded joints, Proc. Fed. Aviat. Adm. JAMS Tech. Rev. Meet. (2014). Seattle, WA.
[29] J. Jumel, S. Chauffaille, M.K. Budzik, M.E.R. Shanahan, J. Guitard, Viscoelastic foundation analysis of single cantilevered beam (SCB) test under stationary loading, Eur. J. Mech. Solid. 39 (2013) 170–179, https://doi.org/10.1016/j.euromechsol.2012.10.005.
[30] G. Jhin, S. Azari, A. Ameli, N.V. Datla, M. Papini, J.K. Spelt, Crack growth rate and crack path in adhesively bonded joints: comparison of creep, fatigue and fracture, Int. J. Adhesion Adhes. 46 (2013) 74–84, https://doi.org/10.1016/j.ijadhadh.2013.05.009.
[31] J. Renart, N. Blanco, E. Pajares, J. Costa, S. Lazcano, G. Santacruz, Side Clamped Beam (SCB) hinge system for delamination tests in beam-type composite specimens, Compos. Sci. Technol. 71 (2011) 1023–1029, https://doi.org/10.1016/j.compscitech.2010.10.005.
[32] MIL-HDBK-17-1F, Composite Materials Handbook: Vol. 1. Polymer Matrix Composites Guidelines for Characterization of Structural Materials, vol. 1, Department of Defense Handbook, 2002 (Chapter 7).

Paper D

Mode I fracture characterisation of rigid and flexible bonded joints using an advanced Wedge-Driven Test

J. Manterola[a], J. Renart[b], J. Zurbitu[a], A. Turon[b], I. Urresti[a]
[a]Ikerlan Technology Research Centre, Applied Mechanics Area, Mondragón, Spain
[b]AMADE, Polytechnic School, Universitat de Girona, Girona, Spain

The paper has been published in
Mechanics of Materials Vol. 148, 103534, 2020.

Mechanics of Materials 148 (2020) 103534

Contents lists available at ScienceDirect

Mechanics of Materials

journal homepage: www.elsevier.com/locate/mechmat

Research paper

Mode I fracture characterisation of rigid and flexible bonded joints using an advanced Wedge-Driven Test

J. Manterola[a,*], J. Renart[b,c], J. Zurbitu[a], A. Turon[b], I. Urresti[a]

[a] Ikerlan Technology Research Centre, Basque Research and Technology Alliance (BRTA), Po. J. Ma. Arizmendiarrieta, 2, 20500 Arrasate-Mondragón, Spain
[b] AMADE, Polytechnic School, University of Girona, Campus Montilivi, s/n, 17071 Girona, Spain
[c] Serra Húnter Fellow, Generalitat de Catalunya, Spain

ARTICLE INFO

Keywords:
Mode I fracture toughness
Bonded joints
Test method
Wedge Test
Flexible adhesive

ABSTRACT

The resistance to fracture of a bonded joint is usually evaluated through the experimental characterisation of its fracture toughness. Different test procedures and data reduction methods are available in the literature, such as the ISO-25217 test standard. The need for crack length measurement has led to inaccurate results when large adhesive thicknesses or flexible adhesives were studied. Advanced test protocols based on the insertion of a wedge, such as the Wedge Test (WT) in ASTM D3762 or the Wedge-Driven Test (WDT), simplify the test procedure, but most such procedures do not allow for the measurement of fracture toughness. Further, experimental results are scarce in the literature, especially when dealing with bonded joints and considerable thicknesses. In the present work, an advanced data reduction method based on the WDT is presented: The Wedge-Driven Test Plus (WDT+). The fracture toughness of specimens made by bonding two aluminium adherends with a rigid and a flexible adhesive was measured, and the effect of wedge thickness and test speed at low displacement rates on the test results was analysed. The results were compared with static tests performed in a double cantilever beam (DCB) following ISO-25217. It has been demonstrated that the proposed data reduction method is less sensitive to test speed and enables different adhesive types, and bondline thickness and wedge thickness configurations, thereby improving the WDT available in the literature.

1. Introduction

The quality of a bonded joint is defined by its mechanical capacity when exposed to external loads and environmental conditions. Since the overall performance of a bonded joint depends on the individual contribution of its constituents and the integration between them, different methods are needed to evaluate its quality. Concerning fracture behaviour, the mode I opening is considered the most critical fracture mode, and therefore different experimental methods are used to evaluate mode I fracture strength and the toughness of bonded joints (da Silva et al., 2012).

The ISO-25217 test standard (ISO-25217, 2009) is the most widespread standardised method for measuring mode I fracture toughness (G_{IC}) in structural adhesives, i.e. critical energy release rate (ERR). Double cantilever beam (DCB) specimens are used as test samples (Manterola et al., 2019a, 2019b) due to their simplicity. However, the data reduction procedures require measuring crack length to determine fracture toughness. The compliance-based beam method (CBBM) is an alternative method used to avoid crack length measurement during the test (De Moura et al., 2008). However, this data reduction scheme is based on beam theory and specimen compliance, and even though crack length monitoring is avoided, the out-of-plane shear modulus of the adherends is needed to iteratively adjust the flexural modulus of the specimen. The CBBM becomes a laborious procedure when specimens with different materials and geometries are tested. The J-integral method is another alternative to characterise fracture toughness in bonded joints (Paris and Paris, 1988). In this case, crack length measurement is avoided since the relative rotation between the adherends is measured, e.g. with inclinometers (Manterola et al., 2019a). In any case, the intrinsic problem of DCB tests is that the crack growth rate decreases during the progress of the test when a constant opening displacement rate is applied, changing the loading conditions during crack propagation.

The Wedge Test (WT) standardised by ASTM D3762 is used to evaluate, in a qualitative manner, the environmental durability of adherend-surface preparations in bonded joints with metal adherends (ASTM D3762-03, 2010). The test procedure consists of inserting a wedge with the same thickness as the adherend into the bonded joint,

* Corresponding author.
E-mail address: jmanterola@ikerlan.es (J. Manterola).

https://doi.org/10.1016/j.mechmat.2020.103534
Received 10 January 2020; Received in revised form 3 July 2020; Accepted 6 July 2020
Available online 08 July 2020

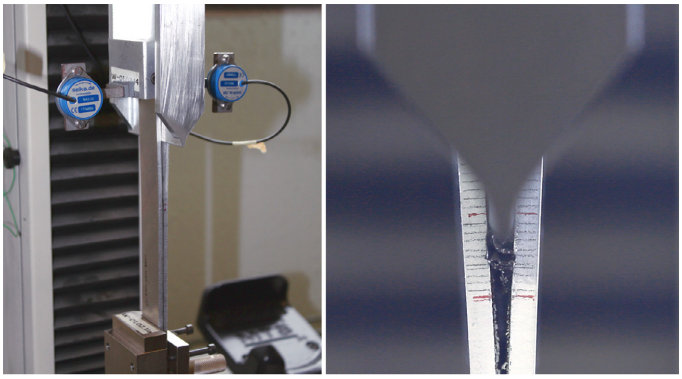

a) b)

Fig. 1. (a) A WDT+ test in progress with attached inclinometers, and (b) tearing and sweeping of the adhesive.

exposing the specimen to an aggressive environment and measuring the crack length when propagation finishes, which is related to the toughness of the joint. A comparative study between crack lengths in different bonded joints may give a qualitative overview of the performance of the joint, but further analysis is needed to obtain a quantitative value of the fracture toughness of the bonded joint (Adams et al., 2009; McCartin et al., 2016; Sargent, 2005; Manterola et al., 2020). In Cognard (1986), a simplified formulation was proposed to calculate the fracture toughness of bonded joints with a negligible bondline thickness. In Plausinis and Spelt (1995), an improvement was proposed which considers the adhesive as an elastic material. However, small errors in crack length measurement result in large errors in fracture toughness (Jumel and Shanahan, 2008), and thus alternative methods to estimate crack length have been analysed, e.g. using strain gauges (Budzik et al., 2009) or acoustic emissions (Manterola et al., 2019b).

In Glessner et al. (1989), a different test procedure based on the wedge test was proposed. The Wedge-Driven Delamination (WDD) method was designed to characterise the mode I interlaminar fracture toughness of unidirectional carbon fibre composites. In the WDD testing design, the sample is forced upon a stationary low-friction wedge and, unlike in DCB tests, the crack front position relative to the contact point between the wedge and the adherends remains constant, on average, during crack propagation. Thus, steady crack growth is obtained, and the data reduction method is simplified to $G_{IC} = P/B$, avoiding crack length measurement. In this scheme, bondline thickness is neglected. In Williams (1998), an analytical expression was developed which considers the equivalent coefficient of friction (COF) between the wedge and adherends. A forced driven wedge is simulated for the separation of a thin adherend bonded to an infinitively rigid adherend. These simulations, however, were not experimentally validated in Williams (1998) so that some experimental data were taken from the literature for comparison. In Renart et al. (2020), the Wedge-Driven Test (WDT) was proposed as an alternative method to evaluate the fracture strength of composite structures bonded with thin adhesive layers. Unlike WDD, this method allows friction between the wedge and adherends, and the wedge design is much simpler. However, in order to avoid crack length measurement, the equivalent COF must be deduced by fitting experimental data to analytical expressions based on the simple beam theory. Furthermore, in Dillard et al. (2011), the WDT was used to characterise mode I fracture resistance over a range of crosshead rates up to 1 m/s, with the conclusion that WDT may offer a useful alternative to the DCB test, since WDT eliminates the dependence of the crack-tip loading rate on debond length or resolution issues associated with imaging the entire specimen, as required for dynamic testing.

Finally, an advanced WDT method named the Smart Wedge (SW) test was presented in Adams et al. (2018). This study proposed a new test tool to obtain experimental results out of a universal testing machine. The vertical opening load is monitored using load transductors, and crack length measuring is avoided for the evaluation of fracture toughness. However, the flexural stiffness ($E_f I$) must be obtained using a post-tested wedge specimen under DCB-type loading and, at this point, the crack length must be measured.

In this contribution, an improvement and simplification of the WDT procedure developed in Renart et al. (2020) is presented to generate fast and fully-objective results. The test procedure is simplified, avoiding crack length measuring, equivalent COF estimation and load tracking by using inclinometers. Moreover, a new data reduction method is developed for application to different adhesives and bondline thickness configurations. The scope of the WDT method in Renart et al. (2020) is increased towards flexible adhesives and thick adhesive layers commonly used for industrial applications.

2. Methodology

A new test methodology based on the WDT was developed to evaluate fracture toughness in bonded joints with both a rigid and a flexible adhesive. The new methodology named Wedge-Driven Test Plus (WDT+) was compared to standard DCB tests. For this purpose, different batches of specimens were manufactured and tested according to the requirements of each test method. Besides, different low displacement rates were applied to evaluate the robustness of the test method for the quasi-static characterisation of the fracture toughness. To enable the adaptation of the WDT+ method to different bonded joint configurations, three different wedge thicknesses were used, and their effect on the test results were evaluated. Since rigid and flexible adhesives were tested, two different data reduction methods were compared for the DCB test: the corrected beam theory (CBT) proposed in the ISO-25217 standard (ISO-25217, 2009), and the J-integral approach (Manterola et al., 2019a).

2.1. Wedge-Driven Test Plus (WDT+)

The test involves the insertion of a wedge between the adherends of a bonded joint at a constant displacement rate to generate a fracture in the adhesive layer (Fig. 1a), while the bonded joint is clamped to the frame of the testing machine. After the test, the wedge is pulled towards its origin.

During insertion, the wedge moves towards the crack front until the crack starts to propagate, positioning the wedge at this moment: $d = d_{ini}$. From here, the wedge ideally moves at the same displacement

rate together with the crack front, having a constant distance (a) between them. However, as demonstrated in Renart et al. (2020), the method is also appropriate for adhesives that exhibit stick-slip behaviour. The wedge stops when the displacement d is equal to 125 mm and then returns to the origin. When the crack starts to propagate ($d > d_{ini}$), the wedge is in contact with the metallic adherend, i.e. the adhesive-free sliding surface. After several millimetres of propagation ($d = d_{lim}$), the wedge is inserted into the adhesive layer. Since in flexible bonded joints the wedge tears and sweeps the adhesive (Fig. 1b), only the data between d_{ini} and d_{lim} are considered of interest to calculate the fracture toughness in bonded joints.

Fracture toughness was obtained following the procedure described in Renart et al. (2020). However, the method was improved by measuring the rotation at the contact point between the wedge and the specimen. To do so, two NA3-30 capacitive inclinometers from SEIKA Mikrosystemtechnik GmbH were fixed to each adherend to measure their rotation (Fig. 1a), provided that the rotation of the adherends at the fractured end was the same as that at the contact point. Moreover, measuring the opening angle allowed to consider the rotation of the specimen arms near the crack front produced by the flexibility of the specimen. Then, a corrected crack length (a_c) was considered for the following instead of a. During wedge insertion, the load needed to move the wedge, and the individual opening angle of each adherend was recorded and averaged. Considering the adherends in the fractured path as cantilever beams, the following geometrical equation was obtained for the corrected crack length (Williams, 1998):

$$a_c = \frac{3}{2}\frac{\delta_y}{\tan\theta}, \tag{1}$$

where θ is the average of the angle at the contact point measured with the inclinometers, δ_y is the opening displacement of the adherends at the contact point between the wedge and the adherends, and a is the distance between the crack-tip and the contact point. Knowing a_c and δ_y, the expression for the energy release rate (ERR) is given as follows:

$$G_I = \frac{3}{4}\frac{E_x h^3 \delta_y^2}{a_c^4}, \tag{2}$$

where E_x is the Young's modulus of the adherend, and h is the adherend thickness.

The equivalent coefficient of friction (COF) between the wedge and the adherends, μ_{eq}, can also be post-processed. For this purpose, loads and contact points between the adherends and the wedge must be analysed first, following the load scheme presented in Fig. 2.

Three forces act on the wedge during its insertion: the load needed to move the wedge forward, F_{push}, a normal contact load between the wedge and the specimen, F_N, and a friction force, F_F. The normal and friction forces can be decomposed into a vertical and a horizontal contact force (in red), where the vertical component is the load needed to open the specimen's arms ($P = F_{Cy}$). A relationship between F_{push} and P may be obtained:

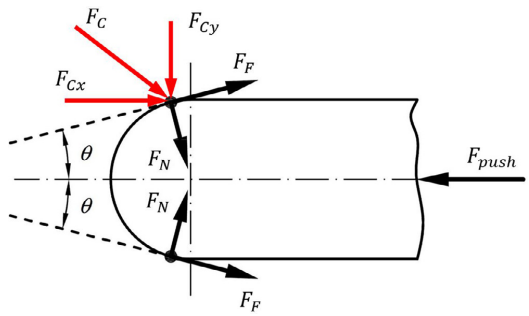

Fig. 2. Loads acting on the wedge during the loading and propagation phases. Adapted from Renart et al. (2020).

$$F_{push} = 2P\frac{\mu_{eq} + \tan\theta}{1 - \mu_{eq}\tan\theta}. \tag{3}$$

Following simple beam theory (SBT) but considering a corrected crack length, the expression for the opening load at the contact point between the wedge and the adherends reads:

$$P = \frac{E_x B h^3 \delta_y}{4a_c^3}, \tag{4}$$

where B is the specimen width. Thus, an expression for the equivalent COF can be determined using Eqs. (3) and (4):

$$\mu_{eq} = \frac{2a_c^3 F_{push}}{E_x B h^3 \delta_y} - \tan\theta. \tag{5}$$

Since small deviations in geometrical measurements result in large errors in the calculated values of fracture toughness, the contact point between a rounded wedge and the adherends was also analysed. Further, simplified (point A) and exact (point B) contact points were considered for the analysis (Fig. 3); and later, in Section 4, the relative error in the estimation of the fracture toughness derived from the simplified contact point is discussed. Besides, the influence of the thickness of the interface or the bonded joint was considered in the formulation.

As anticipated in Renart et al. (2020), if the ratio a/r_w is large enough, point A can be assumed as the contact point instead of B. Thus, the opening displacement of the adherends at the contact point A is:

$$\delta_y^A = \frac{D_w - t_a}{2}, \tag{6}$$

where D_w is the total thickness of the wedge, and t_a is the thickness of the bonded joint (for thin adhesives or delamination tests $t_a \approx 0$). If the exact contact point (point B) is considered in the analysis, the crack length is $a = \bar{a} - \zeta$, and the exact opening displacement reads:

$$\delta_y^B = \sqrt{\left(\frac{D_w}{2}\right)^2 - \zeta^2} - \frac{t_a}{2}, \tag{7}$$

where ζ is the distance between the exact (a) and the simplified ($\bar{a}$) crack lengths. Since the distance ζ is difficult to measure, it can be estimated using Euler's beam theory. The angle of rotation of the adherends in the contact point B, θ_B, is:

$$\tan\theta_B = \left.\frac{dy}{dx}\right|_{x=\bar{a}-\zeta} = \frac{3\sqrt{\left(\frac{D_w}{2}\right)^2 - \zeta^2}}{2(\bar{a} - \zeta)}. \tag{8}$$

The angle θ_B can also be estimated though the geometrical relationship:

$$\tan\theta_B = \frac{\zeta}{\sqrt{\left(\frac{D_w}{2}\right)^2 - \zeta^2}}. \tag{9}$$

Combining Eqs. (8) and (9), the distance ζ is obtained:

$$\zeta = \sqrt{\bar{a}^2 + 3\left(\frac{D_w}{2}\right)^2} - \bar{a}. \tag{10}$$

However, the evaluation of δ_y^B requires the measurement of $\bar{a}$. To avoid this, the formulation proposed in Eq. (11) for the reduction of data in the WDT+ assumes a simplified contact point between the wedge and the adherends, contact point A Fig. 3b). Using Eqs. (1), ((2) and (6), an expression for the ERR was obtained, and it reads:

$$G_I = \frac{16}{27}\frac{E_x h^3 \tan^4\theta}{(D_w - t_a)^2}. \tag{11}$$

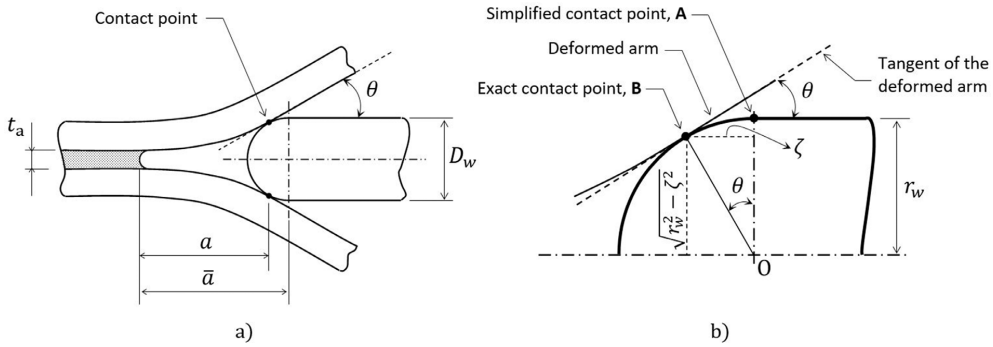

Fig. 3. (a) Contact points between the wedge and the adherends, and (b) geometrical analysis of the contact point. Adapted from Renart et al. (2020).

2.2. DCB tests

DCB tests were run following the DCB test protocol described in the ISO-25217 test standard. The CBT and J-integral data reduction methods were applied to obtain G_{IC}. For the CBT data reduction method, the crack position was recorded using an optical system (Canon 550D and macro EF100) during the test. The mode I critical ERR was obtained with the following equation:

$$G_{IC} = \frac{3P\delta}{2B(a + |\Delta|)}\frac{F}{N}, \tag{12}$$

where P is the applied load, δ is the displacement of the load application point, B is the total width of the bonded area, a is the crack length, Δ is a correction factor for the crack length based on the compliance of the bonded joint, F is the large-displacement correction and N is the load-block correction (ISO-25217, 2009).

For the J-integral method, the rotation of the adherends and the applied load were measured. Thus, the same two capacitive inclinometers used for the WDT+ were fixed to the adherends (Fig. 4). The formulation proposed for the reduction of data in the J-integral method reads (Manterola et al., 2019a):

$$J_I = \frac{P}{B}\sin\theta, \tag{13}$$

where θ is the relative rotation between the adherends at the applied load position with respect to the bondline of the DCB specimen.

2.3. Experimental test campaign

DCB test specimens were manufactured by bonding two aluminium adherends, 3-mm thick and 200-mm long, with two different adhesives:

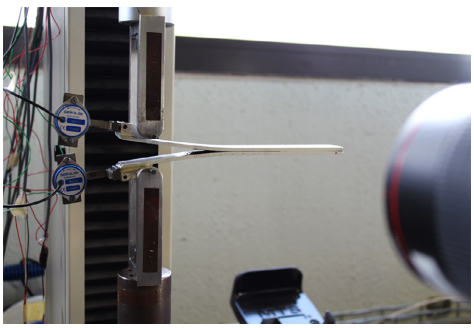

Fig. 4. DCB specimen with inclinometers during the test.

a methacrylate rigid adhesive (Araldite 2021) and a silicone-based flexible adhesive (SIKASIL SG-500). Both adhesives are two-component, high-strength structural adhesives, but completely different behaviours were expected due to their different natures. High-strength aluminium alloy (type Al 7075-T6) adherends were used to prevent any plastic deformation during the test, with a Young's modulus of 71 GPa and a yield strength of 550 MPa.

The aluminium substrates were first rough-filed (rigid adhesive) or sanded (flexible adhesive) then cleaned with acetone to remove the native metal oxide. Prior to bonding, the substrates were cleaned again with isopropyl alcohol. Teflon-calibrated spacers were placed in-between the adherends to ensure a constant thickness of the adhesive layer throughout the whole specimen and also to delimit an edge in the crack front. The specimens were cured to allow the crosslinking of the adhesive to occur. Different curing cycles were applied for each adhesive type. In the case of the Araldite 2021, a curing temperature of 60 °C and a relative humidity of 50% for 12 h was applied; and in the case of the SIKASIL SG-500, the curing was performed under ambient room temperature conditions for 72 h. To validate manufacturer recommendations for the curing cycle of the Araldite 2021, a differential scanning calorimetry (DSC) test was carried out on a small piece of bulk adhesive to measure its glass transition temperature (T_g). Regarding the heat flow versus temperature curve obtained in the DSC test, a T_g of 79.5 °C was determined.

A sharp artificial crack was produced by cutting the adhesive with a knife, and different initial crack lengths (a_0) were set for the specimens depending on the test method and the type of adhesive. Initial crack lengths of 60 mm and 40 mm were set for the rigid and flexible bonded joints for the DCB test, respectively. Whereas for the WDT+, initial crack lengths of 100 mm and 90 mm were set for the rigid and flexible adhesives, respectively (Fig. 5). Additionally, a 45° chamfer was machined in the frontal part of the substrates to allow for a softer insertion of the wedge into the bonded joint in WDT+ (Fig. 5b). All manufactured specimens had a total width of 25 mm.

Finally, the specimens manufactured for the DCB tests were painted with white spray, and then a ruler was marked in the lateral side of the joint following the requirements of ISO-25217 to measure the crack length during the test. In addition, end blocks were bonded to the adherends to apply the load for the DCB tests (Fig. 5a).

All tests were carried out in an MTS Insight 5 kN universal tensile testing machine at a temperature of 23 ± 2 °C and a relative humidity of 50 ± 5%, but they were run at different displacement rates (DR). Test specimens were separated into seven different specimen batches (T1–T7) classified by the test method, displacement rate, type of adhesive and wedge thickness in the case of specimens manufactured for the WDT+ method.

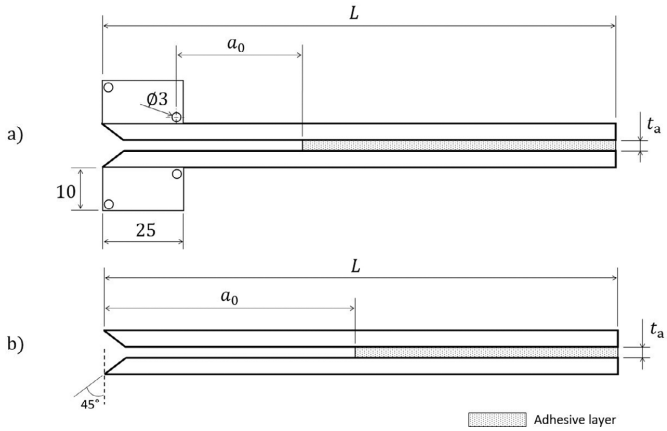

Fig. 5. Specimens for (a) DCB tests and (b) WDT+. Dimensions in mm. t_a is the bondline thickness. See values in Tables 1 and 2.

2.3.1. DCB tests

For the DCB tests, three specimen batches were tested (named T1, T2 and T3): T1 and T2 were tested at a displacement rate of 2 mm/min according to the test standard ISO-25217 to ensure quasi-static crack growth. Specimens of T3 were tested at displacement rates of 10 mm/min, 30 mm/min and 50 mm/min to evaluate the effect of test speed on test performance for the quasi-static characterisation. Regarding the type of adhesive, T1 comprised rigid bonded joints and T2 and T3 comprised flexible bonded joints. Three specimens per batch were tested. The bondline thickness, t_a, and the number of specimens tested for each batch are summarised in Table 1. Thickness measurement refers to the average (AVG) thickness measured for each batch of specimens plus/minus the standard deviation (SD).

2.3.2. WDT+ tests

For the WDT+, test conditions analogous to those in the DCB tests were applied. For this purpose, the crack position data obtained in the DCB tests were analysed, and the crack growth rate was calculated to specify equivalent displacement rates since, in WDT+, the crack growth rate is assumed to be the same as the wedge displacement rate. To do so, four different specimen batches were prepared (T4–T7): T4 and T5 were tested at displacement rates of 10 mm/min and 6 mm/min and were analogous to the displacement rates applied to T1 and T2, respectively. The specimens of batch T6 were tested at 250 mm/min, while the specimens of batch T7 (analogous to T3) were tested at displacement rates of 30 mm/min, 90 mm/min and 150 mm/min. Regarding the type of adhesive, T4 and T6 were assigned to rigid bonded joints, and T5 and T7 were assigned to flexible bonded joints. Besides, three different aluminium wedges with different thicknesses – 3.00 mm, 5.00 mm and 6.60 mm – were used to analyse the influence of wedge diameter on the results with D_w. The different wedge thicknesses were used in batches T4 and T5 – but in batches T6 and T7, only a 3.00-mm thickness was used.

For the WDT+, a total of 14 specimens were tested. The wedge thickness employed, D_w, the bondline thickness, t_a, and the number of specimens tested for each batch are summarised in Table 2. The average and standard deviation of the thickness measured were assigned to each batch of specimens.

Section 3 presents the test results of all specimens examined, while Section 4 analyses and discusses the results.

Table 1
Configuration of the specimens tested following the DCB test protocol.

Batch	Method	DR (mm/min)	Adhesive	t_a (mm)	No. tested specimens
T1	DCB	2	A2021	0.42 ± 0.07	3
T2	DCB	2	SG500	0.63 ± 0.05	3
T3	DCB	10 − 50	SG500	0.64 ± 0.03	3

*DR: Displacement Rate; t_a: bondline thickness.

Table 2
Configuration of the specimens tested following the WDT+ method.

Batch	Method	DR (mm/min)	Adhesive	D_w (mm)	t_a (mm)	No. tested specimens
T4	WDT+	10	A2021	3.00 − 6.60	0.55 ± 0.08	5
T5	WDT+	6	SG500	3.00 − 6.60	0.74 ± 0.08	5
T6	WDT+	250	A2021	3.00	0.56 ± 0.00	1
T7	WDT+	30 − 150	SG500	3.00	0.70 ± 0.03	3

*DR: Displacement Rate; D_w: wedge thickness; t_a: bondline thickness.

3. Results

First, the fracture toughness results obtained from the WDT+ with inclinometers were compared to the results obtained with the DCB tests; second, the results from the WDT+ and DCB tests were compared for different displacement rates; finally, the influence of wedge diameter on the WDT+ results was analysed.

The load displacement and R-curves are presented for the DCB tests (batches T1 and T2 are depicted in Fig. 6 and Fig. 7, respectively). The DCB tests were carried out at a displacement rate of 2 mm/min; and during the tests, the crack growth rate (da/dt) was measured. Later, an average da/dt was used to set the displacement rate for WDT+.

A fully cohesive and stable crack growth predominated in all tests, thus having continuous load-displacement curves. Some adhesive failure was detected at the beginning of crack propagation in the T1-01 specimen but did not affect test performance, since good repeatability was achieved. Following the ISO-25217 test standard, 65 mm of crack propagation was allowed in all tests. The curves obtained had the characteristic shape of a DCB test, with a linear behaviour before crack initiation in the rigid adhesive samples, and a non-linear behaviour in the flexible adhesive samples due to the viscoelastic behaviour of the adhesive (Fig. 6).

R-curves are shown in Fig. 7 for the rigid and flexible adhesives, respectively, following the CBT data reduction method. Fracture toughness was calculated following Eq. (12), and a constant and slightly decreasing curve was obtained as the crack grew. Fracture toughness

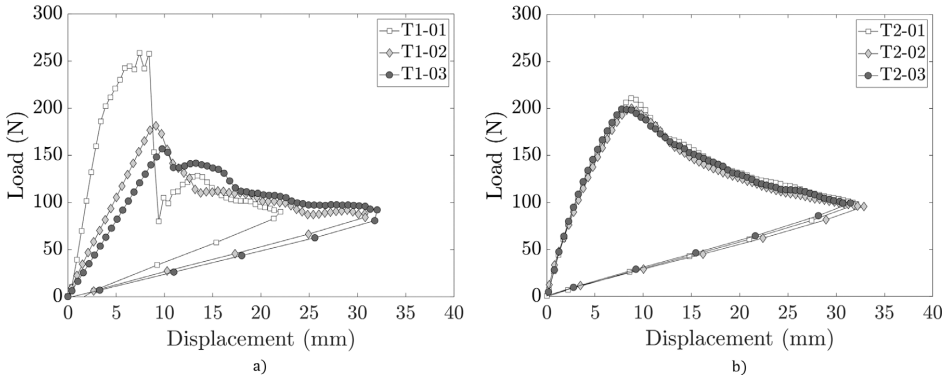

Fig. 6. DCB load-displacement curves for (a) rigid adhesive samples and (b) flexible adhesive samples.

was determined as the average value of the calculated critical ERR over the 65 mm of crack propagation.

The discrete sampling of the crack growth rate (da/dt) measured during the DCB tests is shown in Fig. 8 and, as expected for DCB tests, a decreasing crack growth rate is observed. The average crack growth rate was also calculated, being 10 mm/min and 6 mm/min for the rigid and flexible bonded joints, respectively.

From each test, the J-integral was measured through Eq. (13). A comparison between the results obtained from the CBT and the J-integral is shown in Fig. 9 for two representative bonded joints: one with a rigid and another with a flexible adhesive. Close results were obtained from both methods.

With regard to the WDT+ tests, the load-displacement curves and the equivalent COF calculated at each point of the insertion process (δ_x) are shown in Fig. 10 for representative specimens of batches T4 and T5 tested with a wedge thickness of 3.00 mm. Cohesive and stable crack growth was observed in all tests, and the crack propagation phase was delimited by d_{ini} and d_{lim}.

The loading phase ($\delta_x > d_{ini}$) showed a small peak of force at $\delta_x \approx 10$ mm when the wedge was inserted between the adherends; then, the force increased monotonically until a second peak, at which point the crack started to propagate ($\delta_x = d_{ini}$). During crack propagation ($\delta_x > d_{ini}$), F_{push} fluctuated around a *plateau* value and then dropped just before the horizontal displacement δ_x reached d_{lim}. This occurred because the sliding surface between the wedge and the adherends underwent changes due to the dirt accumulated on the adherend surface during the manufacturing process. F_{push} showed a strong peak value when the wedge was inserted into the adhesive layer ($\delta_x = d_{lim}$) of the rigid adhesive samples. The wedge hit the adhesive layer, and an increment in compressive forces was registered for a short period of time. This behaviour was not observed in the flexible adhesives. Then, the wedge was inserted into the adhesive layer. Since undesirable phenomena, such as adhesive tearing and sweeping, occurred during this latter stage, this part of the test was not used for the data post-processing. The introduction of the wedge finished when $\delta_x = 125$ mm; next, the wedge was pulled back from the specimen. Some traction forces occurred at the beginning of the removal process due to the friction between the wedge and the adhesive; however, once the wedge arrived at the adhesive-free region ($\delta_x < d_{lim}$), the traction forces were nearly zero.

According to Renart et al. (2020), the equivalent friction coefficient (COF) between the adherends can be estimated during the displacement range [10, d_{ini}] if it remains constant. However, in the present study, it was observed that the equivalent COF varied during the whole insertion process and showed strong fluctuation around a *plateau* value during the propagation phase.

The evolution of the rotation angle of the adherends measured with the inclinometers is shown in Fig. 11. The angle increased while $\delta_x < \delta_{ini}$, but then reached a *plateau* value around which the angle fluctuated during the crack propagation phase [δ_{ini}, δ_{lim}].

In the WDT+, the ERR was calculated for the experimental points with $\delta_x < d_{lim}$ through Eq. (11). ERR-displacement curves are shown in

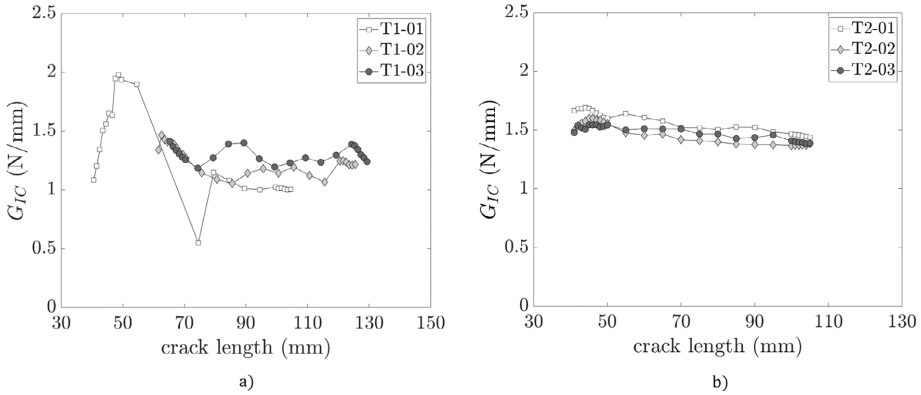

Fig. 7. R-curves for (a) rigid adhesive samples and (b) flexible adhesive samples.

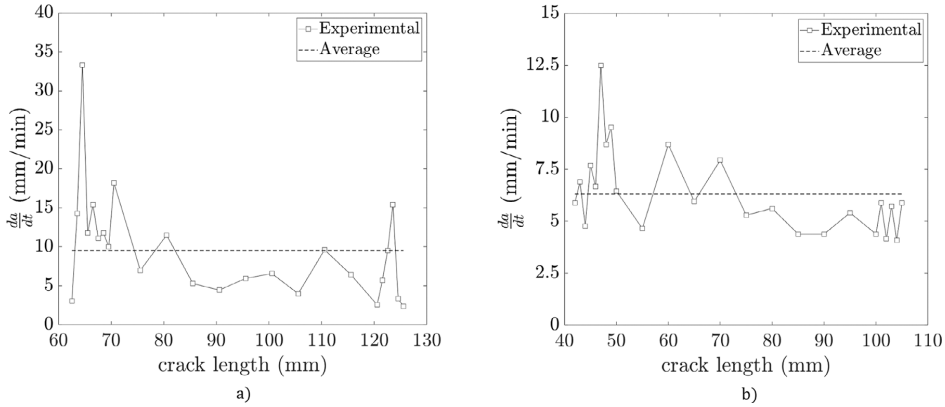

Fig. 8. Crack growth rates in (a) rigid adhesive samples (T1-02) and (b) flexible adhesive samples (T2-01), tested at a displacement rate of 2 mm/min.

Fig. 12. The ERR increased monotonically during the loading phase, then fluctuated during crack propagation. Some tests exhibited a rising ERR curve behaviour since the opening angle increased due to the dirt stuck between the wedge and adherends. However, good repeatability was achieved for both adhesive types, and the fracture toughness was determined as the average value of the ERR over the crack propagation phase delimited by d_{ini} and d_{lim}.

In Table 3, the average values and the standard deviation of the critical ERR, F^c_{push}, the equivalent COF, and the contact angle (θ^c) between d_{ini} and d_{lim} of each batch of specimens are summarised.

The G_{IC} values obtained from the DCB and WDT+ tests were similar and, concerning the WDT+, higher F^c_{push} values were needed for crack propagation in the flexible joints than in their rigid counterparts, which culminated in a higher equivalent COF. The contact angle was also higher in the flexible than in the rigid bonded joints.

Additionally, rigid and flexible bonded joints were tested at different displacement rates with the DCB (T3) and the WDT+ (T6, T7). Fig. 13 shows the load-displacement curves of flexible bonded joints tested with the DCB at different displacement rates.

The respective R-curves are shown in Fig. 14. The CBT data reduction method was applied following Eq. (12), and fracture toughness was determined as the average value of the calculated critical ERR over the 65 mm of crack propagation.

With regard to the WDT+, Fig. 15(a) and (b) shows the load-displacement curves and the equivalent COF at displacement rates of 250 mm/min and 150 mm/min, respectively.

ERR-displacement curves at different displacement rates obtained with the WDT+ are compared in Fig. 16(a) and (b) for rigid and flexible samples, respectively. Unlike in DCB tests, the fracture toughness did not increase with the displacement rate for the WDT+.

Fig. 17 summarises the fracture toughness obtained from DCB and WDT+ run at different displacement rates, for the rigid and flexible bonded joints. For comparison, the corresponding average crack growth rates have been considered although DCB tests exhibited a variable crack growth rate during propagation. The points are the average values of each batch, and the bars are the standard deviation.

The average values and the standard deviation of the critical ERR for the DCB and WDT+ tested at different displacement rate conditions, the critical load for crack propagation, the equivalent COF and the contact angle (θ^c) obtained from the WDT+ are all summarised in Table 4.

As shown in Fig. 17, in WDT+, it was possible to obtain quasi-static fracture toughness values at higher displacement rates than in DCB tests as specified in ISO-25217. Concerning the WDT+, there was an increase of F^c_{push} with the displacement rate, whereas the rotations at the contact point between the wedge and the specimen remained almost

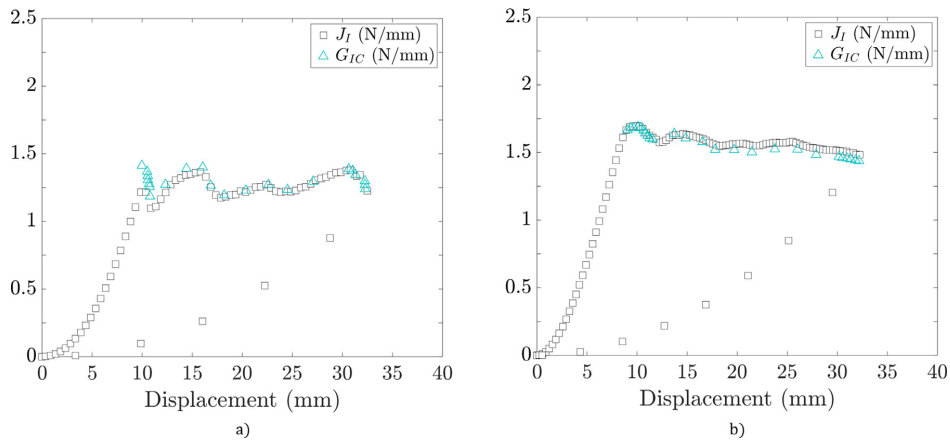

Fig. 9. CBT versus J-integral data reduction methods at a displacement rate of 2 mm/min for (a) rigid (T1-03) and (b) flexible (T2-01) adhesives.

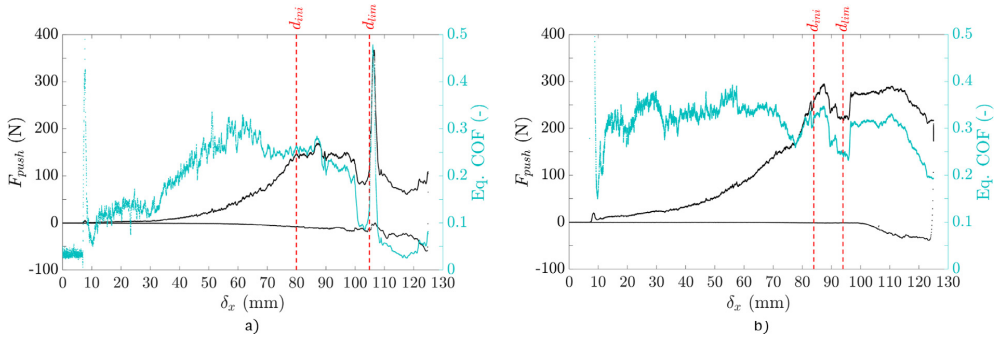

Fig. 10. Load-displacement (left axis) and equivalent COF-displacement (right axis) curves for (a) rigid (T4-01) and (b) flexible (T5-01) adhesive samples, tested following the WDT+ method.

constant. The equivalent COF also remained almost constant with the increase of the displacement rate.

The effect of wedge diameter on the results was analysed for the rigid (T4) and flexible (T5) bonded joints. Three different diameters (D_w= 3.00 mm, 5.00 mm and 6.60 mm) were tested. The ERR versus the wedge displacement curves obtained are depicted in Fig. 18, in which it can be observed that the initiation of crack propagation (d_{lim}) was reduced with the wedge thickness. Simultaneously, the crack length (distance between the crack-tip and the contact point between the wedge and the specimens) increased with the wedge diameter, e.g. the crack length was 25 mm, 35 mm and 45 mm for the rigid bonded joints, and 10 mm, 20 mm and 30 mm for their flexible counterparts, when using the 3.00 mm, 5.00 mm and 6.60 mm wedge diameters, respectively. The test carried out with the rigid adhesive bonded joint and the wedge thickness of 6.60 mm (specimen T4–05) was stopped before the rest because the crack front reached the clamped end of the specimen.

Table 5 lists the average values and standard deviation of the critical ERR, F^c_{push}, the equivalent COF and the contact angle (θ^c) between d_{ini} and d_{lim}. The results of Table 5 and Fig. 18 show that wedge thickness does not affect the G_{IC}.

4. Discussion

Fracture toughness obtained from the WDT+ method matched that obtained from the DCB tests, in both rigid and flexible bonded joints (Table 3). Concerning the DCB test, the CBT and J-integral data reduction methods yielded close values of fracture toughness (see Fig. 9). Therefore, the fracture behaviour of both adhesives meets linear elastic fracture mechanics (LEFM) conditions. Since the proposed data reduction method for the WDT+ is also based on these assumptions, the fracture toughness evaluated by the WDT+ is reliable.

The evolution of the contact angle during the test (Fig. 11) was much more stable than the evolution of the equivalent COF or the force measured with the load cell, F_{push} (see both parameters in Fig. 10). Besides, it was observed that the COF did not remain completely constant during the test and strongly depended on the adherend surface, test speed and interfacial friction coefficient, among other variables (Shi et al., 2017). Therefore, the data reduction method proposed in Eq. (11) was shown to be more robust than the data reduction method proposed in Renart et al. (2020), which strongly depends on the equivalent COF to calculate the ERR.

Load cell and inclinometer output data are compared in Fig. 19 to analyse the effect of the displacement rate on the different parameters used in the data reduction. Generally, it can be observed that the inclinometers exhibited a smoother response than the load cell. This became more evident when the wedge stopped, i.e. when it stopped from the current displacement rate to 0 mm/min. When this occurred (e.g. 1250 s in Fig. 19(a) and 50 s in Fig. 19(b)), there was a significant drop in the force, whereas the angle remained the same. As in Eq. (11), the ERR only depended on the angle and neither in the force nor the crack length, the ERR almost did not vary with the increase of the displacement rate, having quasi-static values of the fracture toughness of bonded joints.

This is an important advantage when compared to the DCB test, presenting the possibility for the WDT+ to test at slightly higher displacement rates, reducing the testing time but obtaining the same

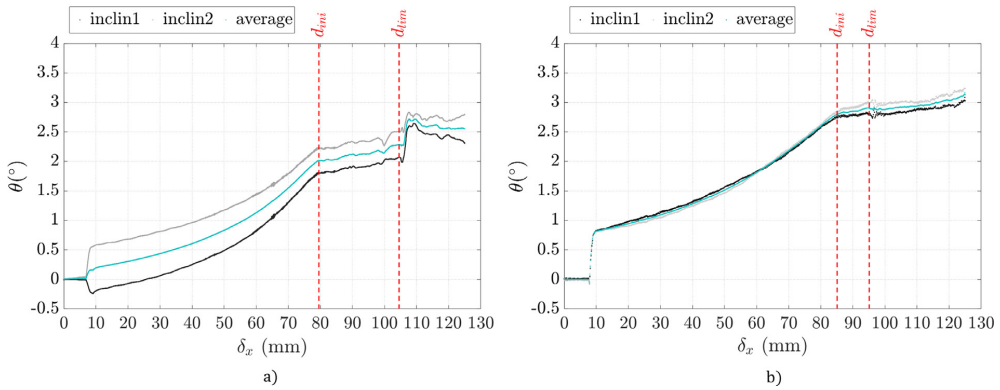

Fig. 11. Adherend rotation measured with the inclinometers in (a) rigid adhesive samples (T4-02) and (b) flexible adhesive samples (T7-03).

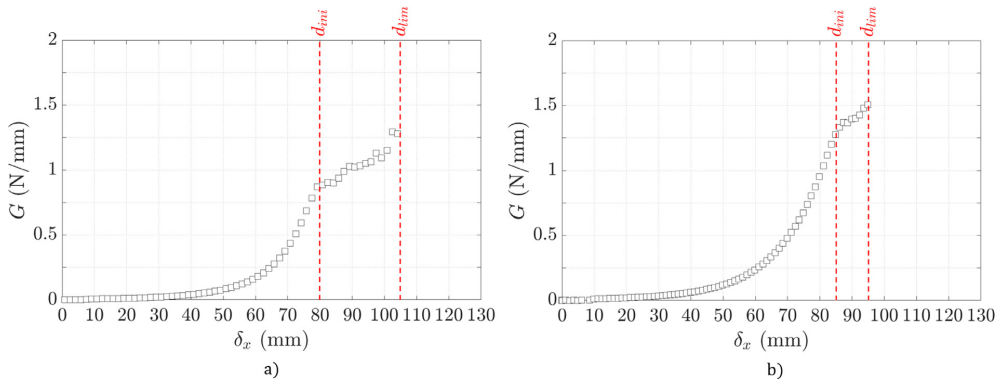

Fig. 12. ERR-displacement curves for (a) rigid (T4-01) and (b) flexible (T5-01) adhesive samples, tested following the WDT+ method. For the sake of clarity, 1 of every 1000 points is represented.

Table 3
Experimental results from DCB and WDT+.

Method	Batch	Adhesive	DR (mm/min)	D_w (mm)	G_{IC} (N/mm)		F^c_{push} (N)		Eq. COF (–)		θ^c (°)	
					AVG	SD	AVG	SD	AVG	SD	AVG	SD
DCB	T1	A2021	2	n/a	1.193	0.143	n/a	n/a	n/a	n/a	n/a	n/a
	T2	SG500	2	n/a	1.503	0.055	n/a	n/a	n/a	n/a	n/a	n/a
WDT+	T4	A2021	10	3.00	1.128	0.071	163.53	15.23	0.268	0.028	2.17	0.10
	T5	SG500	6	3.00	1.440	0.082	234.39	23.79	0.315	0.024	2.72	0.02

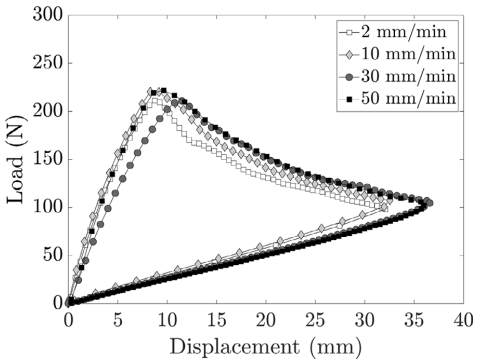

Fig. 13. Load-displacement curves from flexible adhesive samples (T2, T3) tested with the DCB test at different displacement rates.

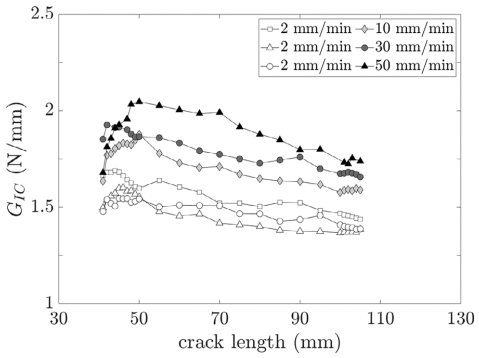

Fig. 14. R-curves from flexible bonded joints at different displacement rates with the DCB.

quasi-static value of fracture toughness (Fig. 17). An increase of the fracture toughness was expected with the increase of the displacement rate beyond the quasi-static conditions suggested in ISO-25217, as evidenced in DCB tests for flexible bonded joints (Fig. 14). However, while Wedge-Driven Tests keep an almost constant distance a during crack propagation, the data reduction method proposed in Eq. (11) is load- and crack-length-independent. Thus, dynamic effects are minimised for the evaluation of the G_{IC} and the range of test speeds at which quasi-static conditions are met is increased. In support of the proposed method, a similar strategy was followed in Dillard et al. (2011), Blackman et al. (1995, 2009) but for high rates of testing. Studies in Blackman et al. (1995) identified strong dynamic effects on the characterisation of G_{IC} in bonded joints and, to avoid so, a load- and a crack-length-independent data reduction method were suggested in Blackman et al. (2009) and Dillard et al. (2011), respectively. Then, the results in Fig. 19 clearly demonstrate that the effect of the displacement rate on the relative opening angle between adherends (θ) is almost negligible at slow displacement rates, but not on the force applied.

With regard to wedge dimension, thick wedges anticipate crack initiation (Fig. 18) and increase crack length. If the wedge diameter increases, then the fracture toughness results will be less influenced by adhesive thickness, which is beneficial for obtaining a more robust data reduction method. However, the thicker the wedge, the greater the error in the results produced due to the assumption of contact point A in Fig. 3(b). The relative error in the evaluation of the critical ERR derived from the assumption of contact point A instead of contact point B is evaluated analytically in Fig. 20(a). Additionally, the relative error in the evaluation of fracture toughness by neglecting bondline thickness in the formulation is shown in Fig. 20(b).

When D_w/t_a approaches 1, the error between the exact and simplified formulation asymptotically becomes infinite (Fig. 20(a)). This occurs because the thickness of the adhesive layer is neglected, and

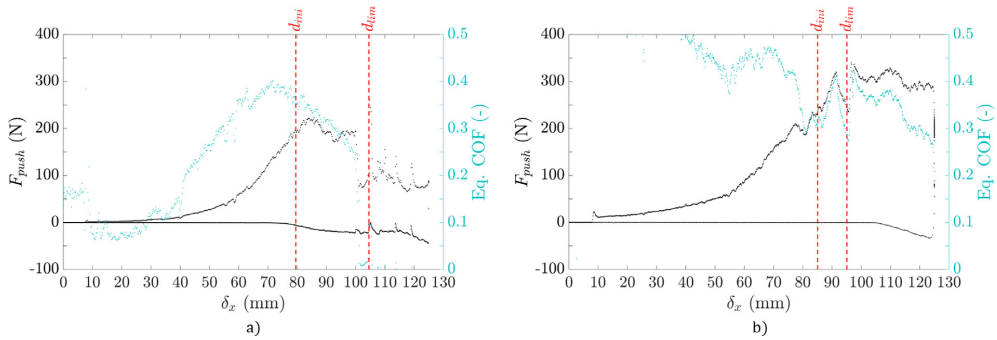

Fig. 15. Load-displacement (left axis) and equivalent COF-displacement (right axis) curves for (a) rigid (T6-01) and (b) flexible (T7-03) adhesive samples, from the WDT+.

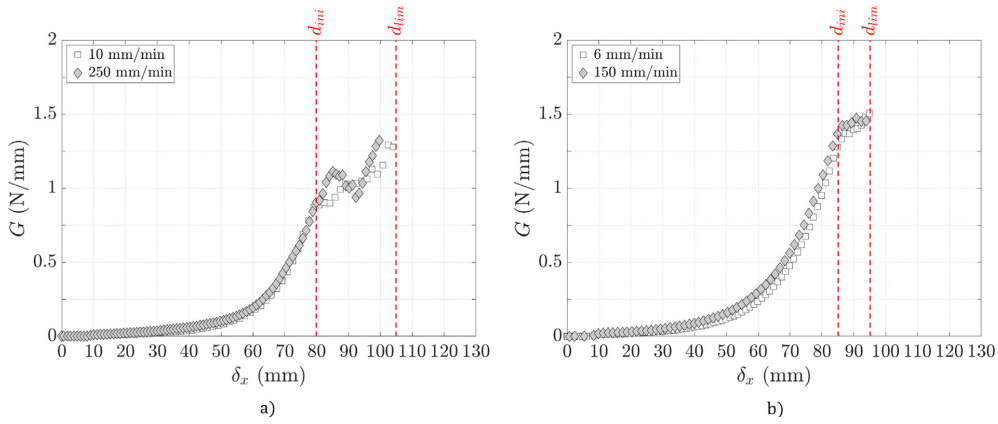

Fig. 16. ERR-displacement curves for (a) rigid (T6-01) and (b) flexible (T7-03) bonded joints, tested following the WDT+.

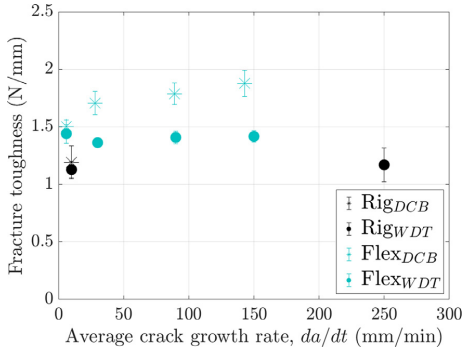

Fig. 17. Fracture toughness vs. the average crack growth rate for rigid and flexible bonded joints tested with the DCB and the WDT+.

therefore fracture toughness is incorrectly estimated, as shown in Fig. 20(b). The error also increases if D_w/t_a increases (for a given t_a), i.e. wedges with larger diameters have larger differences in the contact points (Renart et al., 2020). These effects are more pronounced for smaller crack lengths and thicker adhesives because both cases involve larger wedge diameters, and thus larger differences in the contact points and, ultimately, large errors in the estimation of fracture toughness.

In any case, the wedge configuration and the data reduction method discussed in this paper provided relative errors in the calculation of fracture toughness that were lower than 1% in all tests, as can be seen in Table 6. However, if the formulation in Renart et al. (2020), which does not consider bondline thickness, is used, significant errors may be encountered in the evaluation of fracture toughness, which depends on the bondline thickness, the wedge diameter and the contact point.

In accordance with Adams et al. (2009) and Sener et al. (2002), the data reduction method must consider the bondline thickness, which is included in Eq. (11) of the present work. Otherwise, strong deviations in the evaluation of fracture toughness will be obtained.

5. Conclusions

A new data reduction method named WDT+ is proposed to evaluate the quasi-static fracture toughness in bonded joints. Unlike Wedge-Driven Test procedures in the literature, crack length measurement, load tracking or equivalent COF estimation are avoided to evaluate mode I fracture toughness in bonded joints. Then, the test procedure is fully-objective and simplified, while human intervention is not required. The WDT+ data reduction method has been shown to be robust and quasi-static tests can be performed at slow displacement rates higher than those suggested by the ISO-25217 for DCB tests. Moreover, the WDT+ method is appropriate for any adhesive type and bondline thickness, increasing the scope of the Wedge-Driven Test method

Table 4
Experimental results of samples tested at different displacement rates.

Method	Adhesive	Batch	DR (mm/min)	D_w (mm)	G_{IC} (N/mm)		F^c_{push} (N)		Eq. COF (–)		θ^c (°)	
					AVG	SD	AVG	SD	AVG	SD	AVG	SD
DCB	SG500	T3	10	n/a	1.707	0.101	n/a	n/a	n/a	n/a	n/a	n/a
			30	n/a	1.787	0.093	n/a	n/a	n/a	n/a	n/a	n/a
			50	n/a	1.877	0.115	n/a	n/a	n/a	n/a	n/a	n/a
WDT+	A2021	T4	10	3.00	1.128	0.071	163.53	15.23	0.268	0.028	2.17	0.10
		T6	250	3.00	1.170	0.147	193.31	15.65	0.323	0.040	2.14	0.11
	SG500	T5	6	3.00	1.440	0.082	234.39	23.79	0.315	0.024	2.72	0.02
		T7	30	3.00	1.363	0.030	286.54	15.90	0.369	0.020	2.88	0.02
			90	3.00	1.408	0.055	285.78	11.11	0.365	0.015	2.85	0.01
			150	3.00	1.417	0.049	293.92	17.29	0.375	0.023	2.85	0.01

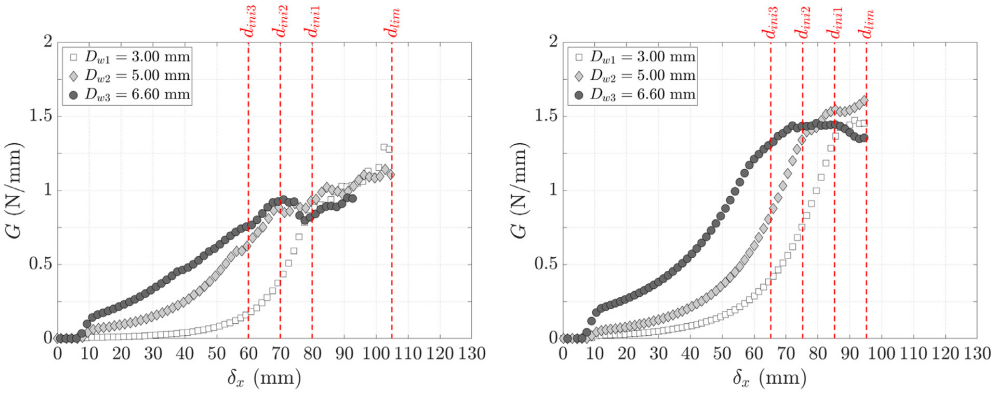

Fig. 18. ERR-displacement curves for (a) rigid and (b) flexible bonded joints tested with different wedge thicknesses. Distances d_{ini1}, d_{ini2} and d_{ini3} correspond to wedge diameters D_{w1}, D_{w2} and D_{w3}, respectively.

Table 5
Experimental average values between d_{ini} and d_{lim} for different wedge thicknesses.

Batch	Adhesive	DR (mm/min)	D_w (mm)	G_{IC} (N/mm)		F^c_{push} (N)		Eq. COF (–)		θ^c (°)	
				AVG	SD	AVG	SD	AVG	SD	AVG	SD
T4	A2021	10	3.00	1.128	0.071	163.53	15.23	0.268	0.028	2.17	0.10
		10	5.00	1.085	0.040	111.30	10.20	0.248	0.044	3.07	0.08
		10	6.60	1.000	0.031	81.86	8.46	0.189	0.042	3.61	0.09
T5	SG500	6	3.00	1.440	0.082	234.39	23.79	0.315	0.024	2.72	0.02
		6	5.00	1.556	0.024	154.69	11.40	0.229	0.005	3.80	0.01
		6	6.60	1.432	0.037	147.40	12.63	0.255	0.029	4.66	0.03

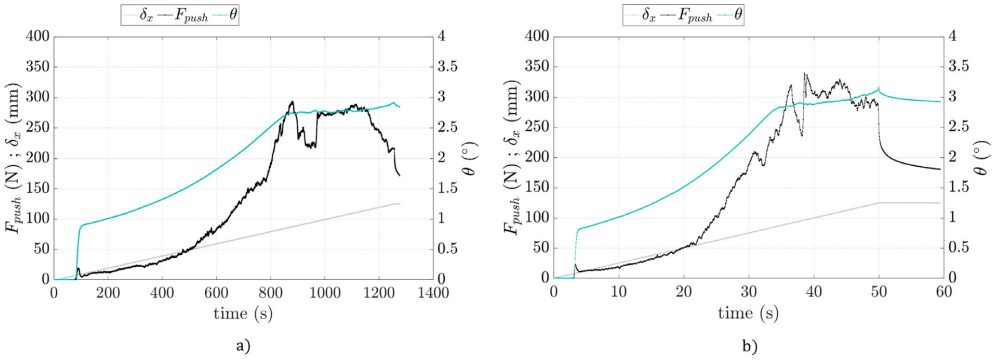

Fig. 19. Evolution of the contact angle and F_{push} in flexible bonded joints tested at (a) 6 mm/min and (b) 150 mm/min with the WDT+.

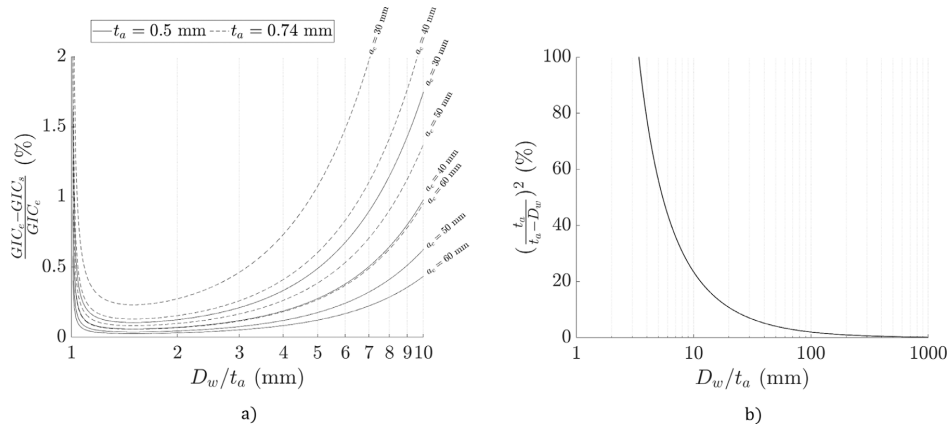

Fig. 20. Relative error in the measurement of fracture toughness: (a) between the exact and simplified formulations in the function of the ratio D_w/t_a (in logarithmic scale) for different crack lengths and adhesive thicknesses, and (b) through the simplified formulation in the function of the ratio D_w/t_a taking into account bondline thickness ($G_{IC_s}(t_a)$) or neglecting it ($G_{IC_s}(t_a = 0)$).

Table 6
Error in the calculation of G_{IC} depending on geometrical parameters.

D_w (mm)	a_c (mm)	Rigid adhesive		Flexible adhesive	
		a (mm)	Error [G_{IC}] (%)	a (mm)	Error [G_{IC}] (%)
3.00	35	25	0.4969	10	0.5499
5.00	45	–	–	20	0.8177
	50	35	0.6265	–	–
6.60	55	–	–	30	0.9155
	60	45	0.7384	–	–

*a: crack length; a_c: corrected crack length; D_w: wedge thickness.

towards flexible adhesives and thick adhesive layers. Its simplicity makes the WDT+ fast and reliable to characterise the quality of structural bonded joints intended for research or industrial applications.

CRediT authorship contribution statement

J. Manterola: Conceptualization, Methodology, Investigation, Writing - original draft. **J. Renart:** Conceptualization, Methodology, Writing - review & editing. **J. Zurbitu:** Supervision, Writing - review & editing. **A. Turon:** Methodology, Writing - review & editing. **I. Urresti:** Resources, Project administration.

Declaration of Competing Interest

The authors declare that they have no known competing financial interests or personal relationships that could have appeared to influence the work reported in this paper.

Acknowledgements

The authors gratefully acknowledge the financial support of the Spanish government through the “Ministerio de Ciencia, Innovación y Universidades” under the contract RTI2018-099373-B-I00.

References

da Silva, L.F.M., Dillard, D.A., Blackman, B., Adams, R.D., 2012. Testing Adhesive Joints: Best Practices. Wiley.

ISO-25217, Determination of the Mode I Adhesive Fracture Energy of Structural Adhesive Joints Using Double Cantilever Beam and Tapered Double Cantilever Beam Specimens, Tech. rep., Rep., Int. Org. Stdzn. (2009).

Manterola, J., Cabello, M., Zurbitu, J., Renart, J., Turon, A., Jumel, J., Urresti, I., 2019a. Effect of the width-to-thickness ratio on the mode I fracture toughness of flexible bonded joints. Eng. Fract. Mech. 218, 106584. https://doi.org/10.1016/j.engfracmech.2019.106584.

De Moura, M.F.S.F., Campilho, R.D.S.G., Gonçalves, J.P.M., 2008. Crack equivalent concept applied to the fracture characterization of bonded joints under pure mode I loading. Compos. Sci. Technol. 68, 2224–2230. https://doi.org/10.1016/j.compscitech.2008.04.003.

Paris, A.J., Paris, P.C., 1988. Instantaneous evaluation of J and C-star. Int. J. Fract. 38, 19–21.

ASTM D3762-03, 2010. Standard Test Method for Adhesive-Bonded Surface Durability of Aluminium (Wedge Test). ASTM International, West Conshohocken, PA. https://doi.org/10.1520/D3762-03R10. 2010.

Adams, R.D., Cowap, J.W., Farquharson, G., Margary, G.M., Vaughn, D., 2009. The relative merits of the Boeing wedge test and the double cantilever beam test for assessing the durability of adhesively bonded joints, with particular reference to the use of fracture mechanics. Int. J. Adhes. Adhes. 29, 609–620 doi:10.1016/j.ijadhadh.2009.02.010.

Manterola, J, Zurbitu, J, Renart, J, Turon, A, Urresti, I, 2020. Durability study of flexible bonded joints: The effect of sustained loads in mode I fracture tests. Polymer Testing 88 (106570). https://doi.org/10.1016/j.polymertesting.2020.106570.

McCartin, H.M., Ricsi, D.M., Brown, N.C., Adams, D.O., DeVries, K.L., 2016. Environmental durability assessment of composite bonded joints using the wedge test. Compos. Adv. Mater. Expo Anaheim.

Sargent, J.P., 2005. Durability studies for aerospace applications using peel and wedge tests. Int. J. Adhes. Adhes. 25, 247–256. https://doi.org/10.1016/j.ijadhadh.2004.07.005. https://doi.org/.

Cognard, J., 1986. The mechanics of the wedge test. J. Adhes. 20 (1), 1–13. https://doi.org/10.1080/00218468608073236. https://doi.org/.

Plausinis, D., Spelt, J.K., 1995. Designing for time-dependent crack growth in adhesive joints. Int. J. Adhes. Adhes. 15, 143–154. https://doi.org/10.1016/0143-7496(95)91625-G. https://doi.org/.

Jumel, J., Shanahan, M.E.R., 2008. Crack front curvature in the Wedge Test. J. Adhes. 84, 788–804. https://doi.org/10.1080/00218460802352975.

Budzik, M., Jumel, J., Imielinska, K., Shanahan, M.E.R., 2009. Accurate and continuous adhesive fracture energy determination using an instrumented wedge test. Int. J. Adhes. Adhes. 29, 694–701. https://doi.org/10.1016/j.ijadhadh.2008.11.003. https://doi.org/.

Manterola, J., Aguirre, M., Zurbitu, J., Renart, J., Turon, A., Urresti, I., 2019b. Using acoustic emissions (AE) to monitor mode I crack growth in bonded joints. Eng. Fract. Mech. 224, 106778. https://doi.org/10.1016/j.engfracmech.2019.106778. https://doi.org/.

ASTM STP 1012Glessner, A.L., Takemori, M.T., Vallance, M.A., Gifford, S.K., 1989. Mode I interlaminar fracture toughness of unidirectional carbon fiber composites using a novel wedge-driven delamination design. In: Paul, A.L. (Ed.), Composite Materials: Fatigue and Fracture Second. American Society for Testing and Materials, Philadelphia, pp. 181–200 ASTM STP 1012.

Williams, J.G., 1998. Friction and plasticity effects in wedge splitting and cutting fracture tests. J. Mater. Sci. 33, 5351–5357. https://doi.org/10.1023/A:1004490015211.

J. Renart, J. Costa, G. Santacruz, S. Lazcano, E. Gonzalez, Measuring Fracture Toughness of Interfaces Under Mode I Loading With the Wedge Driven Test, Under Submission (2020).

Dillard, D.A., Pohlit, D.J., Jacob, G.C., Starbuck, J.M., Kapania, R.K., 2011. On the use of a driven wedge test to acquire dynamic fracture energies of bonded beam specimens. J. Adhes. 87, 395–423. https://doi.org/10.1080/00218464.2011.562125.

Adams, D.O., McCartin, H.M., Sievert, Z., 2018. Development of environmental durability

test methods for composite bonded joints. In: Proceedings of the Joint Advanced Materials & Structures Technical Review Meeting. Long Beach.
Shi, X., Pan, Y., Ma, X., 2017. Modeling and analysis of the rope-sheave interaction at traction interface. J. Appl. Mech. 84 (3). https://doi.org/10.1115/1.4035584.
Blackman, B.R.K., Dear, J.P., Kinloch, A.J., MacGillivray, H., Wang, Y., Williams, J.G., Yayla, P., 1995. The failure of fibre composites and adhesivel bonded fibre composites under high rates of test. Part I: mode I loading – experimental studies. J. Mater. Sci. 30, 5885–5900. https://doi.org/10.1007/BF01151502.
Blackman, B.R.K., Kinloch, A.J., Rodriguez Sanchez, F.S., Teo, W.S., Williams, J.G., 2009. The fracture behaviour of structural adhesives under high rates of testing. Eng. Fract. Mech. 76, 2868–2889. https://doi.org/10.1016/j.engfracmech.2009.07.013. https://doi.org/.
Sener, J.Y., Ferracin, T., Caussin, L., Delannay, F., 2002. On the precision of the wedge-opened double cantilever beam method for measuring the debonding toughness of adhesively bonded plates. Int. J. Adhes. Adhes. 22, 129–137. https://doi.org/10.1016/S0143-7496(01)00046-X. https://doi.org/.